



MSIS  
3  
2002



This is to certify that the

dissertation entitled

- I. Kinetic Evaluation of the Copolymerization of Lactide with Substituted Lactides
- II. Synthesis and Characterization of Polyacenes

presented by

Chun Wang

has been accepted towards fulfillment  
of the requirements for

Ph.D. degree in Chemistry

  
Major professor

Date July 10, 2001

**PLACE IN RETURN BOX** to remove this checkout from your record.  
**TO AVOID FINES** return on or before date due.  
**MAY BE RECALLED** with earlier due date if requested.

DATE DUE	DATE DUE	DATE DUE

**I. KINETIC EVALUATION OF COPOLYMERIZATION OF LACTIDE  
WITH SUBSTITUTED LACTIDES**

**II. SYNTHESIS AND CHARACTERIZATION OF POLYACENES**

**By**

**Chun Wang**

**A DISSERTATION**

**Submitted to  
Michigan State University  
in partial fulfillment of the requirements  
for the degree of**

**DOCTOR OF PHILOSOPHY**

**Department of Chemistry**

**2001**

## ABSTRACT

### I. KINETIC EVALUATION OF COPOLYMERIZATION OF LACTIDE WITH SUBSTITUTED LACTIDES. II. SYNTHESIS AND CHARACTERIZATION OF POLYACENES

By

Chun Wang

Because of its environmental and biodegradability, polylactide has important applications as materials in medicine and as an environmentally friendly commodity plastic. One major deficiency of polylactide is its limited range of physical properties. Copolymerization of lactide with substituted lactides is a strategy that can provide polylactides with new properties. Evaluation of the kinetics of these copolymerizations is necessary since the kinetics define the structure of polylactide copolymers, which in turn defines the physical properties of the copolymers. A protocol was developed to analyze the compositions of LA/substituted LA copolymers, which allowed us to evaluate the kinetic parameters of the copolymerization of lactide with ethylglycolide, isopropyl glycolide, and D-ethylglycolide. The data show that these copolymerizations can be described as ideal polymerizations, but due to the monomer reactivity differences, poly(lactide-co-isopropylglycolide) and Poly(lactide-co-D-ethylglycolide) tend to be blocky. These polymers show single glass transitions. A study of the degradation of poly(lactide-co-isopropylglycolide) showed that the degradation process can be described by a random chain scission mechanism.

Polyacene is expected to have the lowest band gap among conjugated polymers. Despite its promise as an electrical conductor, and as a material for optics and battery electrodes, it has yet to be synthesized. We developed the synthesis of polyacene materials through the acid-catalyzed condensation of bis(methoxymethyl)benzenes. TGA, IR and Raman characterization support the formation of an extended  $\pi$ -conjugated system. To improve solubility, we developed a scheme to prepare *n*-octylated bis(methoxymethyl)benzene. Polymerization of this monomer yielded materials with molecular weights as high as 7000. However, fluorescence data show that the acene segments have a maximum length of only ~5 units. We also designed a synthesis of two-dimensional graphite by applying similar chemistry to poly(*p*-phenylene). TGA, IR and Raman data support formation of a graphitic structure after the material is heated to >500 °C.

**To my Father and family**

## **ACKNOWLEDGMENTS**

My first acknowledgment goes to my advisor: Professor Baker. He is not the reason I came to MSU, however, it is because of him, I chose to stay as a Spartan. Thank you very much for your guidance and attention in all these years, I just wish I had accomplished more to deserve such a great mentor.

I would also like to thank Professor Borhan, Blanchard, Berglund, Reusch, Scraton and. Chang. What I learned from you will continue to influence me in the future.

It's time to say good-bye, my dear group. My special thanks goes to Cory, who helped me turn into today's "Chun". Micah, Tara, Erin, Fadi, Gao, JB, Kirk, Tianqi, Wenxi, Jingpin, Sue, Hou, Qiao, Yiyan, Mao. I learn a bit from each of you. Thanks for your help and companionship, I have had a great time.

My friends, Don and Ellen, Xiaoxiao, Winnie, Zigang, Heather, Lisa and Dan, Tong, Qingqing, Ning, Ying, for all the valleys and peaks that we have been through, thanks for always being there with me. I appreciate your sincere friendship.

The last toast goes to my family: Mom, for your eternal love, Dad, you have always been my example in research, my dentist sister and brother-in-law, for your sweet support, and Yijun, my husband, for your love and friendship.

Most important of all, all the success and glory attributes to my mighty Father.

## Table of Contents

List of Schemes	xi
List of Figures	xiv
List of Tables	xviii

### I. KINETIC EVALUATION OF COPOLYMERIZATION OF LACTIDE WITH SUBSTITUTED LACTIDES

<b>INTRODUCTION</b> .....	<b>2</b>
<b>1. Structure and Physical Properties of Polylactide</b> .....	<b>2</b>
2. Polylactide Degradation .....	4
<b>3. Applications of Polylactides</b> .....	<b>6</b>
3.1. Biomedical Applications .....	6
3.1.1. General Medical Applications .....	6
3.1.2. Controlled Drug Delivery .....	6
3.1.3. Tissue Engineering.....	7
3.2. Applications as Conventional Thermoplastics.....	7
<b>4. Copolymerization</b> .....	<b>9</b>
4.1. Lactide Copolymerization.....	10
4.1.1. Copolymerization of Lactide with Lactones and Carbonates .....	11
4.1.1.1. Copolymerization with Caprolactone.....	11
4.1.1.2. Copolymerization with Other Lactones.....	12

4.1.1.3. Copolymerization with Carbonates.....	12
4.1.2. Copolymerization with Glycolide.....	13
4.1.3. Copolymerization of Substituted Glycolides and Lactide.....	15
4.1.4. Copolymerization with Lysine and Other Amino Acids .....	16
4.2. Block and Graft Copolymers .....	18
4.2.1. Copolymerization of Lactide with Poly(ethylene glycol).....	18
4.2.2. Graft Copolymers from Natural Polymers.....	20
4.2.3. Lactide Copolymers with Blocks from Vinyl and Acrylic Monomers ...	21
4.2.4. Copolymerization with Other Comonomers .....	23
4.3. Copolymerization Characterization .....	23
4.4. Kinetic Studies of Copolymerization .....	25
4.4.1. Monomer Reactivity Ratios.....	25
4.4.2. Types of Copolymerization Behavior.....	27
4.4.2.1. Ideal copolymerization: $r_1 r_2 = 1$ .....	27
4.4.2.2. Alternating Copolymerization: $r_1 = r_2 = 0$ .....	28
4.4.2.3. Block Copolymerization: $r_1 > 1, r_2 > 1$ .....	28
4.4.3. Experimental Evaluation of Monomer Reactivity Ratios .....	28
4.4.4. Monomer Reactivity Ratio Analysis of Lactide Copolymerizations ...	29
<b>EXPERIMENTAL.....</b>	<b>31</b>
5.1. General.....	31
5.2. Monomer Preparation and Synthesis.....	32
5.3. Copolymerization .....	33
5.4. Copolymer Composition: Direct Determination .....	33

<b>5. 5. Biodegradation .....</b>	<b>34</b>
<b>RESULTS AND DISCUSSION .....</b>	<b>35</b>
<b>6.1. Copolymerization of Lactide with Ethylglycolide .....</b>	<b>35</b>
6.2. Kinetic Evaluation of the Copolymerization of Lactide with Ethylglycolide	40
6.2.1. Copolymer Composition Determination.....	40
6.2.1.1. <sup>13</sup> C NMR.....	40
6.2.1.2. Normal Phase High Pressure Liquid Chromatography (HPLC) .....	41
6.2.1.3. Reverse Phase HPLC .....	44
6.2.1.4. Kinetic Evaluation Based on Reverse Phase HPLC Results .....	45
6.2.1.5. Direct Determination of Copolymer Composition. ....	49
6.3. Kinetic Evaluation of the Copolymerization of Lactide with Isopropylglycolide .....	60
6.4. Copolymerization of Lactide with R-ethylglycolide .....	69
6.5. Physical Properties and Structure of Copolymers.....	76
6.6. Biodegradation of the Copolymers.....	81
<b>BIBLIOGRAPHY .....</b>	<b>87</b>
<b>II. SYNTHESIS AND CHARACTERIZATION OF POLYACENES</b>	
<b>INTRODUCTION .....</b>	<b>94</b>
1. Structure of Polyacene.....	94
1.1. Chemical Structure.....	94
1.2. Electronic Structure and Properties.....	95

1.2.1. Electronic structure of unsubstituted polyacene .....	95
1.2.2. Electronic structures of alkyl substituted polyacene .....	102
1.2.3. Properties of polyacenes.....	104
1.3. Applications.....	104
1.3.1. Electronically conductive materials.....	104
1.3.2. Optical limiters.....	109
1.3.3. Electrodes for lithium ion batteries .....	111
1.3.3. Capacitors .....	118
1.4. Synthetic Approaches to Polyacenes .....	118
1.4.1. The Diels-Alder approach.....	120
1.4.2. Topochemical polymerizations .....	123
1.4.3. Acene-like materials .....	124
1.5.4. Soluble polyacenes .....	127
1.6. Characterization of Polyacenes.....	128
1.6.1. X-ray diffraction .....	129
1.6.2. <sup>13</sup> C NMR.....	129
1.6.3. ESR (Electron Spin Resonance) .....	130
1.6.4. UV and fluorescence .....	130
1.6.5. Raman spectroscopy.....	131
<b>EXPERIMENTAL.....</b>	<b>132</b>
2.1. General .....	132
2.2. Synthesis .....	133
<b>RESULTS AND DISCUSSION .....</b>	<b>141</b>

3.1. Polyacenic materials. ....	141
3.1.1. Simple routes to acene-like materials .....	141
3.1.2. Chemical dehydrogenation.....	150
3.1.3. Polymerization in solution.....	150
3.1.4. Characterization of acene-like materials .....	154
3.1.4.1. Infrared .....	154
3.1.4.2. Raman.....	155
3.1.4.3. Elemental Analysis .....	155
3.2. Well-defined Soluble Polyacene .....	159
3.2.1. Monomer design and synthesis.....	159
3.2.2. Polymerization condition development .....	163
3.2.3. Model cyclization study.....	164
3.2.4. Characterization .....	173
3.2.5. Discussion .....	174
3.3. Acene/poly ( <i>p</i> -phenylene) hybrids. ....	175
3.4. Conclusion .....	180
<b>BIBLIOGRAPHY .....</b>	<b>182</b>

## LIST OF SCHEMES – KINETIC EVALUATION OF THE COPOLYMERIZATION OF LACTIDE WITH SUBSTITUTED LACTIDES

<b>Scheme 1.</b>	Preparation of polylactide.	2
<b>Scheme 2.</b>	Ring opening polymerization mechanism of lactide.	3
<b>Scheme 3.</b>	Copolymerization of lactide with $\epsilon$ -caprolactone.	11
<b>Scheme 4.</b>	Copolymerization of lactide with TMC.	13
<b>Scheme 5.</b>	Copolymerization of lactide with glycolide.	13
<b>Scheme 6.</b>	Copolymerization of lactic acid with mandelic acid.	15
<b>Scheme 7.</b>	Copolymerization of lactide with BMD and DMD.	16
<b>Scheme 8.</b>	Polymerization of D,L-3-methylglycolide.	16
<b>Scheme 9.</b>	Synthesis of PLA-PEG copolymers.	20
<b>Scheme 10.</b>	Synthesis of poly(lactide- <i>b</i> -isoprene- <i>b</i> -lactide).	22
<b>Scheme 11.</b>	Synthesis of poly(HEMA- <i>graft</i> -lactide).	23
<b>Scheme 12.</b>	Chain propagation steps in the copolymerization of two monomers.	26
<b>Scheme 13.</b>	Copolymerization of racemic lactide with ethylglycolide.	36
<b>Scheme 14.</b>	Reactivity differences leads to “blocky” copolymers.	40
<b>Scheme 15.</b>	Protocol for the determination of copolymer composition.	52
<b>Scheme 16.</b>	Copolymerization of racemic lactide with racemic isopropylglycolide.	60
<b>Scheme 17.</b>	Chain propagation mechanism for lactide copolymerization.	68
<b>Scheme 18.</b>	Copolymerization of lactide with R-ethylglycolide.	69
<b>Scheme 19.</b>	The relationship between monomer reactivity ratio and the structure of copolymers.	80

## LIST OF SCHEMES – SYNTHESIS AND CHARACTERIZATION OF POLYACENES

<b>Scheme 1.</b>	Polyacene oligomer synthesized by via Diels-Alder adduction.	120
<b>Scheme 2.</b>	Polyacene oligomer synthesized via Diels-Alder addition and retro Diels-Alder elimination.	122
<b>Scheme 3.</b>	Topochemical polymerization of butadiyne and 1-buten-3-yne to prepare polyacene.	124
<b>Scheme 4.</b>	Preparation acene-like material from phenol-formaldehyde resin.	125
<b>Scheme 5.</b>	Acene-like material synthesized from styrene-divinylbenzene copolymers and poly( <i>p</i> -phenylene).	126
<b>Scheme 6.</b>	Synthesis of highly alkyl-substituted pentacene derivatives by homologation.	127
<b>Scheme 7.</b>	Acid catalyzed polymerization of methoxymethylbenzene.	142
<b>Scheme 8.</b>	Acid-catalyzed polymerization of bis(methoxymethyl) benzenes.	143
<b>Scheme 9.</b>	Possible outcomes from the polymerization of bis(methoxymethyl)benzenes.	148
<b>Scheme 10.</b>	The substitution pattern on the benzene ring leads to different condensation products.	149
<b>Scheme 11.</b>	Alkyl substituted polyacene.	159
<b>Scheme 12.</b>	First approach to the synthesis of 1,4- <i>bis</i> -(methoxymethyl)-2,5-dialkyl benzenes.	161
<b>Scheme 13.</b>	Modified synthesis of 1,4- <i>bis</i> -(methoxymethyl)-2,5-dialkyl benzenes.	162
<b>Scheme 14.</b>	Control experiment used to develop polymerization conditions.	163
<b>Scheme 15.</b>	Control experiment to prove BF <sub>3</sub> caused side reactions.	163

<b>Scheme 16.</b>	Synthesis of a model compound for the cyclization study.	164
<b>Scheme 17.</b>	Model cyclization condition study.	165
<b>Scheme 18.</b>	Model dehydrogenation test.	166
<b>Scheme 19.</b>	Intramolecular cyclization vs. intermolecular bridge formation.	171
<b>Scheme 20.</b>	Synthesis of alkylated polyacenes.	172
<b>Scheme 21.</b>	Proposed approach for the preparation of a soluble linear polyacene.	175
<b>Scheme 22.</b>	Synthesis of a methoxymethyl-substituted polyphenylene.	176
<b>Scheme 23.</b>	Synthesis of sheet structures from methoxymethyl-substituted polyphenylenes.	178

## LIST OF FIGURES – KINETIC EVALUATION OF THE COPOLYMERIZATION OF LACTIDE WITH SUBSTITUTED LACTIDES

<b>Figure 1.</b>	Four generic copolymer architectures.	9
<b>Figure 2.</b>	Examples of lactones that copolymerize with lactide.	12
<b>Figure 3.</b>	A poly(lactide-co-L-Lysine) derivative.	17
<b>Figure 4.</b>	Copolymerization of lactide with Hpr.	18
<b>Figure 5.</b>	DSC runs (second heating after flash quenching from 100 °C) for lactide and ethylglycolide copolymers. Heating rate: 10 °C/min under helium.	37
<b>Figure 6.</b>	Glass transition temperatures of lactide and ethylglycolide copolymers.	38
<b>Figure 7.</b>	Mole fraction of lactide in the copolymer ( $F_1$ ) as a function of the feed ratio ( $f_1$ ) during the copolymerization of lactide with ethylglycolide as determined from reverse phase HPLC	47
<b>Figure 8.</b>	$r_1$ and $r_2$ determination by the Fineman-Ross method.	48
<b>Figure 9.</b>	Mole fraction of lactide in the copolymer ( $F_1$ ) as a function of the feed ratio ( $f_1$ ) during the copolymerization of lactide with ethylglycolide as determined from $^1\text{H}$ NMR.	54
<b>Figure 10.</b>	$r_1$ $r_2$ determination by Fineman-Ross method.	55
<b>Figure 11.</b>	$r_1, r_2$ Determination by the Telen-Tudos Method.	59
<b>Figure 12.</b>	Mole fraction of lactide in the copolymer ( $F_1$ ) as a function of the feed ratio ( $f_1$ ) during the copolymerization of lactide with poly(lactide-co-rac-isopropylglycolide).	64
<b>Figure 13.</b>	$r_1$ $r_2$ determination using the Fineman-Ross method.	65
<b>Figure 14.</b>	$r_1, r_2$ Determination using the Kelen-Tudos method.	66
<b>Figure 15.</b>	Melt polymerization of D-ethylglycolide at 130 °C catalyzed by $\text{Sn}(\text{Oct})_2 + t\text{-BBA}$	70
<b>Figure 16.</b>	Mole fraction of lactide in the copolymer ( $F_1$ ) as a function of the feed ratio ( $f_1$ ) during the copolymerization of lactide	72

with D-ethylglycolide.

<b>Figure 17.</b>	$r_1, r_2$ determination by Fineman-Ross method.	73
<b>Figure 18.</b>	$r_1, r_2$ determination by Kelen-Tudos method.	74
<b>Figure 19.</b>	Glass transition temperature of lactide and isopropylglycolide copolymers.	77
<b>Figure 20.</b>	The weight loss of polymer samples during hydrolytic degradation.	83
<b>Figure 21.</b>	The molecular weight loss of poly(LA-co-iPRGL) during hydrolytic degradation.	84
<b>Figure 22.</b>	Decrease in the molecular weight of P(LA-co-iPRGL) during hydrolytic degradation fitted to the random chain scission model.	85
<b>Figure 23.</b>	The decrease in the degree of polymerization of polymer samples during hydrolytic degradation.	86

## LIST OF FIGURES – –SYNTHESIS AND CHARACTERIZATION OF POLYACENES

<b>Figure 1.</b>	Chemical structure of polyacene.	94
<b>Figure 2.</b>	Four possible double bond configurations for polyacene.	96
<b>Figure 3.</b>	Empirical determination of the band gap ( $E_g$ ) of polyacene.	99
<b>Figure 4.</b>	Six methyl-substituted polyacenes studied by Wang and Hou.	101
<b>Figure 5.</b>	Three possible isomers of structure 5.	102
<b>Figure 6.</b>	Band gaps of conductive materials.	105
<b>Figure 7.</b>	Molecular orbital energy diagram of polyacene and doped polyacene.	108
<b>Figure 8.</b>	Relationship between output fluence and input fluence of a 70% transmitting solution of a polyacene-based oligomer in toluene.	109
<b>Figure 9.</b>	Five-level energy diagram of polyacene.	110
<b>Figure 10.</b>	Cell structure and electrochemistry of electrodes in PAS batteries.	112
<b>Figure 11.</b>	The $C_6Li$ configuration observed in the first stage Li-graphite intercalation compound (Li-GIC).	113
<b>Figure 12.</b>	An illustrative model of PAS.	115
<b>Figure 13.</b>	Other acene derivatives made by Clardy's group.	121
<b>Figure 14.</b>	Thermogravimetric analysis results for poly(methoxymethylbenzene). Heating rate: 10 °C/min.	143
<b>Figure 15.</b>	Thermogravimetric analysis results for poly(methoxybenzene) and poly(bis(methoxymethyl)benzene) when $O_2$ is rigorously excluded. Heating rate: 10 °C/min.	144
<b>Figure 16.</b>	Thermogravimetric analysis results for poly(methoxymethylbenzene) and poly(bis(methoxymethyl)benzene) run under nitrogen	146

contaminated with 10% oxygen. Heating rate: 10 °C/min.

<b>Figure 17.</b>	Thermogravimetric analysis results for poly (bis-1,2-(methoxymethyl)benzene) in nitrogen. Heating rate: 10 °C/min.	151
<b>Figure 18.</b>	Thermogravimetric analysis results for poly(bis-1,4-(methoxymethyl)benzene) in nitrogen. Heating rate: 10 °C/min.	152
<b>Figure 19.</b>	Thermogravimetric analysis results for poly(1,2-bis(methoxymethyl)benzene) prepared via solution and bulk reactions.	153
<b>Figure 20.</b>	Infrared absorption spectra of the polybenzyl network formed from 1,2-bis(methoxymethyl)benzene, taken after being heated in nitrogen at 10 °C/min to 30 °C, 380 °C, 500 °C, 650 °C, and 800 °C	157
<b>Figure 21.</b>	Raman spectra of polymers derived from <i>ortho</i> , <i>para</i> and <i>meta</i> -bis(methoxymethyl)benzene after being heated to 800 °C.	158
<b>Figure 22.</b>	UV and fluorescence spectra of soluble polyacene products.	172
<b>Figure 23.</b>	Thermogravimetric analysis of methoxymethyl-substituted polyphenylene.	177
<b>Figure 24.</b>	Infrared of cross-linked and heat treated samples of a methoxymethyl-substituted polyphenylene.	179
<b>Figure 25.</b>	Raman spectrum of a cross-linked and heat treated sample of a methoxymethyl-substituted polyphenylene.	180

## LIST OF TABLES – KINETIC EVALUATION OF THE COPOLYMERIZATION OF LACTIDE WITH SUBSTITUTED LACTIDES

<b>Table 1.</b>	Properties of copolymers.	39
<b>Table 2.</b>	Determination of Conversion in the Copolymerization of Lactide (LA) and Ethylglycolide (EG) by Normal Phase HPLC.	43
<b>Table 3.</b>	Monomer Determination by Reverse Phase HPLC.	44
<b>Table 4.</b>	Copolymerization behavior of lactide with ethylglycolide.	46
<b>Table 5.</b>	Comparison of the GC and <sup>1</sup> H NMR methods for analyzing the copolymer composition.	53
<b>Table 6.</b>	Copolymerization behavior from Fineman-Ross method.	56
<b>Table 7.</b>	Copolymerization behavior from Kelen-Tudos method.	58
<b>Table 8.</b>	Comparison of copolymer composition analysis obtained from parallel runs.	61
<b>Table 9.</b>	Copolymerization behavior from Fineman-Ross method.	67
<b>Table 10.</b>	Copolymerization behavior from Kelen-Tudos method.	67
<b>Table 11.</b>	Copolymerization behavior from Fineman-Ross method.	75
<b>Table 12.</b>	Copolymerization behavior from Kelen-Tudos method.	75
<b>Table 13.</b>	Properties of P(LA- <i>co</i> - <i>t</i> PrGL).	76

## LIST OF TABLES – SYNTHESIS AND CHARACTERIZATION OF POLYACENES

<b>Table 1.</b>	Electronic properties of structures 1-6.	103
<b>Table 2.</b>	Concentration vs. yield in model cyclization study.	167
<b>Table 3.</b>	Reaction temperature vs. yield in model cyclization.	167
<b>Table 4.</b>	Reaction time vs. yield in model cyclization study.	168

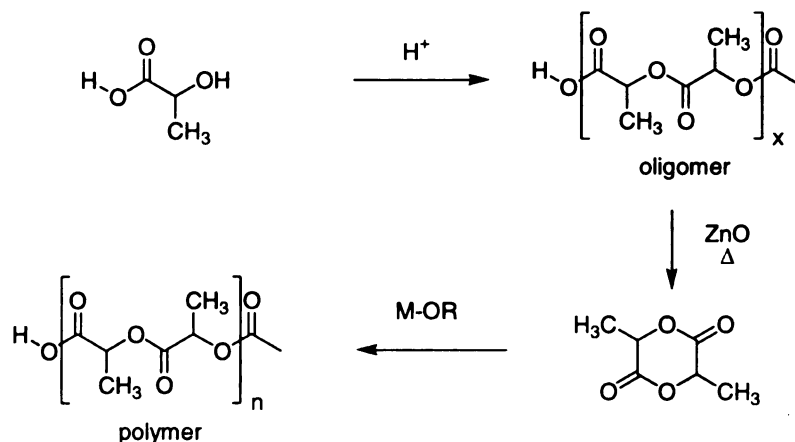
<b>Table 5.</b>	Argon purge vs. yield in model cyclization study.	168
<b>Table 6.</b>	Acid ratio vs. yield in model cyclization study.	169
<b>Table 7.</b>	The rate of adding the acid vs. yield in model.	169
<b>Table 8.</b>	Different solvent vs. yield in model cyclization.	170

# **I. KINETIC EVALUATION OF COPOLYMERIZATION OF LACTIDE WITH SUBSTITUTED LACTIDES**

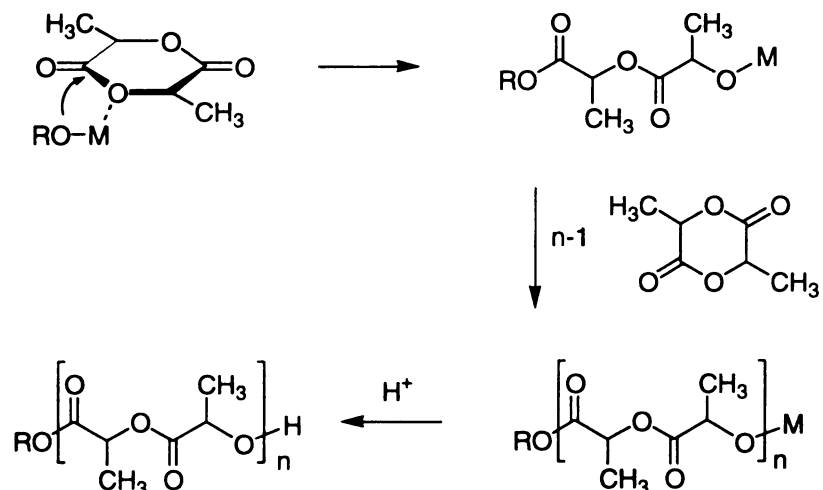
# INTRODUCTION

## 1. Structure and Physical Properties of Polylactide

Polymers based on lactic acid are an increasingly important class of polymers. Because they are biocompatible and degrade to environmentally benign products, applications for these polyesters are increasing rapidly. Lactic acid polymers are prepared by the Ring Opening Polymerization (ROP) of lactide, the cyclic dimer of lactic acid. As shown in **Scheme 1**, lactides are obtained by depolymerizing lactic acid oligomers, which in turn are produced by the acid catalyzed polycondensation of lactic acid. This scheme is the method of choice since ROP leads to fast polymerization rates and excellent control over the polymer architecture. The key step in initiating ROP of lactide (**Scheme 2**) is the nucleophilic attack at the lactide carbonyl by a metal alkoxide, formed *in situ*, or directly added to the polymerization. Propagation



**Scheme 1. Preparation of polylactide**



### Scheme 2. Ring opening polymerization mechanism of lactide.

steps extend the polymer chain by an analogous process. The attack by the alkoxide is affected by the steric hindrance posed by the lactide and the nucleophilicity of the alkoxide. Although not proven, it is thought that attack by the metal alkoxide is the rate determining step in lactide polymerization.<sup>1</sup>

Lactic acid is chiral, and thus there are three lactide diastereomers, the R,R (D-lactide), S,S (L-lactide), and the R,S or *meso* form (DL-lactide). A 1:1 mixture of the R,R and S,S diastereomers is often termed *rac*-lactide. L- and D,L-lactide are used almost exclusively for polymerization. The physical properties of polylactides are sensitive to the stereochemistry of the monomers and the stereoregularity of the resulting polymer chain. Polymerization of the R,R or S,S diastereomer yields a crystalline polymer with a glass transition temperature ( $T_g$ ) of 55-64°C,<sup>2</sup> while *rac*-lactide yields amorphous materials<sup>3,4</sup>.

Poly(L-lactide), PLLA, is a semi-crystalline polymer with a melting temperature ( $T_m$ ) of 180 °C and a crystallinity of about 70%.<sup>5</sup> The  $T_g$  is reported to be 55-64 °C,<sup>6-8</sup> depending on the degree of crystallinity. PLLA has good

mechanical properties such as a high modulus and high strength, and for this reason, PLLA was the material of choice for the development of practical degradable polymers. For example, PLLA is widely used in orthopedic devices since it can be processed by thermal processes such as injection-molding and extrusion. However, due to its high crystallinity, PLLA shows the slowest degradation rate of all resorbable polylactides.

Polymerization of the R,S diastereomer results in poly(D,L-lactide), (PDLLA). Because of the random distribution of L- and D-units along the polymer backbone, crystallization is inhibited and the polymer is an amorphous, glassy material with a  $T_g$  of about 50-60 °C.<sup>9</sup> Compared to crystalline PLLA, the stiffness of PDLLA is significantly lower, and because the amorphous structure allows water to diffuse easily into the bulk polymer, its degradation rate is much faster than PLLA.

## **2. Polylactide Degradation**

The dominant degradation pathway for high molecular weight polylactides is hydrolysis of the ester bonds along the polymer chain.<sup>10</sup> Ester hydrolysis is a well-known reaction in organic chemistry that can be catalyzed by acid or base. In the case of polylactide, cleavage of ester bonds generates carboxyl end groups that autocatalyze further degradation. The hydrolytic degradation of polylactide is generally regarded as a homogeneous process, rather than heterogeneous-surface erosion, and includes two stages. The first stage is characterized by a decrease in molecular weight due to random

hydrolytic ester cleavage, while the second is the onset of weight loss once the chains are short enough to be mechanically unstable or soluble.<sup>11</sup>

Several factors favor high degradation rates: a low  $T_g$  that facilitates transport of water in the polymer matrix, a hydrophilic structure that enhances the solubility of water in the polymer, and the presence of acid or base to catalyze ester hydrolysis. Since degradation occurs fastest in amorphous regions, the crystallinity and morphology of the polymer also help determine the overall degradation rate. In amorphous samples, ester hydrolysis occurs randomly along the polymer chain and the decrease in the degree of polymerization can be fit to a random scission model.

Enzymatic degradation becomes important in glassy samples only at the latter stages of degradation, when short, flexible chains become soluble and are accessible to enzymes. In contrast, rubbery polymers seem to be able to degrade polylactide much earlier via surface erosion. Proteinase K,<sup>12,13</sup> pronase and bromelain<sup>13</sup> were also reported to effect enzymatic degradation of polylactide.

### **3. Applications of Polylactides**

#### **3.1. Biomedical Applications**

##### **3.1.1. General Medical Applications**

The driving force for the use of PLLA in medical applications is that PLLA degrades in the body to benign products. Good mechanical properties make polylactides the materials of choice for surgical fixation materials, such as: sutures, clips, bone pins and plates.<sup>14</sup> The degradation rates of polylactides must be matched to their application so they persist in the body long enough to fulfill their function as a support. Copolymerization of lactide with glycolide is commonly used to increase the degradation rate. For example, most resorbable sutures are either pure poly(glycolide) or glycolide-rich copolymers.

##### **3.1.2. Controlled Drug Delivery**

Biodegradable polymers such as polylactide are often used in controlled drug release systems, often as carriers for drugs. Polymer-mediated controlled release systems have many advantages over conventional delivery systems:<sup>15</sup> 1) agents can be delivered to tissues in a sustained, continuous and predictable fashion; 2) they are well protected before being released; 3) site specific delivery (such as in brain) can be achieved by simple implantation or direct injection; 4) repeated drug administration is not necessary.

Many classes of drugs benefit from time-release approaches to delivery. Time release can provide a near-constant level of therapeutic agents, maximizing the effectiveness of drugs and minimizing toxicity and adverse

reactions caused by “spikes” in concentration. Controlled delivery strategies also have important applications in agrochemical fields with the timed-release of nutrients and pesticides providing obvious advantages. Here again control over the polymer degradation profile is critical, since it largely defines the rate of release from the drug carrier.

### **3.1.3. Tissue Engineering**

A major application of biodegradable polymers is tissue engineering, in which they act as a scaffold for the regeneration of autografted new skin, wound covers and delivery vehicles for transplanting cells.<sup>16,17</sup> Tissue engineering involves the creation of natural tissue by transplanting cells removed from the patient or from a close relative and seeding the cells into a scaffold that serves both as an adhesive substrate and a physical support for the cells. The design and fabrication of suitable scaffolds from polylactide and lactide copolymers is a significant challenge and extensive studies are aimed at evaluating these polymers as scaffolds for tissue growth.<sup>18,19</sup> However, the degradation of the scaffold must be tightly controlled, and the degradation profile of polylactide is complicated, partly due to its crystallinity. Copolymerization of L-lactide with glycerol<sup>20</sup> and blending of PDLLA with biodegradable rubbery materials<sup>21,22</sup> have been proposed as partial solutions to this problem.

### **3.2. Applications as Conventional Thermoplastics**

Poly lactides are well-behaved thermoplastics with a reasonable shelf life for applications ranging from fibers for clothing to packaging materials. Because lactic acid is derived from the fermentation of starch, poly lactides are

a renewable alternative to petroleum-based polymers. In even slightly moist environments, PLLA degrades by hydrolysis to environmentally-friendly products over a period of several months to a year, which compares to 100 to 500 years for conventional plastics such as polystyrene and polyethylene. Its general physical properties and melt processing ease are similar to conventional packaging resins. PLLA is a clear, colorless thermoplastic when quenched from the melt and is similar in many respects to polystyrene. When plasticized with its own monomer, PLLA becomes increasingly flexible so that a continuous series of products can be prepared that can mimic polyvinyl chloride, low density polyethylene, linear low density polyethylene, polypropylene and polystyrene. Besides mechanical properties comparable to traditional packaging plastics and biodegradability, another advantage of polylactide is that it can be produced from renewable sources. Cargill-Dow is commercializing polylactide production using dextrose from corn.<sup>23</sup> Technology to convert food wastes into polylactide has also been developed.<sup>24</sup>

To overcome the poor processability of PLLA and its poor impact strength, the most common composition for high volume packaging resins is the 90/10 copolymer of L-/D,L lactide. The addition of D,L lactide reduces the crystallinity of the polymer and improves the impact strength. This material can be readily polymerized in the melt, can be oriented above its  $T_g$ , and is easily melt processable. To modify the mechanical properties, lactide is often copolymerized with glycolide and  $\epsilon$ -caprolactone.<sup>25</sup> All of these materials are biodegradable and compostable.

#### 4. Copolymerization

Copolymerizations are polymerization processes in which a mixture of two or more monomers is polymerized in the same reaction vessel to give a copolymer, a polymer where each of the monomers is incorporated into the

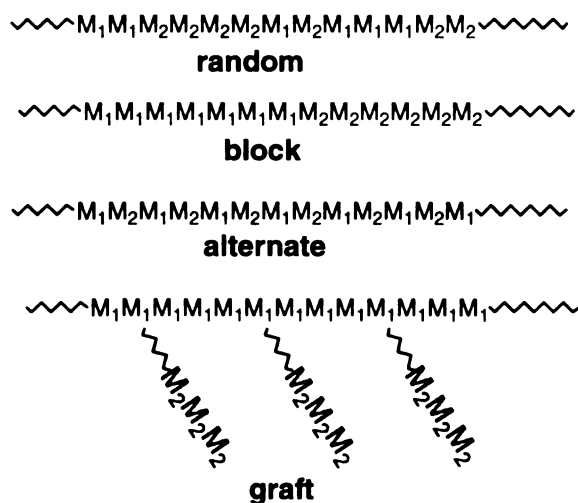


**Figure 1.** Four generic copolymer architectures.

polymer.<sup>26</sup> Copolymerization is important in that it greatly increases the ability of a polymer scientist to tailor-make polymer products with specific properties. Copolymerization studies also provide important information about the reactivities of monomers. As illustrated in **Figure 1**, polymers can be categorized into four general architectures: random, block, alternate and graft, according to the distribution of the comonomer units along the copolymer chain. In random copolymers, there is no preference for the placement of monomers along the chain, and therefore random copolymers should be homogeneous. Similarly, a perfectly alternating copolymerization yields a homogeneous product. Both random and alternating copolymerizations

produce materials with properties intermediate between those of the parent homopolymers. In contrast, block and graft copolymerizations generally result in multiphase materials where each phase exhibits the properties of one of the homopolymers. This provides an effective way of combining the individual properties of each polymer in a single material. In addition to the four cases shown in **Figure 1**, there are many intermediate cases. For example, most “random” copolymerizations deviate from true random incorporation of monomer units and show a preference for the incorporation of one monomer. When the preference is high, the polymers resemble block copolymers and are termed tapered block copolymers. In the limit of a large difference in reactivity, the complete polymerization of one monomer is followed by the polymerization of a second monomer, and one obtains a true block copolymer.

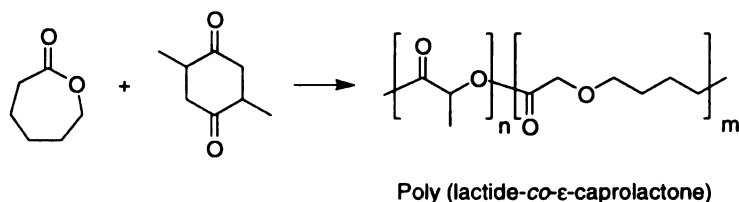
#### **4.1. Lactide Copolymerization**

The copolymerization of lactide with other monomers has been recognized as an important strategy to obtain materials with modified physical properties and degradation rates that meet the needs of specific applications. The four major parameters that can be varied to achieve an expected physical property are: copolymer structure, molecular weight, chemical composition (mole fraction of the monomers) and the chemical structure of the comonomers. A variety of monomers have been copolymerized with lactide and the next section provides a brief review of the major classes of lactide copolymers.

#### 4.1.1. Copolymerization of Lactide with Lactones and Carbonates

##### 4.1.1.1. Copolymerization with Caprolactone

$\epsilon$ -Caprolactone has been copolymerized with both L-lactide and D,L-lactide (**Scheme 3**).<sup>27-30</sup> Poly( $\epsilon$ -caprolactone) (PCL) itself is biocompatible and permeable to many drugs, however, the polymer is hydrophobic and its hydrolytic degradation rate is very slow. PLA is more hydrophilic, and thus is more permeable to drugs, but degrades rapidly. The major reason to copolymerize lactide with  $\epsilon$ -caprolactone is to combine the permeability of PCL with the rapid degradation rate of PLA to optimize properties such as permeability, hydrophilicity, the  $T_g$  and crystallinity for use in drug delivery devices.<sup>30</sup> When caprolactone and lactide are added simultaneously to a polymerization, the poly(lactide-*co*- $\epsilon$ -caprolactone) that is obtained is rarely



**Scheme 3.** Copolymerization of lactide with  $\epsilon$ -caprolactone.

random because  $\epsilon$ -caprolactone is much more reactive than lactide. This leads to non-random monomer incorporation and tapered copolymers. A well-defined block structure can be achieved when these two monomers are added sequentially.<sup>31</sup> Besides sutures and drug delivery systems,<sup>32</sup> one of the major applications of poly(lactide-*co*-caprolactone) is for wound treatment, especially

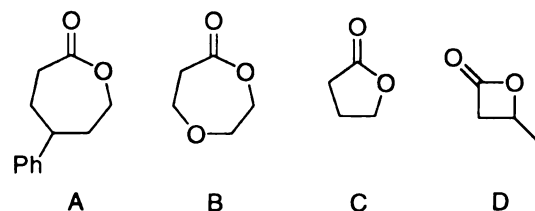


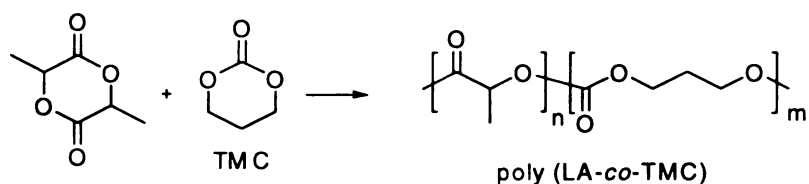
**Figure 2.** Examples of lactones that copolymerize with lactide. for burns.<sup>33-35</sup> The  $T_g$  of poly(lactide) is 50-60 °C, which is too high for the convenient application of PLA films on the surface of a wound. Incorporation of a more flexible comonomer such as  $\epsilon$ -caprolactone is needed to obtain flexible films with  $T_g$ 's near body temperature. It was reported that incorporation of 10-20 mole % of  $\epsilon$ -caprolactone units in PLA reduced the  $T_g$  to 28-38 °C (poly( $\epsilon$ -caprolactone has a  $T_g$  around  $-50$  °C).

#### 4.1.1.2. Copolymerization with Other Lactones

Besides  $\epsilon$ -caprolactone, a number of other cyclic lactones are reported to copolymerize with lactide (**Figure 2**) including: 5-phenyl- $\epsilon$ -caprolactone (A),<sup>36</sup> 1,5-dioxapan-2-one (B),<sup>37,38</sup>  $\gamma$ -butyrolactone (C),<sup>39</sup> and  $\beta$ -butyrolactone (D).<sup>40,41</sup> When polymerized, each of these polymers degrades to benign products that are harmless to the environment. When used as comonomers, each monomer tends to impart flexibility and permeability to hard polymers such as polylactide. The copolymers of lactide with these cyclic lactones have been proposed for various applications either in medicine or in packaging.

#### 4.1.1.3. Copolymerization with Carbonates

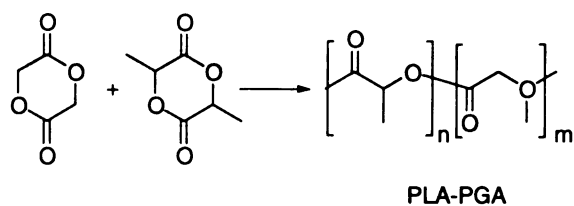
The major advantage of copolymerizing lactide with cyclic carbonates is to introduce the carbonate linkage into the polylactide chain. The carbonate linkage is expected to be enzymatically hydrolyzable and more hydrolytically stable than an ester linkage. The most common example is the copolymerization of lactide with trimethylene carbonate (TMC).<sup>42</sup> 2,2-Dimethyltrimethylene carbonate was also reported that have copolymerized with lactide.<sup>43</sup>



**Scheme 4.** Copolymerization of lactide with TMC

#### 4.1.2. Copolymerization with Glycolide

Glycolide and lactide are both based on the 1,4-dioxan-2,5-dione ring, and structurally, they differ in that the methyl groups of lactide are absent in glycolide. Because of reduced steric hindrance, glycolide is much more reactive than lactide and the copolymerization rates of glycolide and lactide are very different. Glycolide has been copolymerized with both L-lactide<sup>44,45</sup> and D,L-lactide to give linear, branched and star-shaped copolymers.<sup>15,46,47</sup> All of these copolymers tend to be “blocky”.



**Scheme 5.** Copolymerization of lactide with glycolide.

Pure poly(glycolide) is poorly soluble in all common organic solvents. Similarly, the blocky segments in glycolide copolymer are sparingly soluble, and thus the “blockiness” is the most important parameter to be controlled during the copolymerization. The mole % of glycolic units in copolymers is generally limited to ~50 % because higher contents render the copolymer insoluble in common solvents.

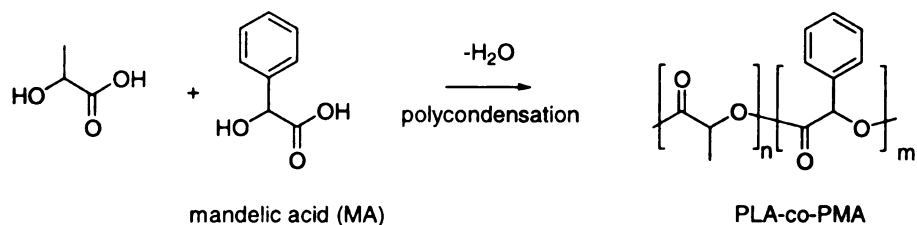
Pure PLLA and PDLLA are not well suited for pharmaceutical applications because their rate of degradation is too slow. However, the absence of methyl groups on the glycolic units renders the polymer more sensitive to hydrolysis and accelerates the degradation rate of the copolymer. Copolymerization is a convenient method for controlling crystallinity in PLLA and PGA. The melting temperature ( $T_m$ ) of polyglycolide ranges from 225 to 230 °C<sup>48</sup> while crystalline PLLA melts near 180 °C. Copolymerization of L-lactide with glycolide tends to suppress crystallinity because of irregular placement of monomer units in the backbone of the copolymer. Even more effective is the use of DL-lactide as a comonomer. PDLLA is amorphous with a  $T_g$  of about 50-60 °C, therefore the inclusion of DL-lactide can be used to fine tune the crystallinity in poly(lactide-*co*-glycolide)s.

Poly(lactide-*co*-glycolide) copolymers undergo bulk degradation by random hydrolytic scission of their ester bonds. The lactide segments yield lactic acid that enters the tricarboxylic acid cycle, whereas PGA segments produce glycolic acid which is either excreted in urine or enters the tricarboxylic acid cycle. Because of their degradation to nontoxic products and their tunable

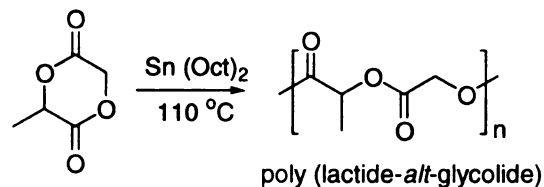
mechanical properties, poly(lactide-*co*-glycolide) has been intensely studied for medical applications. They are widely used as suture materials and have been approved by the FDA for drug delivery.<sup>49</sup> In addition, these copolymers are the starting materials in the production of implantable medical devices, primarily in orthopedic applications, and as scaffolds for tissue growth.<sup>9</sup>

#### 4.1.3. Copolymerization of Substituted Glycolides and Lactide

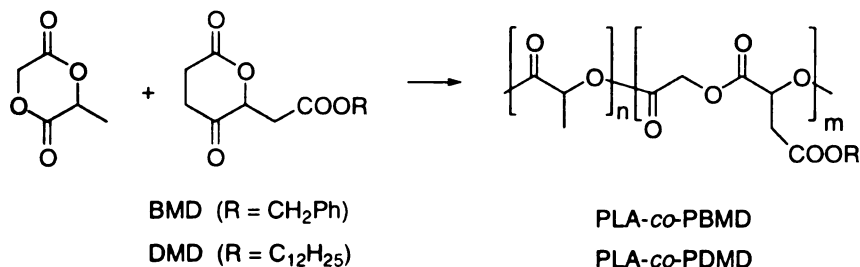
There are only a few examples where lactide has been copolymerized with substituted lactides or glycolides, partially because of the limited availability of substituted lactides. The synthesis of a series of alkylated<sup>50</sup> and benzyl substituted<sup>51</sup> glycolides were recently reported, and the copolymerizations of these substituted lactides are being studied. Several papers were published on the synthesis of poly(lactide-*co*-mandelide) by the



**Scheme 6.** Copolymerization of lactic acid with mandelic acid



**Scheme 8.** Polymerization of D,L-3-methylglycolide.



**Scheme 7.** Copolymerization of lactide with BMD and DMD

direct condensation of lactic acid and mandelic acid (**Scheme 6**). Although the molecular weight of these copolymers were low, inclusion of the mandelic acid units led to a significant increase in  $T_g$  (from 57 °C for polylactide to 77 °C for the copolymer) suggesting that copolymerization of mandelide with lactide may be a successful strategy for obtaining polymers with high  $T_g$ s.

Another copolymerization example is the polymerization of lactide with 3-(S)-[(benzyloxycarbonyl)methyl]-1,4-dioxane-2,5-dione (BMD) and 3-(S)-[(dodecyloxycarbonyl)methyl]-1,4-dioxane-2,5-dione (DMD) (**Scheme 7**). Treatment of the copolymers with alkali forms a carboxyl-functionalized surface designed to enhance cell binding.<sup>52</sup> D,L-3-Methylglycolide was synthesized by Dong *et al.* (**Scheme 8**).<sup>46</sup> Homopolymerization of this monomer resulted in a copolymer with alternating lactyl and glycolyl units in the polymer backbone. An alternating structure for the polymer was claimed from an analysis of <sup>13</sup>C NMR spectra of the polymer, but no physical properties or degradation data were reported.

#### 4.1.4. Copolymerization with Lysine and Other Amino Acids

One limitation of polylactides in tissue engineering is that the adhesion and growth of cells cannot be easily controlled since polylactides do not contain functional groups (other than end groups) that would allow chemical modification of its properties. Copolymerization of functionalized lactide monomers can overcome this problem. Langer *et al.* prepared a monomer that contained a lactic acid and a lysine residue.<sup>53,54</sup> Homopolymerization incorporated lysine into the polylactide backbone (**Figure 3**), enabling a variety of functionalities to be introduced onto the polymer through reaction at the  $\epsilon$ -amine group of the lysine units. These potential functionalities include peptide sequences or growth factors that help to improve polymer-cell interactions.

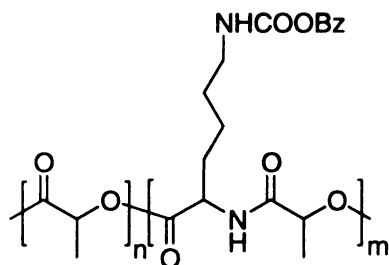


**Figure 3. A poly(lactide-co-L-Lysine) derivative.**

Another approach to improving polylactide-cell interactions is the direct copolymerization of lactide with amino acids. *Trans*-4-hydroxy-L-proline (Hpr)<sup>55</sup> was reported to copolymerize with lactide to give the copolymer structure shown in **Figure 4**.

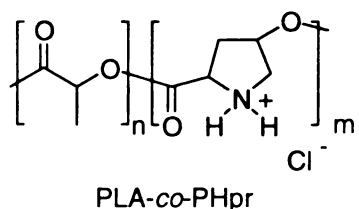


**Figure 4.** Copolymerization of lactide with Hpr.

## 4.2. Block and Graft Copolymers

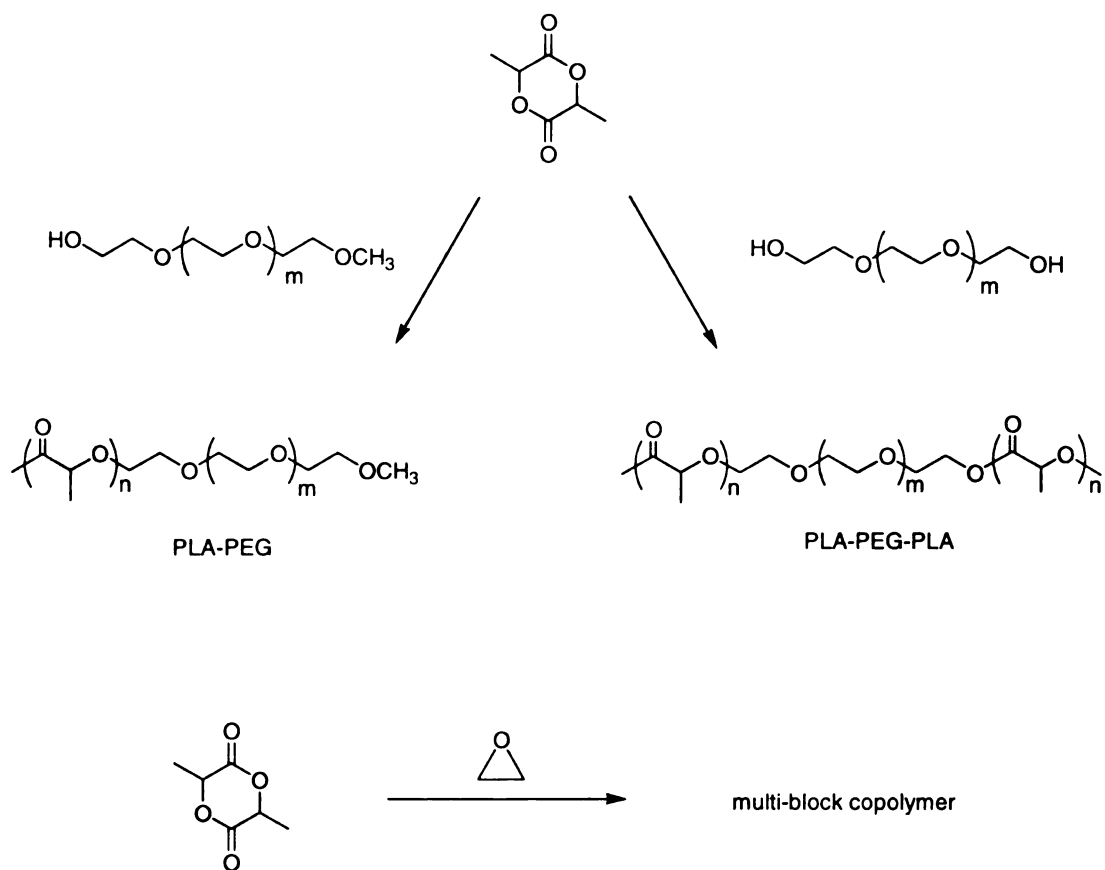
Block and graft copolymers that contain polylactide segments can be prepared by the sequential polymerization of two different lactide monomers, or by isolating a polymer and using it to initiate a second polymerization. The first approach is limited to monomers that polymerize by the same mechanism, while the second allows for the use of two different polymerization mechanisms. There are many examples where hydroxy terminated polymers were used as macroinitiators for the polymerization of lactide to give block and graft architectures. There also are reports of the polymerization of lactide-based macromonomers to comb-like graft copolymers.

### 4.2.1. Copolymerization of Lactide with Poly(ethylene glycol)

Poly(ethylene glycol) (PEG), also referred to as poly(ethylene oxide) (PEO) at high molecular weights, is commonly terminated with chain-end hydroxyl groups which can serve as initiators for the ring-opening polymerization of lactide. Using a PEG with only one end terminated with a hydroxyl group yields a PLA/PEG diblock copolymer,<sup>56-61</sup> while a PEG with both ends terminated with hydroxyl groups yields a PLA/PEG/PLA triblock copolymer (Scheme 9).<sup>62</sup> Jeong *et al.* prepared thermosensitive PLA-PEG

hydrogels that have a temperature-dependent sol-gel transition. These materials can be used in injectable drug delivery systems. Han and Hubbell demonstrated the broad synthetic utility of PLA-PEG systems by attaching acrylate moieties at the end of the chains to form cross-linkable systems.<sup>63</sup>

Biocompatibility is one of the most noted advantages of these materials. PLA-PEG copolymer systems act as surfactants because the PEG block is very hydrophilic while the PLA block is hydrophobic. Therefore, when a PLA-PEG copolymer is subjected to a fabrication process that uses an aqueous external phase, PEG enriches the surface. The inclusion of PEG in copolymer systems can impart extremely beneficial surface properties within the body because of its ability to inhibit the adsorption of proteins to the polymer surface and, as a result, prevents many polymer-cell interactions. Thus, PLA-PEG copolymers are often the material of choice for scaffolds for tissue engineering and drug delivery systems.



**Scheme 9.** Synthesis of PLA-PEG copolymers

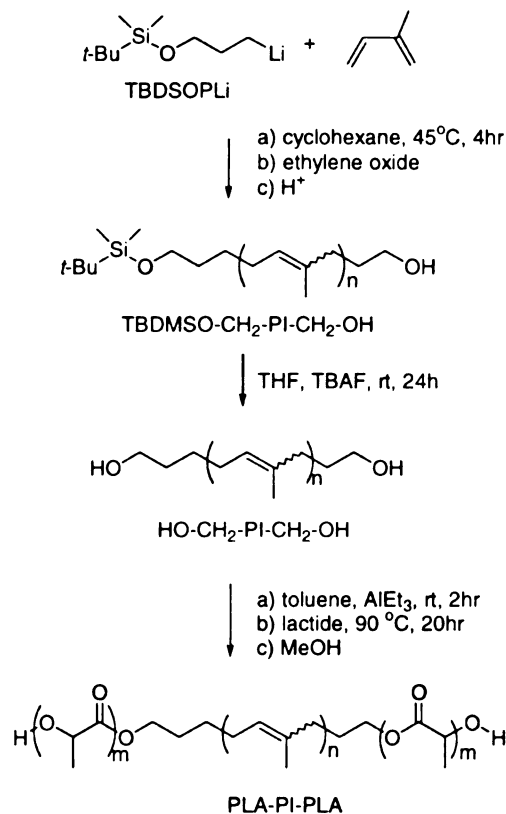
#### 4.2.2. Graft Copolymers from Natural Polymers

Cellulose is the most abundant renewable biomass in the world, however, its biodegradability and bioabsorbability is very poor. By using the multiple hydroxyl groups of cellulose as initiators, this natural polymer can be converted to poly(cellulose-*g*-lactide). Materials obtained from lactide and cellulose combine the advantages of both and can be used in tissue engineering.<sup>64,65</sup> Similarly, poly(saccharide-*g*-lactide) materials were synthesized and characterized.<sup>66</sup> Polysaccharides have the advantage of

targeting carbohydrate-binding proteins located on mammalian cells. Therefore, this type of copolymer has potential as gene delivery vehicles with the capability to target specific cell types. Starch/lactide graft copolymers were synthesized by You by reacting lactide with corn starch. Since both starch and polylactide are degradable, this graft copolymer can be completely degraded by acid, base and enzymes. Lactide also has been copolymerized with comonomers such as xylofuranose,<sup>67</sup> sorbitol,<sup>68</sup> 1,3-propanediol,<sup>22</sup> and mannitol.<sup>69</sup>

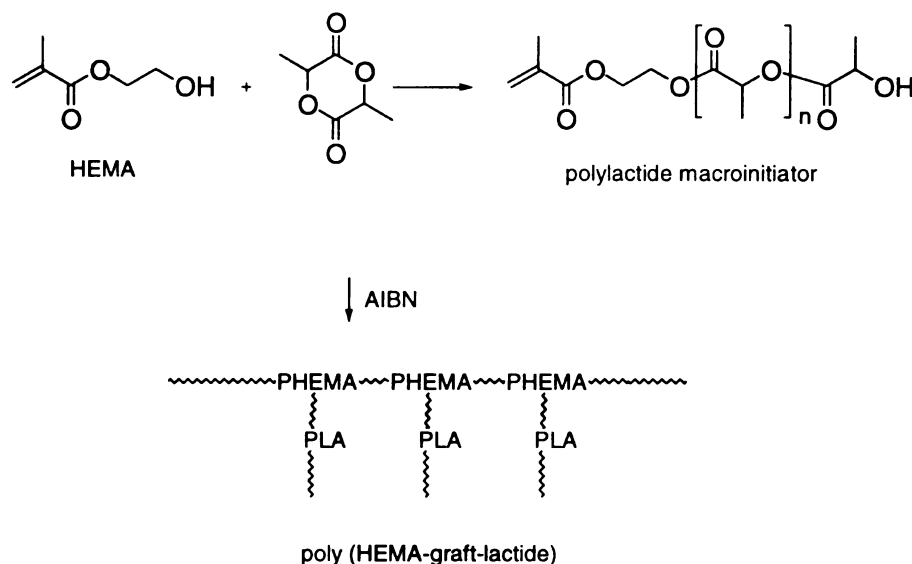
#### 4.2.3. Lactide Copolymers with Blocks from Vinyl and Acrylic Monomers

Using the macroinitiator approach, lactide has been copolymerized with polybutadiene,<sup>70</sup> polyisoprene,<sup>71</sup> polystyrene,<sup>72</sup> and poly(2-hydroxyethyl methacrylate) (HEMA).<sup>73-75</sup> These copolymers usually have either block (with vinyl monomers) or graft architectures (with acrylic monomers). **Scheme 10** illustrates the preparation of a poly(lactide-*b*-isoprene-*b*-lactide) triblock copolymer through a combination of living anionic polymerization (isoprene) and controlled ring opening polymerization (lactide). Since the polyisoprene segment is amorphous and has a low  $T_g$ , PLA is toughened by the polyisoprene. The resulting block copolymer is a degradable thermoplastic elastomer that can be used in packaging applications. Using the same method, poly(butadiene-*b*-lactide)<sup>70</sup> was synthesized for similar applications.



**Scheme 10.** Synthesis of poly(lactide-*b*-isoprene-*b*-lactide)

A common strategy used to prepare comb-like graft polymers is to use an end-functionalized macromonomer to start a second polymerization. As shown in **Scheme 11**, HEMA terminated PLA, a macromonomer, can undergo radical initiated polymerization to yield poly(HEMA-*graft*-lactide). Since the HEMA segments increase the hydrophilicity of the copolymer, this degradable graft copolymer can be used as a hydrogel for the controlled delivery of macromolecular protein drugs.<sup>73</sup>



**Scheme 11.** Synthesis of poly(HEMA-*graft*-lactide)

#### 4.2.4. Copolymerization with Other Comonomers

Poly(lactide-*co*-amide)s are an emerging class of degradable graft copolymers, which combine the mechanical properties of polyamides and the biodegradability of the polylactides.<sup>76</sup> Lactide polymerization was initiated with N-isopropylacrylamide<sup>77</sup> and N,N-dimethylacrylamide.<sup>77</sup> These copolymers have been reported to be effective in drug delivery systems that target solid tumors.

#### 4.3. Copolymerization Characterization

The most important structural information needed to characterize copolymers include the determination of the molar composition of the copolymers and the distribution of the comonomers in the polymer backbone. <sup>1</sup>H NMR is the most popularly used method to analyze the composition of

lactide copolymers,<sup>31,45,78</sup> because the methyl and methine signals of the lactide unit in <sup>1</sup>H NMR spectra are generally well-separated from resonances from most of the monomers that copolymerize with lactide. Near IR spectroscopy has been used to determine the composition of poly(lactide-*co*-glycolide),<sup>79</sup> Raman spectroscopy for poly(lactide-*co*- $\epsilon$ -caprolactone),<sup>80</sup> and HPLC and MALDI-TOF for poly(ethylene oxide-*b*-L-lactide).<sup>81</sup> However, these methods cannot be considered to be general analytical approaches since they have only been applied to copolymers on a case by case basis.

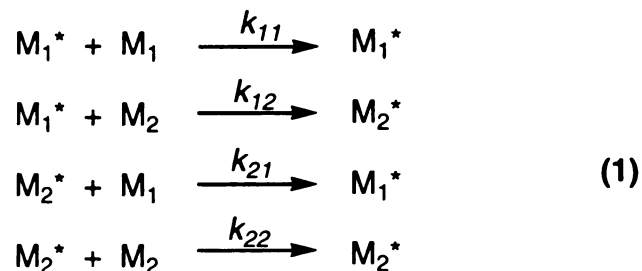
Among all lactide copolymerizations, the most thoroughly analyzed cases are copolymers of lactide with  $\epsilon$ -caprolactone and lactide with glycolide. Quantitative <sup>13</sup>C NMR is best suited for analyzing the sequence distribution of these copolymers since the carbonyl signal is very sensitive to the sequence effects. From high resolution <sup>13</sup>C spectra, tetrad and even pentad peaks can be clearly detected, and after assignment, the intensities of these peaks can be used to calculate the average block length of each component. Poly(lactide-*co*- $\epsilon$ -caprolactone)<sup>82</sup> and poly(lactide-*co*-glycolide)<sup>82,83</sup> are block or tapered copolymers due to the large difference in the monomer reactivity for the lactide/caprolactone and lactide/glycolide pairs.

## 4.4. Kinetic Studies of Copolymerization

### 4.4.1. Monomer Reactivity Ratios

The composition of a copolymer is usually different from the composition of the comonomer feed from which it is produced, since some monomers are more reactive to copolymerization and some are less.<sup>26</sup> Staudinger and Schneiders observed that the relative tendencies for monomers to copolymerize often bore little resemblance to their relative rates for homopolymerization. Thus the composition of a copolymer cannot be determined directly from the homopolymerization rates of the two monomers. There are several models that can be used to analyze and predict copolymer composition, with the best known being the *first-order Markov* or *terminal model* of copolymerization. The principal assumption of this model is that the chemical reactivity of the propagating chain in a copolymerization depends only on the identity of the monomer unit at the end of the growing chain; the chain composition preceding the last monomer unit does not influence the reactivity. For the copolymerization of two monomers,  $M_1$  and  $M_2$ , the *first-order Markov Model* describes four possible steps for chain growth, since both  $M_1$  and  $M_2$  can each add to a propagating chain ending in  $M_1$  or to one ending in  $M_2$ , as elucidated in **Scheme 12**. There are four rate constants for the processes,  $k_{11}$  for adding monomer  $M_1$  to a propagating chain ending in  $M(M_1^*)$ ,  $k_{12}$  for adding monomer  $M_1$  to a propagating chain ending in  $M(M_2^*)$ ,  $k_{22}$  for adding monomer  $M_2$  to a propagating chain ending in  $M(M_2^*)$ , and  $k_{21}$  for

adding monomer  $M_2$  to a propagating chain ending in  $M(M_1)$ . The processes with rate constants  $k_{11}$  and  $k_{22}$  describe *homopolymerization* or *self-propagation*; while  $k_{12}$  and  $k_{21}$  describe *cross-propagation*.



**Scheme 12.** Chain propagation steps in the copolymerization of two monomers.

From these four kinetic steps, the copolymerization equation can be derived:

$$\frac{d[M_1]}{d[M_2]} = \frac{[M_1](r_1[M_1] + [M_2])}{[M_2]([M_1] + r_2[M_2])} \quad (2)$$

where the parameters  $r_1$  and  $r_2$  are termed the monomer reactivity ratios of  $M_1$

$$r_1 = k_{11}/k_{12} \text{ and } r_2 = k_{22}/k_{21} \quad (3)$$

and  $M_2$ , and are defined as

The significance of the copolymerization equation is that it relates the copolymer composition  $d[M_1]/d[M_2]$  to the concentration of the two monomers in the feed,  $[M_1]$  and  $[M_2]$ .

#### 4.4.2. Types of Copolymerization Behavior

The monomer reactivity ratio ( $r$ ) is very useful since it can be used to define different types of copolymerization behavior.

##### 4.4.2.1. Ideal copolymerization: $r_1 r_2 = 1$

A copolymerization is termed as *ideal* when the  $r_1 r_2$  product is unity. An ideal copolymerization occurs when the two types of propagating species  $M_1^*$  and  $M_2^*$  show the same preference for adding one or the other of the two monomers. Under these conditions, the relative rates of incorporation of the two monomers into the copolymer are independent of the identity of the unit at the end of the propagating species. Most ionic copolymerizations are characterized by the ideal type of behavior.

When  $r_1 = r_2 = 1$  the two monomers show equal reactivities toward both propagating species. The copolymer composition is the same as the comonomer feed with random placement of the two monomers along the copolymer chain. This behavior is referred to as *random* or *Bernoullian*. For the case where the two monomer reactivity ratios are different, that is  $r_1 > 1$  and  $r_2 < 1$  or  $r_1 < 1$  and  $r_2 > 1$ , one monomer is more reactive than the other toward both propagating species. The copolymer will contain a larger proportion of the more reactive monomer placed randomly along the chain. Therefore, a very important practical consequence of ideal copolymerization is that it becomes progressively more difficult to produce copolymers containing appreciable amounts of both monomers as the difference in reactivities of the two monomers increases. Only when  $r_1$  and  $r_2$  do not differ substantially will there

exist a large range of comonomer feed compositions, which yield copolymers containing appreciable amounts of both monomers.

#### **4.4.2.2. Alternating Copolymerization: $r_1 = r_2 = 0$**

When  $r_1 = r_2 = 0$ , the two monomers enter into the copolymer in equimolar amounts in a nonrandom, alternating arrangement along the copolymer chain. This type of copolymerization is referred to as *alternating* copolymerization. Many radical copolymerizations show a tendency toward alternation. The behavior of most comonomer systems lies somewhere between the two extremes of ideal and alternating copolymerization.

#### **4.4.2.3. Block Copolymerization: $r_1 > 1, r_2 > 1$**

If both  $r_1$  and  $r_2$  are greater than unity there is a tendency to form a block copolymer in which there are blocks of both monomers in the chain. This type of behavior has been encountered in only a few copolymerizations of olefins initiated by Ziegler-Natta catalysts.

#### **4.4.3. Experimental Evaluation of Monomer Reactivity Ratios**

The experimental procedures for evaluating  $r_1$  and  $r_2$  involve determining the copolymer composition for several different comonomer feed compositions. Copolymerizations must be carried out to low degrees of conversion (ca. 5%) to minimize deviation of the monomer ratio from its initial value. The copolymer composition is determined either directly by analysis of the copolymer, or indirectly by analysis of comonomer feed.

Several methods have been used to extract monomer reactivity ratios from the copolymer composition data. Among them, the most widely used are

the Fineman-Ross<sup>84</sup> and Kelen-Tudos methods,<sup>85,86</sup> both are schemes to linearize the experimental data. However, the more statistically sound methods for analyzing composition data are nonlinear methods, which involve plotting the instantaneous copolymer composition as a function of the comonomer feed ratio for various feeds, and then using an iterative process to determine the  $r_1$  and  $r_2$  values that best fit the data.<sup>87,88</sup>

In general, both the linearization and nonlinearization methods are based on the differential form of the copolymerization equation (**equation 2**) which requires that the conversion be held as low as possible to assure that the monomer ratios does not differ much from the feed ratio. In practice, there are limitations since one must be able to isolate a sample of the copolymer for analysis. This requirement can be hard to meet, especially when the reactivities of the two monomers are quite different. This issue will be discussed further in the “Results and Discussion” section.

#### **4.4.4. Monomer Reactivity Ratio Analysis of Lactide Copolymerizations**

To date, three lactide copolymerization systems have been evaluated kinetically, the copolymerization of lactide with glycolide,<sup>89</sup> the copolymerization of  $\epsilon$ -caprolactone with lactide,<sup>31</sup> and the copolymerization of 3-methylglycolide with lactide.<sup>90</sup> The Fineman-Ross and Kelen-Tudos methods were used for data analysis in these kinetic studies. For the copolymerization of lactide with glycolide, the experimentally determined reactivity ratios were  $r_1$  (lactide) = 0.22, and  $r_2$  (glycolide) = 3.4. Therefore, lactide is less active toward chain propagation as can be predicted by considering the steric hindrance caused by

the methyl group. In the copolymerization of lactide with 3-methylglycolide,  $r_1$  (lactide) = 0.92, and  $r_2$  (3-methylglycolide) = 1.71. Again a simple steric argument provides a reasonable explanation of the data. Note that difference between the  $r$ -values for these two comonomers is not as large as was seen for the lactide/glycolide pair.

At first glance, the copolymerization of  $\epsilon$ -caprolactone and lactide might seem confusing. Although the homopolymerization of  $\epsilon$ -caprolactone is much faster than lactide ( $k_{22} > k_{11}$ ),  $r_1$  (lactide) = 17.9 while  $r_2$  (caprolactone) = 0.6. This result can be explained by consideration of the growing polymer chain. Compared to  $\epsilon$ -caprolactone, the alkoxide chain end derived from lactide is less basic due to the proximity of the carbonyl group. Thus, the lactide chain end should be less reactive. The slowest rate constant in the copolymerization is  $k_{12}$ , the addition of caprolactone to the lactide chain end. This leads to the overall value of  $r_1$  ( $k_{11}/k_{12}$ ) being greater than  $r_2$  ( $k_{22}/k_{21}$ ).

## EXPERIMENTAL

### 5.1. General

Unless otherwise specified, ACS reagent grade starting materials and solvents were used as received from commercial suppliers without further purification. Proton nuclear magnetic resonance ( $^1\text{H}$  NMR) and carbon nuclear magnetic resonance ( $^{13}\text{C}$  NMR) analyses were carried out at room temperature in deuterated chloroform ( $\text{CDCl}_3$ ) on Varian Gemini-300 and Varian Vax-500 spectrometers with the signals from residual protons in the solvent being used as chemical shift standards. Mass spectral analyses were carried out on a VG Trio-1 Bench top GC-MS.

The molecular weights of polymers were determined by gel permeation chromatography (GPC) using a PLgel 20m Mixed A column at room temperature with THF as the eluting solvent at a flow rate of 1 mL/min. The peaks were detected using a Waters R401 Differential Refractometer and a Varian 2050 Variable Wavelength detector set at 254 nm. The concentration of the polymer solutions used for GPC measurements was 1 mg/mL, and the GPC molecular weights are reported relative to monodisperse polystyrene standards. Differential scanning calorimetry (DSC) analyses of the polymers were obtained using a Perkin-Elmer DSC 7. Samples were run under a helium atmosphere at a heating rate of 10  $^\circ\text{C}/\text{min}$ , with the temperature calibrated with an indium standard. Gas Chromatography (GC) was carried out on Perkin-Elmer 8500 with a fused silica capillary column (SE-54-60W, J & W Sci. Inc.).

High Pressure Liquid Chromatography (HPLC) data was collected from Waters 600 system equipped with a Waters 996 Photodiode Array Detector

## 5. 2. Monomer Preparation and Synthesis

**3,6-Diethyl-1,4-dioxane-2,5-dione (ethylglycolide).** A mixture of 10 g of 2-hydroxybutyric acid and 0.2 g of *p*-toluenesulfonic acid in 700 mL of toluene was heated at reflux for four days, with the water removed azeotropically using a Barrett trap. The toluene solution was then cooled, washed with sat. NaHCO<sub>3</sub>, and dried over MgSO<sub>4</sub>. After removing the toluene, 0.1 g of ZnO was added and the residue was distilled under reduced pressure using a Kugelrohr distillation apparatus. Ethylglycolide was collected at 180 °C (100 mtorr), and was dissolved in the minimum amount of ether needed to dissolve the product. The solution was cooled to -30 °C, and petroleum ether was added drop-wise until the solution turned cloudy. The colorless crystals were collected by cold filtration and dried under vacuum to give 5.2 g (63%) of ethylglycolide as colorless oil. <sup>1</sup>H NMR indicates that the product is a statistical mixture of diastereomers. <sup>1</sup>H NMR (300 MHz, CDCl<sub>3</sub>): δ 4.88 (dd), 4.83 (dd, 1H total for the signals at 4.88 and 4.83), 2.08 (m, 2H), 1.15 (tt, 3H). <sup>13</sup>C NMR (75 MHz, CDCl<sub>3</sub>) δ: 167.62, 166.58, 76.4, 75.6. mp 19.5 - 20.5°C.

### **3,6-Diisopropyl-1,4-dioxane-2,5-dione (isopropylglycolide).**

Isopropylglycolide was synthesized by the procedure described by Yin.<sup>1</sup> <sup>1</sup>H NMR (300 MHz, CDCl<sub>3</sub>): δ 4.95 (d, 1H), 2.30 (m, 1H), 1.03 (d, 3H), 1.01 (d, 3H). <sup>13</sup>C NMR (75 MHz, CDCl<sub>3</sub>) δ 166.38, 79.55, 29.36, 19.55, 15.81. MS (m/z) 201.4 (M+1), mp 137-138 °C (lit.<sup>91</sup> (136 °C)).

### **3R,6R-Diethyl-1,4-dioxane-2,5-dione (R-ethylglycolide) R-**

ethylglycolide was prepared by the procedure described by Yin.<sup>1</sup> <sup>1</sup>H NMR (300 MHz, CDCl<sub>3</sub>): δ 4.85 (dd), 2.03 (m, 2H), 1.08 (tt, 3H). m.p. 120.5-122 °C.

### **5. 3. Copolymerization**

**General conditions for the bulk copolymerization of racemic lactide with substituted glycolides.** Solvent-free polymerizations were carried out in sealed tubes prepared from 3/8 inch diameter glass tubing. Lactide and substituted glycolides were added to the tubes to give the desired feed ratios, and then were transferred into a dry box. Catalyst (Sn(Oct)<sub>2</sub>) and co-initiator (*tert*-butyl benzyl alcohol (*t*-BBA)) were added to the tubes to at a mole ratio of 1 (catalyst) to 400 (monomer). The solvent was removed under vacuum, and the tubes was sealed and immersed in an oil bath at 130 °C (at 165 °C for copolymerization of lactide with isopropylglycolide). At the end of the polymerization, each tube was cooled in ice, opened, and the polymer was dissolved in CHCl<sub>3</sub>. A portion of the sample was evacuated to dryness and analyzed by GPC, NMR and DSC.

### **5. 4. Copolymer Composition: Direct Determination**

Copolymerizations were quenched at low conversion (<10%), and then the mixture of monomer and copolymer was dissolved in CHCl<sub>3</sub> and passed through a short column prepared from a 9-inch long Pasteur pipette filled two-thirds with silica gel. Pre-weighed 20-mL vials were used as receivers. The eluent that collected in the vials was evaporated to dryness until the weight of

vials remained constant.  $^1\text{H}$  NMR showed that the recovered material was free of polymer.

After the separation was complete, the copolymer adsorbed onto the silica was transferred to a 25 mL round bottom flask. To this flask were added  $\text{Sn}(\text{Oct})_2$  (200 mg) and methanol (15 mL). A condenser was added and the slurry was heated at reflux for 48 hrs. The reaction mixture was then centrifuged for 40 minutes, and the clear solution was decanted into a 25 mL round bottom flask. The flask was cooled in an acetonitrile-dry ice bath at  $-20^\circ\text{C}$ , and the methanol was evaporated under vacuum over a period of 2 hours. The composition of the resulting methyl esters was then analyzed by GC or  $^1\text{H}$  NMR.

## **5. 5. Biodegradation**

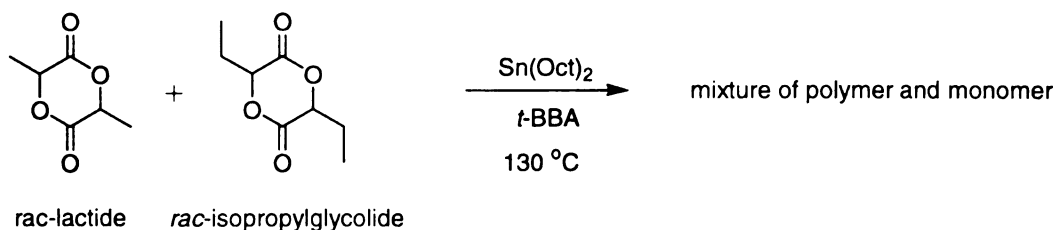
About 50 mg of polymer sample was accurately weighed and chopped into 1mm by 1mm pieces. The chopped sample was immersed in 15 mL of 0.1M phosphate buffer solution ( $\text{pH}=7.4$ ). The degradation was carried out at  $55 \pm 0.1^\circ\text{C}$ . After a predetermined period of time, samples were removed from the buffer solution, washed thoroughly with distilled water and dried under vacuum. The samples were weighed to determine the weight loss and the molecular weight was determined by GPC.

## RESULTS AND DISCUSSION

### 6.1. Copolymerization of Lactide with Ethylglycolide

Poly(lactide), PLA, and its copolymers<sup>30,92</sup> are an important class of biodegradable and biocompatible polymers with numerous applications in medicine and as packaging materials, but a major deficiency of polylactide is its limited range of physical properties. Therefore, an important area of polylactide research is the preparation of copolymers and derivatives of polylactide that extend the range of properties that can be obtained from polylactide. A number of “random” and block copolymers have been prepared to date, primarily with glycolide and  $\epsilon$ -caprolactone. Yin explored another strategy for obtaining new properties from polylactide, the synthesis and polymerization of lactides derived from substituted lactic acids.<sup>50</sup> Copolymers prepared from these new monomers should provide new families of copolymers and provide properties not currently available from PLA.

The copolymerization of lactide with ethylglycolide was briefly examined by Yin.<sup>1</sup> Since ethylglycolide (EG) and lactide (LA) have very similar structures, their copolymers should retain the biodegradability of the homopolymers, but have different physical properties. Yin used bulk polymerization at 130 °C to synthesize a series of copolymers (EG/LA=1/5, EG/LA=1/3, EG/LA=1, EG/LA=3, EG/LA=5) as illustrated in **Scheme 13**. The polymerizations were catalyzed by Sn(Oct)<sub>2</sub> with *t*-butylbenzyl alcohol (BBA) as the initiator. All of the copolymers had  $M_n > 40,000$  g/mol. The thermal and molecular properties of



**Scheme 13.** Copolymerization of racemic lactide with ethylglycolide

these polymers are summarized in **Figures 5** and **6** and in **Table 1**. The DSC plots (**Figure 5**) show one glass transition temperature ( $T_g$ ) for each copolymer, an indication that the copolymers are not phase separated. Considering the structural similarity of the monomers, it is not surprising that copolymers are single phase. The glass transition temperatures listed in **Table 1** fall between those of polylactide and poly(ethylglycolide) and increase with the increase of the mole fraction of the lactide comonomer. The glass transition temperatures of copolymers can be predicted using the Fox equation:

$$\frac{1}{T_g} = \frac{w_A}{T_{gA}} + \frac{w_B}{T_{gB}} \quad (4)$$

where  $T_g$ ,  $T_{gA}$  and  $T_{gB}$  are the glass transition temperature of the copolymer and the pure homopolymers derived from monomers A and B respectively, and  $w$  represents the mass fraction of the polymer. The Fox equation successfully predicts the glass transition temperatures of random copolymers and plasticized systems. An underlying assumption is that the polymer is homogeneous in composition, and that the comonomers are distributed randomly along the chain. As shown in **Figure 6**, the glass transition

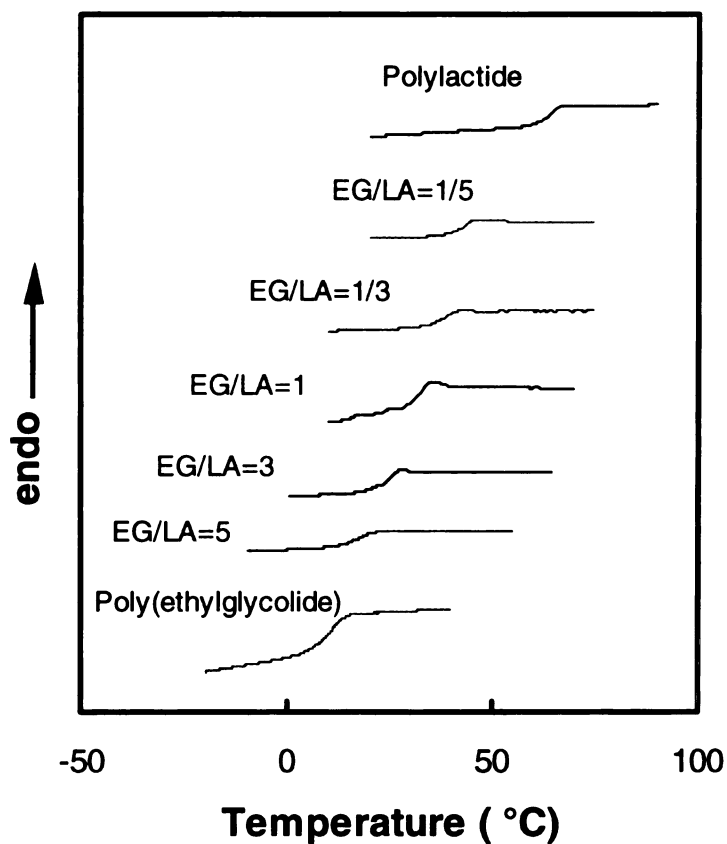


**Figure 5.** DSC runs (second heating after flash quenching from 100 °C) for lactide and ethylglycolide copolymers. Heating rate: 10 °C/min under helium.

temperature of the copolymers fit the Fox equation fairly well. However, whether the copolymer is truly a random copolymer or not must be defined by a characterization technique such as NMR,<sup>45</sup> which is sensitive to structure at the molecular level.

Based on copolymerizations of lactide and glycolide,<sup>93,94</sup> the distribution of monomer units in the polymers is probably far from random because of differences in reactivity for the monomers. As illustrated in **Scheme 14**, these

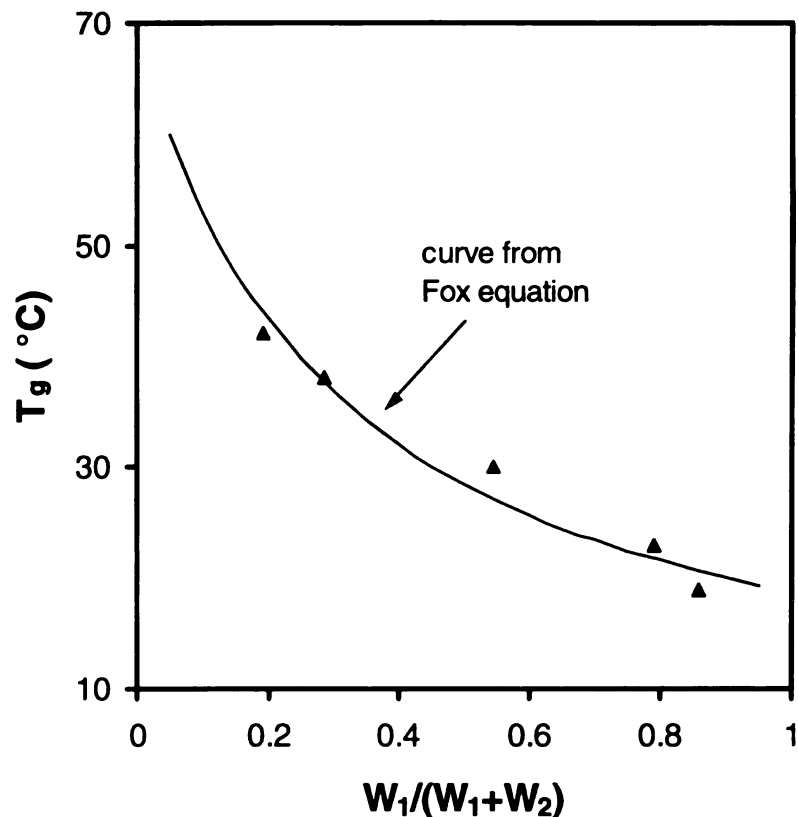


**Figure 6.** Glass transition temperatures of lactide and ethylglycolide copolymers.

effects are likely due to differences in the steric bulk at the carbon  $\alpha$  to the carbonyl. Lactide and glycolide share the same ring structure, but the absence of lactide's methyl groups makes glycolide far more reactive and thus “blocky” polymers are obtained from copolymerizations. However, transesterification reactions can increase the randomness of copolymers.

The results from the copolymerization of lactide with ethylglycolide show that the physical properties of the copolymer can be readily tuned by adjusting the monomer feed ratio. Nevertheless, these sterically hindered lactides should

be less reactive than lactide. Thus a batch copolymerization where all of the monomer is charged into the polymerization at one time will give a polymer whose composition varies with conversion. Special steps must be taken to compensate for changes in the monomer feed ratio and maintain a constant rate of addition of the comonomer into the polymer structure. To gain the control over the copolymer structure and achieve certain physical properties in the copolymers, we need to evaluate the kinetic parameters of these copolymerizations.

**Table 1.** Properties of copolymers

<b>Polymers</b>	<b><math>M_n \times 10^{-3}</math> <sup>a</sup></b>	<b><math>M_w/M_n</math></b>	<b><math>T_g</math> °C <sup>b</sup></b>
Poly(lactide)	35.2	1.89	66
EG/LA=1/5	41.5	1.85	42
EG/LA=1/3	47.8	1.76	38
EG/LA=1	41.7	1.88	30
EG/LA=3	50.8	1.92	23
EG/LA=5	43.6	1.85	19
Poly(ethylglycolide)	45.6	1.78	15

a. measured by GPC in THF using polystyrene as standard

b. measured by DSC under He at a rate of 10 °C/min

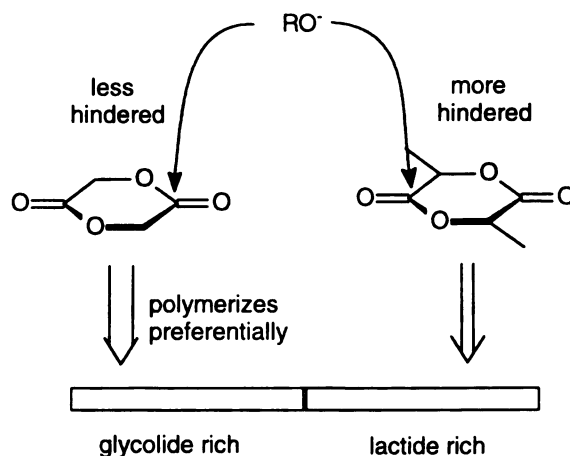
## 6.2. Kinetic Evaluation of the Copolymerization of Lactide with Ethyglycolide

### 6.2.1. Copolymer Composition Determination.

As illustrated in the Introduction, a copolymerization system with two comonomers can be defined by the reactivity ratios of the two monomers,  $r_1$  and  $r_2$ . Experimental determination of these values requires precise measurement of the copolymer compositions ( $F_1$  and  $F_2$ ) that result from several different comonomer feed compositions. The copolymerizations must be terminated at low conversions to avoid significant changes in the monomer feed ratios, and thus the main experimental challenge is to accurately characterize the composition of small polymer samples.

#### 6.2.1.1. $^{13}\text{C}$ NMR

$^{13}\text{C}$  NMR can be used to analyze the conversion for each monomer and



**Scheme 14.** Reactivity differences leads to "blocky" copolymers.

the copolymer composition since the chemical shifts of the monomers and the lactide and ethylglycolide residues in the copolymer are well-separated. The principal drawback of this method is that the spin-lattice relaxation times ( $T_1$ ) of carbon atoms in polymers are usually long and the longest  $T_1$ , that from the carbonyl group, was measured as 30 sec. Since each NMR scan requires 5×30 sec of acquisition time, and the polymer solutions were relatively dilute, 8-hour runs were required to obtain a signal to noise ratio that would provide reliable quantitative integration data. Given the large number of samples, this proved to be impractical.

#### **6.2.1.2. Normal Phase High Pressure Liquid Chromatography (HPLC)**

HPLC is an alternative method for analyzing copolymer composition. However, HPLC analysis is an indirect method in that comonomer composition is obtained by analyzing the change in the monomer composition after polymerization. The conversion must be maintained below 10 % to avoid significant changes in the initial feed ratio during the reaction, and thus the HPLC method is based on measuring the difference of two large numbers. The best conditions for separating the monomers was to use  $\text{CHCl}_3$  as the mobile phase at a flow rate of 1 mL/min. Biphenyl was used an internal standard. The response factors for the monomers and the standard were calculated from the results from a solution of lactide 7.6 mg (0.053 mmol) and ethylglycolide 9.0 mg (0.052 mmol) dissolved in 1mL of a solution of biphenyl in chloroform ( $6.75 \times 10^{-3}$  M). Using the optimized conditions, four peaks were observed, the two ethylglycolide diastereomers (4.6 min, 5.9 min) followed by

lactide (9.2 min). The results in **Table 2** show that the HPLC method gives unreasonably high conversions for both lactide and ethylglycolide, considering the copolymerization time was limited to 30 seconds. One potential problem is poor recovery; i.e, a fraction of one or both monomers was retained on the column or hydrolyzed and retained on the silica packing. To test this hypothesis, we prepared a chloroform solution containing known amounts lactide, ethylglycolide, and biphenyl. This sample was injected into the HPLC, collected, and re-injected. After the 1st injection, the integrated areas of the ethylglycolide and lactide peaks relative to the biphenyl standard were 0.79 and 0.98, respectively. After the second injection, the ratios were 0.07 and 0.20. Assuming no loss of biphenyl, the recovery of lactide and ethylglycolide were 9% and 20%, respectively. Thus, normal phase HPLC is unsuitable for analysis of the monomer composition. Since this problem is most likely caused by the acidic hydroxyl group of the silica packing, we turned to reverse phase HPLC.

**Table 2.** Determination of Conversion in the Copolymerization of Lactide (LA) and Ethylglycolide (EG) by Normal Phase HPLC

	<b>LA feed (mg)</b>	<b>LA (LC) (mg)</b>	<b>LA conv%</b>	<b>EG feed (mg)</b>	<b>EG (LC) (mg)</b>	<b>EG conv%</b>
1	7.6	4.9	35	1.0	0.14	86
2	2.7	1.1	19	0.7	0.03	95
3	10.4	7.5	28	1.4	0.16	85
4	23.8	12.7	47	6.3	0.23	96
5	26.5	10.8	59	14.0	0.20	98
6	9.4	7.3	23	9.1	0.40	97
7	6.7	2.6	60	11.9	0.31	98
8	5.6	.3	95	6.8	0.28	93
9	4.4	1.2	98	9.7	0.43	96
10	3.0	1.5	95	14.9	0.76	95

### 6.2.1.3. Reverse Phase HPLC

Reverse phase HPLC was run in 1:1 acetonitrile/H<sub>2</sub>O at a flow rate of 0.5 mL/min. The stationary phase was Nova-pak C18, and anisole was used as the standard. Response factors were calculated from the results from an injection of a standard solution of 10.0 mg lactide (0.069 mmol) and 19.2 mg ethylglycolide (0.112 mmol) dissolved in 1 mL of a 0.012M solution of anisole in 1:1 acetonitrile/H<sub>2</sub>O. As expected, the compounds eluted in reverse order compared to the normal phase HPLC results. The first compound eluted was lactide (4.2 min), followed by the two ethylglycolide diastereomers (5.6 min, 6.1 min), and finally anisole (9.1 min). The results are summarized in **Table 3**.

**Table 3.** Monomer Determination by Reverse Phase HPLC

	LA feed (mg)	EG feed (mg)	LA Conv%	EG Conv%	f <sub>1</sub> (LA)	F <sub>1</sub> (LA)
3-4	0.6	4.6	7.8	9.8	0.14	0.12
5-4	1.2	2.1	14	14	0.41	0.43
5'-4	1.8	1.9	17	6.3	0.53	0.66
7-4	4.1	3.7	13	7.5	0.57	0.70
8-4	2.8	1.9	13	5.7	0.64	0.77
9-4	4.5	1.2	11	8.5	0.82	0.88

#### 6.2.1.4. Kinetic Evaluation Based on Reverse Phase HPLC Results

The premise of the first order Markov model for copolymerization is that only the repeat unit at the end of the growing polymer chain plays a role in determining the next monomer to be added to the chain. In a copolymerization of lactide (monomer 1) and ethylglycolide (monomer 2),  $k_{11}$  and  $k_{22}$  are the rate constants for homopolymerization, while  $k_{12}$  and  $k_{21}$  describe cross-propagation rates, the addition of ethylglycolide to a lactide chain end, and the addition of lactide to an ethylglycolide chain end. As shown earlier, this model leads to the copolymerization equation:

$$f_1 (1-2F_1)/F_1(1-f_1) = r_2 + [f_1^2(F_1-1)/F_1(1-f_1)^2]r_1 \quad (5)$$

where  $f_1$  is the fraction of monomer 1 in the feed, and  $F_1$  is the fraction of monomer 1 incorporated into the copolymer. A plot of  $[f_1^2(F_1-1)/F_1(1-f_1)^2]$  (x axis) vs.  $f_1 (1-2F_1)/F_1(1-f_1)$  (y axis) should yield a straight line with a slope of  $r_1$  (the monomer reactivity ratio of lactide, defined as  $k_{11}/k_{12}$ ) and a y intercept axis of  $r_2$  (the monomer reactivity ratio of ethylglycolide, defined as  $k_{22}/k_{21}$ ). This is known as the Fineman-Ross<sup>84</sup> method for analyzing copolymerization data. Since rate constants  $k_{11}$  and  $k_{22}$  can be obtained from the homopolymerization of lactide and ethylglycolide, respectively, we can calculate the cross-propagation rate constants  $k_{12}$  and  $k_{21}$  from the experimentally determined values of  $r_1$  and  $r_2$ . The kinetic results are summarized in **Figures 7 and 8** and **Table 4**.

**Table 4.** Copolymerization behavior of lactide with ethylglycolide

	$K_p[I] \text{ (sec}^{-1}) \times 10^3$	
monomer	lactide	ethylglycolide
lactide	6.2 ( $k_{11}$ )	3.5 ( $k_{12}$ )
ethylglycolide	5.4 ( $k_{21}$ )	4.8 ( $k_{22}$ )

The shape of the  $f_1$  vs  $F_1$  curve in **Figure 7** resembles an ideal copolymerization where the reactivities of the two monomers are similar. Given the structural similarity of lactide and ethylglycolide, it is not surprising that these two monomers incorporate randomly into the chain (ideal copolymerization). These results are consistent with previous DSC data, which showed one  $T_g$  for each copolymer, an indication that the copolymer is homogeneous. **Figure 8** shows that the Fineman-Ross determined reactivity ratios are similar, with  $r_1 = 1.78$  and  $r_2 = 0.92$ . From the experimentally determined rate constants (**Table 4**), we find that lactide enters the polymer chain at a faster rate, whether the chain end is a lactide or ethylglycolide unit. This is reasonable, since the longer alkyl chain of ethylglycolide makes it a more sterically hindered monomer.

However, the uncertainty of the data in **Table 4** is large. The monomer reactivity ratios obtained from the Fineman-Ross method were used to generate the theoretical  $f_1$  vs.  $F_1$  curve for the copolymerization. We can see that the experimental data shows some deviation from the theoretical  $f_1$  vs  $F_1$  curve (**Figure 7**). From repeat analyses, we estimate the error in determining

the monomer concentrations from HPLC could be as high as 20%. Since the copolymer composition is indirectly determined by measuring the small change in the concentration of monomer during copolymerization, the error in determining the copolymer composition could be much higher. This problem might be overcome by increasing the concentration of the sample, but the solubility of lactide and ethylglycolide in the eluent (1:1 acetonitrile/water) is limited. An improved protocol for determining the copolymer composition is needed.

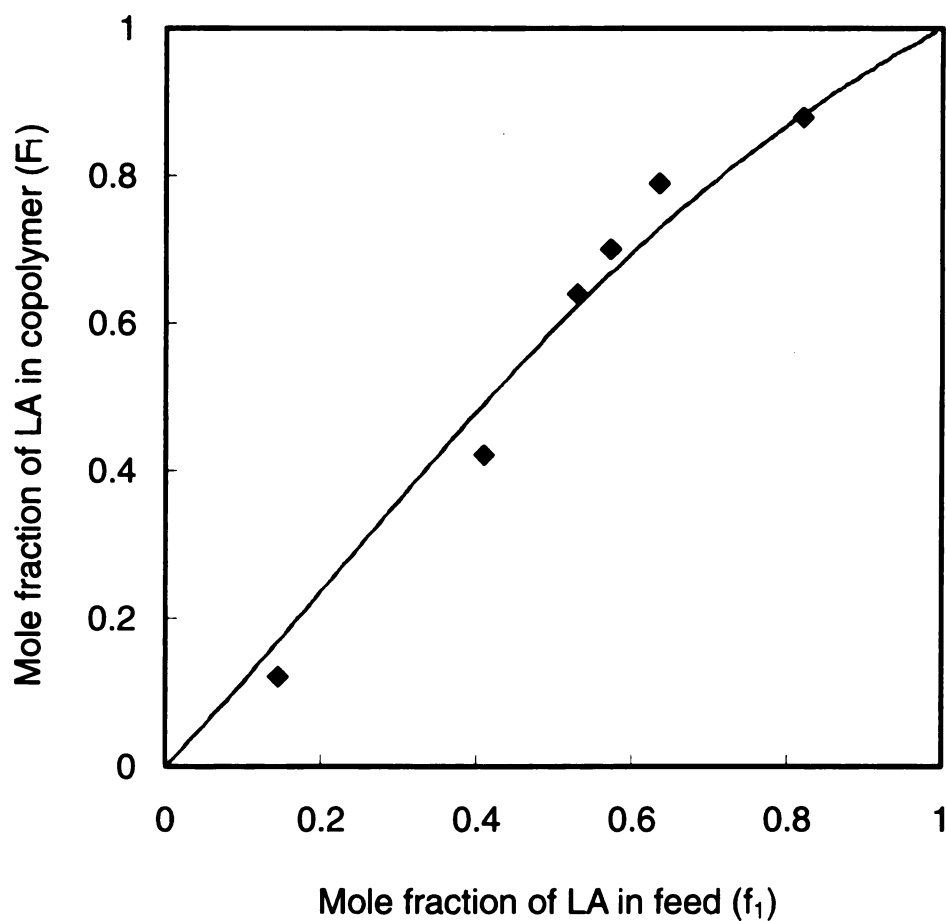


**Figure 7.** Mole fraction of lactide in the copolymer ( $F_1$ ) as a function of the feed ratio ( $f_1$ ) during the copolymerization of lactide with ethylglycolide as determined from reverse phase HPLC

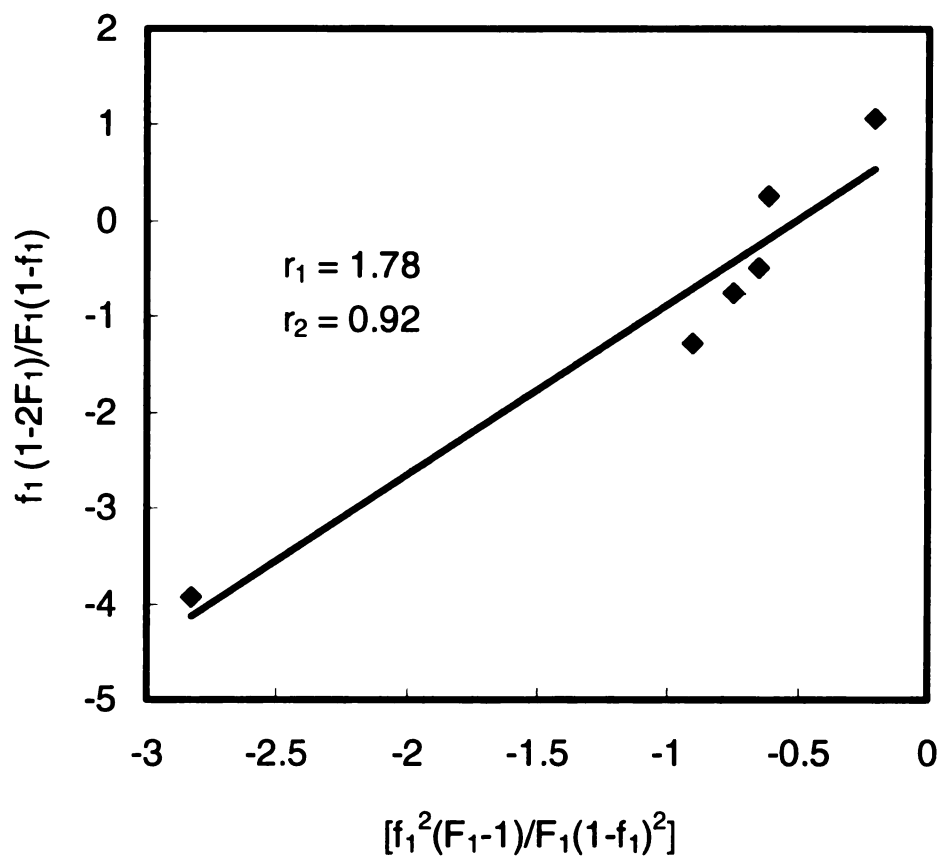


**Figure 8.**  $r_1$  and  $r_2$  determination by the Fineman-Ross method

#### 6.2.1.5. Direct Determination of Copolymer Composition.

Considering the limitations of the NMR and HPLC approaches to copolymer composition analysis, we devised a strategy that allows direct determination of the copolymer composition (**Scheme 15**). After stopping the copolymerization at the desired conversion, the copolymer was separated from the monomer, and converted to small molecules via hydrolysis or transesterification. Since quantitative analysis of this derivative by LC, GC or NMR, is facile, the composition of copolymer can be directly obtained. There are two critical steps in this method: the separation of monomer from the copolymer, which must be complete and without side reactions such as hydrolysis, and the hydrolysis/transesterification reaction, which must convert the copolymer to the desired small molecules in quantitative yield.

**Separation.** Because of the low recoveries seen in our HPLC results and our concern that silica might hydrolyze lactide and ethylglycolide, we examined both silica gel and silica deactivated with 3% triethylamine as stationary phases for the separation of the copolymer from the monomer. Surprisingly, lactide quantitatively hydrolyzed to lactic acid and its linear dimer on the treated column, while both lactide and ethylglycolide were stable to untreated silica gel. The monomer and polymer can be cleanly separated on a silica column using  $\text{CHCl}_3$  as the eluent provided the  $M_n$  of the polymer is  $> 8,000$  g/mol. Assuming the conversion to polymer is limited to 10%, the monomer to catalyst ratio must be at least 400 to 1. Two examples describe the effectiveness of the method. A solution of lactide (22.0 mg) and polylactide

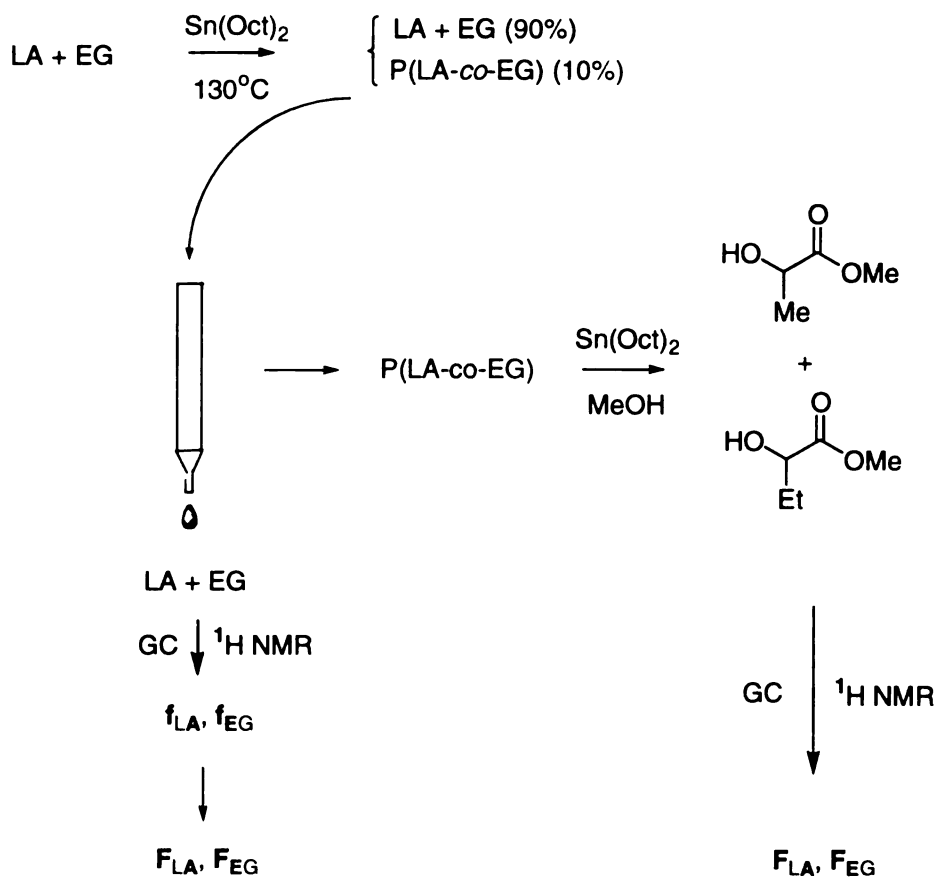
(19.0 mg) in  $\text{CHCl}_3$  was poured onto a silica column prepared from a 9 inch Pasteur pipette. Rinsing the column with 15 mL of  $\text{CHCl}_3$  resulted in recovery of 21.7 mg (98%) of lactide uncontaminated by polymer. Applying the same method to a solution of 21.5 mg of ethylglycolide and 19.0 mg of polylactide resulted in the recovery of 20.5 mg (95%) of ethylglycolide, again uncontaminated by polymer. These results show that the monomer can be cleanly separated from the polymer, and devising a method for recovering the polymer from the silica would complete the separation scheme.

**Transesterification.** Transesterification is an attractive approach for recovering the polymer since it allows direct conversion of the copolymer to esters that can be easily analyzed by GC, HPLC, or NMR. After treating PLA with conc. HCl and methanol for two days at reflux,  $^1\text{H}$  NMR showed 90% conversion of PLA to lactic acid methyl ester, and 10 % to lactic acid. The lactic acid is a problem as we were unable to devise a reverse phase HPLC protocol to separate lactic acid methyl ester, lactic acid, ethylglycolic acid, and its methyl ester. To overcome this problem, the mixtures of acids and esters were treated with diazomethane. We wanted to avoid the routine use of diazomethane, and we reasoned that this step probably can be omitted since the rates of hydrolysis to lactic and glycolic acids should be similar.

We examined alternatives to the use of HCl, and  $\text{Sn}(\text{Oct})_2$ , the catalyst commonly used to polymerize lactide, proved to be the most efficient catalyst for converting polylactide to its methyl ester. The optimized transesterification conditions, refluxing the polymer for 48 h with a large excess of methanol and

$\text{Sn}(\text{Oct})_2$  (30 eq. per polylactide repeat), gave quantitative yields of the methyl esters. Thus, we developed a reliable protocol for obtaining the copolymer composition

The analyses of the copolymers were completed by using GC, LC and NMR to characterize the mixtures of methyl esters. The temperature program used for GC analyses held the sample at 35 °C for 10 minutes, heated the sample at 20 °C/min to 150 °C, and then held at that temperature for 10 minutes. Both the lactic acid methyl ester (b.p. 140-145 °C) and ethylglycolic acid methyl ester (b.p. is 246 °C) are quite volatile, and the two compounds were detected at 2.1 and 4 minutes, while *o*-chlorotoluene, the standard, was detected at 8.7 min. GC-MS was used to prove the identity of the two peaks. Preparation of the sample is critical. The methanol must be removed under conditions that do not lead to loss of the esters. Evacuation of the methanol on a vacuum line with the temperature kept below -10 °C and the pressure >300 mTorr gave good results. The GC analyses of samples prepared by transesterification using HCl as the catalyst were complicated and contained unexpected peaks, but those prepared using  $\text{Sn}(\text{Oct})_2$  were clean and showed only the two expected esters.



**Scheme 15.** Protocol for the determination of copolymer composition.

**Comparison of GC and  $^1\text{H NMR}$ .** Both GC and  $^1\text{H NMR}$  are convenient methods for analyzing the methyl esters of lactic acid and ethylglycolic acid. Having two techniques is important, since copolymers prepared from other pairs of comonomers may yield methyl esters that are nonvolatile or have NMR spectra that cannot be integrated accurately due to overlapping peaks. To assay which technique is best for the lactide/ethylglycolide pair, we prepared and analyzed 4 samples by both methods. The two methods gave comparable  $F_1$  values (**Table 5**), but  $^1\text{H NMR}$

was the preferred technique because it is faster and more convenient. **Figure 9** shows the copolymerization data obtained via the protocol and analysis by NMR, and **Figure 10** shows the data plotted in the Fineman-Ross format to extract the values of  $r_1$  and  $r_2$ . The rate constants for the copolymerization of lactide and ethylglycolide are listed in **Table 5**. The data based on  $^1\text{H}$  NMR analysis (**Figure 10**) are more consistent and have a lower uncertainty that

**Table 5.** Comparison of the GC and  $^1\text{H}$  NMR methods for analyzing the copolymer composition

	$f_1$ (LA)	$F_1$ (LA) from GC	$F_1$ (LA) from NMR
1	0.17	0.29	0.25
2	0.29	0.35	0.29
3	0.79	0.68	0.71
4	0.88	0.84	0.82

those obtained from the original HPLC scheme (**Figure 7**).

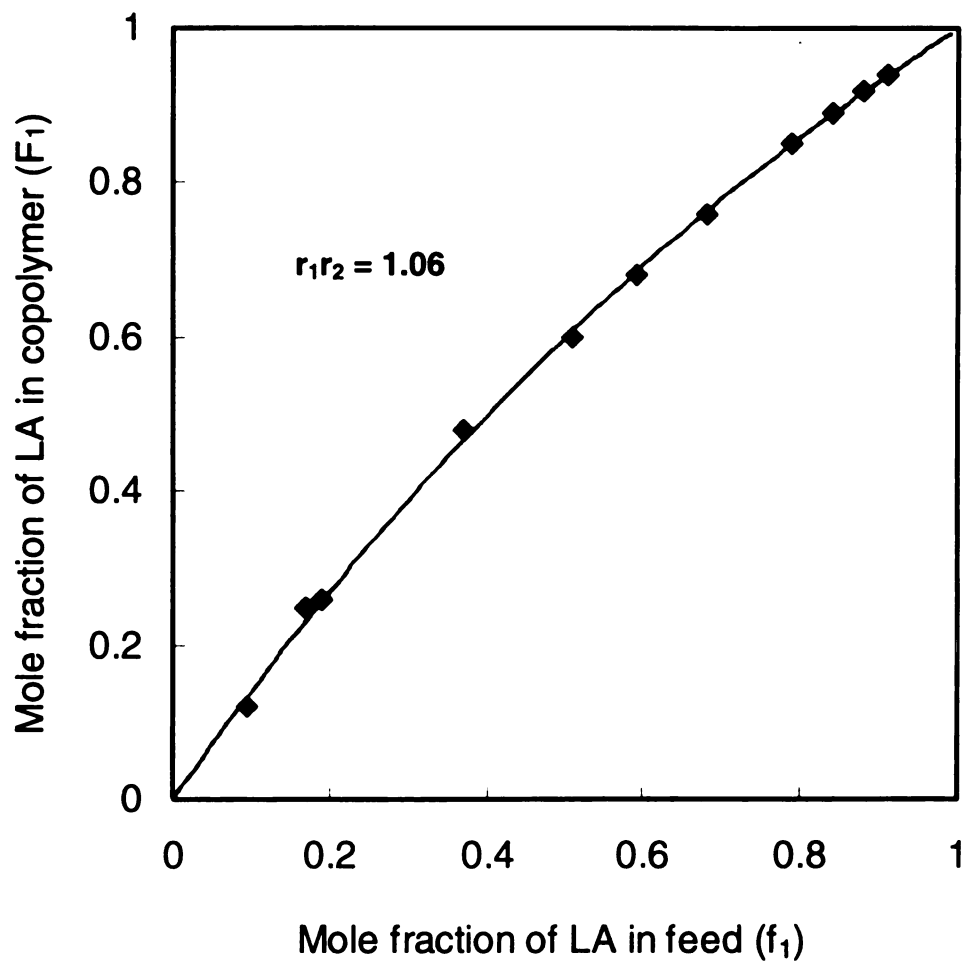


**Figure 9.** Mole fraction of lactide in the copolymer ( $F_1$ ) as a function of the feed ratio ( $f_1$ ) during the copolymerization of lactide with ethylglycolide as determined from  $^1\text{H}$  NMR

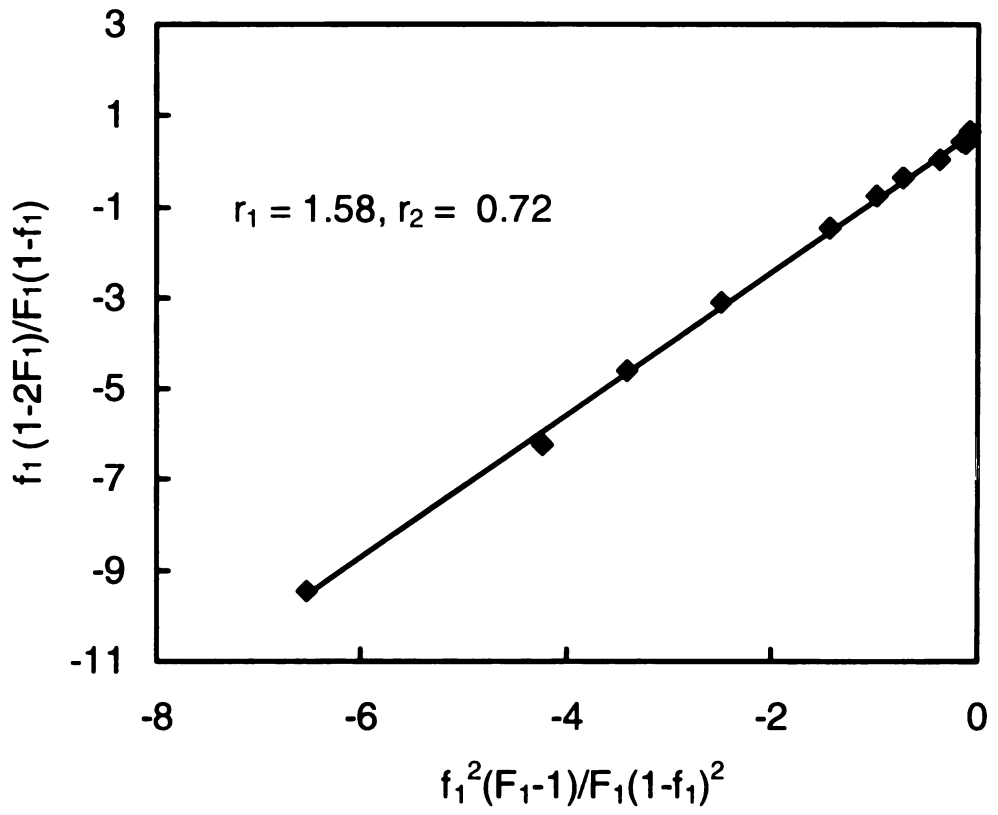


**Figure 10.**  $r_1$   $r_2$  determination by Fineman-Ross method

**Table 6.** Copolymerization behavior from Fineman-Ross method

monomer	$K_p[I] \text{ (sec}^{-1}) \times 10^3$	
	lactide	ethylglycolide
lactide	6.2 ( $k_{11}$ )	3.9 ( $k_{12}$ )
ethylglycolide	6.7 ( $k_{21}$ )	4.8 ( $k_{22}$ )

Recently, the Kelen-Tudos method<sup>85,86</sup> has emerged as a popular method for extracting  $r_1$  and  $r_2$  from experimental data. Like the Fineman-Ross method, this

method is based on the copolymerization equation:

$$\frac{d[M_1]}{d[M_2]} = \frac{[M_1](r_1[M_1] + [M_2])}{[M_2]([M_1] + r_2[M_2])} \quad (3)$$

in which  $d[M_1]$ ,  $d[M_2]$  are defined as the monomer concentration of monomer 1, 2 being incorporated into the copolymer at monomer feed concentrations of  $[M_1]$  and  $[M_2]$ . If we further define  $x = [M_1]/[M_2]$ ,  $y = d[M_1]/d[M_2]$  and  $G = x(y-1)$ , then  $F = x^2/y$ ,  $\xi = F/(\alpha + F)$ ,  $\eta = G/(\alpha + F)$ , and  $\alpha = (F_{\text{Max}}F_{\text{Min}})^{1/2}$ , the copolymerization can be transformed into:

$$\eta = (r_1+r_2/\alpha)\varepsilon - r_2/\alpha$$

Plotting  $\eta$  (y axis) vs  $\varepsilon$  (X axis) yields a straight line with a slope of  $(r_1+r_2/\alpha)$  and an x-intercept of  $r_2/\alpha$ . Since  $\alpha$  is known,  $r_1$  and  $r_2$  can therefore be calculated.

The kinetic data plotted according to this method are shown in **Figure 11** and **Table 5**. Comparing the kinetic results obtained from Fineman-Ross method with those from Kelen-Tudos method, we can see that they are very similar.

**Figure 9** shows the theoretical  $f_1$  vs  $F_1$  curve and the experimental data obtained by the direct determination of copolymer composition. Compared to the analogous data obtained from reverse phase HPLC, the data are more consistent with theoretical values, which is consistent with the direct copolymer determination protocol being a more accurate approach than the indirect composition analysis based on reverse HPLC.

A copolymerization is termed as “ideal” when the product of  $r_1r_2$  is unity. In the case of the copolymerization of lactide with ethylglycolide,  $r_1r_2$  is 1.06 (Kelen-Tudos method), which is very close to 1, so the polymerization can be classified as ideal. Because the  $r_1$  and  $r_2$  values are not that different, both monomers add to the growing polymer chain end randomly (**Figure 5**). An important practical consequence of an ideal copolymerization is that it becomes progressively more difficult to produce copolymers containing appreciable amounts of both monomers as the difference in the reactivities of the two monomers increases. However, because  $r_1$  and  $r_2$  do not differ markedly in the copolymerization of lactide with ethylglycolide, there will exist a large range of comonomer feed compositions that yield copolymers containing appreciable amounts of both monomers.

Steric hindrance from the substituent on the glycolide ring plays an important role in the polymerization rate,<sup>1</sup> and not surprisingly, the

homopolymerization of lactide is faster than that of ethylglycolide ( $k_{11} > k_{22}$ ). Lactide, the more active monomer, adds faster to the growing chain end whether the chain ends in lactide or ethylglycolide ( $k_{11} > k_{12}$ ,  $k_{21} > k_{22}$ ). Nevertheless, the data show that ethylglycolide is the more reactive chain end, suggesting that the ethyl glycolide terminated chains are less stable, probably for steric reasons. This effect should be magnified if the glycolide ring is made more congested. The results for a glycolide with a more sterically demanding alkyl group, isopropylglycolide, are summarized in the subsequent section.

**Table 7.** Copolymerization behavior from Kelen-Tudos method

monomer	$K_p[I] (\text{sec}^{-1}) \times 10^3$	
	lactide	ethylglycolide
lactide	6.2 ( $k_{11}$ )	4.1 ( $k_{12}$ )
ethylglycolide	6.9 ( $k_{21}$ )	4.8 ( $k_{22}$ )

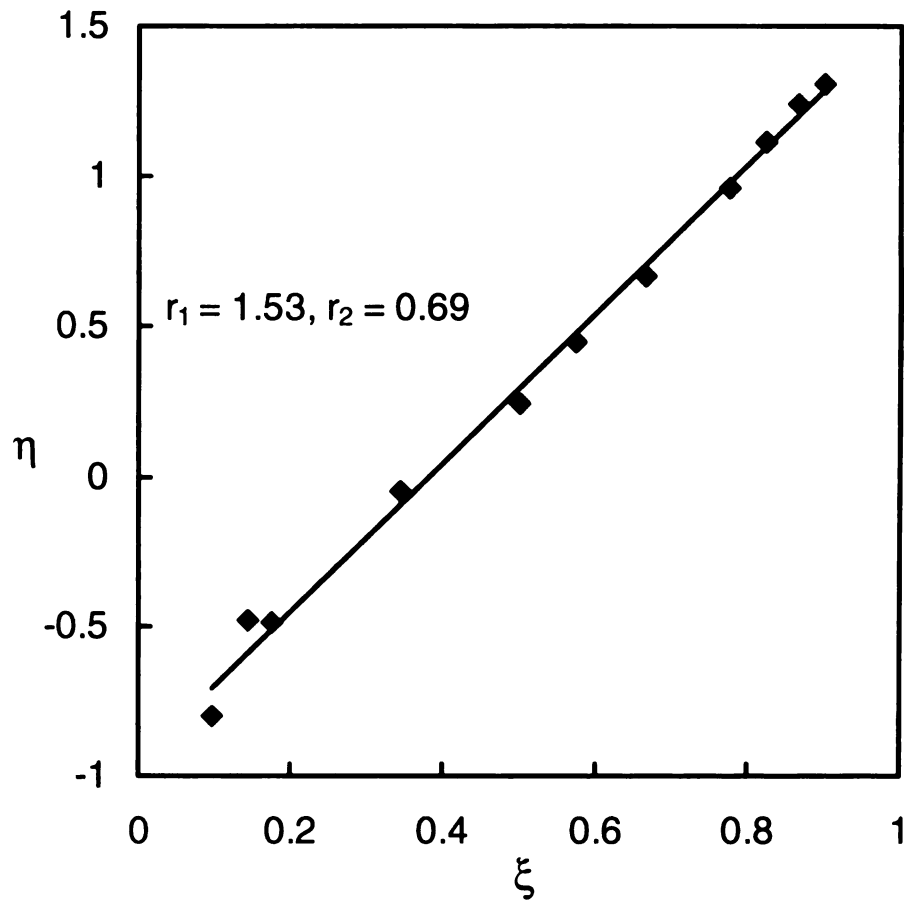
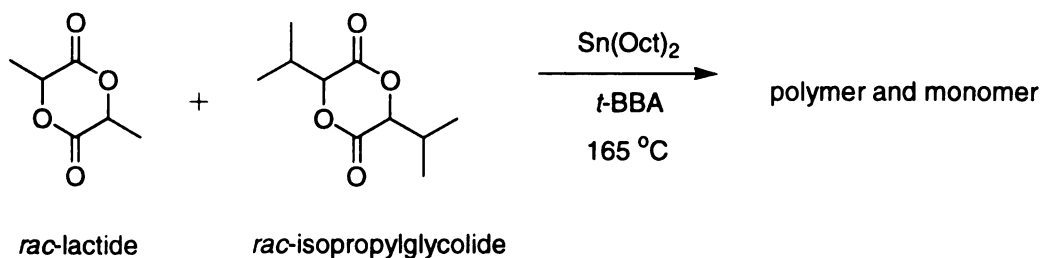


**Figure 11.**  $r_1, r_2$  Determination by the Telen-Tudos Method

### 6.3. Kinetic Evaluation of the Copolymerization of Lactide with Isopropylglycolide

The melting point of *rac*-isopropylglycolide (*rac*-iPrGL) is 161-163 °C, and thus the temperature for the melt copolymerization of lactide with *rac*-isopropylglycolide was set at 165 °C. Initially, the protocol used to analyze the copolymer composition was identical to that used for ethylglycolide. However, the transesterification reaction, the key step in the analysis of copolymer composition, proved problematic. After 6 days, the conversion of poly(*rac*-iPrGL) to the methyl ester of isopropylglycolic acid methyl ester was only 40%, with the remainder consisting of the linear dimer (30%) and oligomeric poly(*rac*-iPrGL) (30%). Switching the solvent to THF, a better solvent for the polymer, did not improve the reaction rate. Thus, we resorted to analysis of the un-polymerized monomer to calculate the copolymer composition. The assumption that the decrease in monomer concentration is directly related to the polymer composition is good (i.e. there are no side reactions), but calculating the small change in monomer concentration requires subtraction of two large numbers, and thus the error associated with the calculation is large.



**Scheme 16.** Copolymerization of racemic lactide with racemic isopropylglycolide

To minimize the error, the monomer feed amount was increased to 500 mg. At 10% conversion for a feed of 90% lactide (45 mg) and 10% isopropylglycolide (5 mg), the uncertainty in the weight of the isopropylglycolide should be  $\pm 0.2$  mg, and the uncertainty associated with measurement of the isopropylglycolide should be  $\pm 4\%$ , which should be acceptable. To test this idea, three sets of experiments were run at different feed ratios, with each set consisting of a pair of duplicate runs. After copolymerization, the compositions of the copolymers were determined; the results of these parallel experiments are summarized in **Table 8**. The data are consistent and thus this method was used for copolymer composition analysis in the poly(lactide-*co-rac*-iPrGL) system. The results of the kinetic study of the copolymerization of lactide with isopropylglycolide are summarized in **Figures 12, 13, and 14** and **Tables 9, 10**.

**Table 8.** Comparison of copolymer composition analysis obtained from parallel runs

	$f_1$ (LA)	$F_1$ (LA)
<b>0-1</b>	0.28	0.63
<b>0-4</b>	0.28	0.63
<b>5-1</b>	0.55	0.94
<b>5-2</b>	0.59	0.97
<b>8-3</b>	0.80	0.97
<b>8-4</b>	0.81	0.99

The data points that define the  $f_1 \sim F_1$  curve for poly(LA-*co-rac*-*i*PrGL) (**Figure 12**) show more scatter than seen in poly(LA-*co*-EG) (**Figure 9**). For poly(LA-*co*-EG), copolymer composition was measured directly, but an indirect approach, with its larger uncertainty, was used for poly(LA-*co-rac*-*i*PrGL). The monomer reactivity ratios obtained from the Kelen-Tudos analysis of the data were used generate the theoretical  $f_1$  vs.  $F_1$  curve for the copolymerization (**Figure 14**). Except for slight deviation in the middle of the curve, the experimental data (diamonds) and the calculated curve are consistent.

The overall shape of the  $f_1 \sim F_1$  copolymerization curves for lactide copolymerized with ethylglycolide and isopropylglycolide are similar, suggesting that both are “ideal”. However, the reactivity ratio product for poly(LA-*co-rac*-*i*PrGL) ( $r_1 r_2 = 0.48$ ) is farther from unity than that of poly(LA-*co*-EG) ( $r_1 r_2 = 1.06$ ), and therefore, we expect the microstructures of these two copolymers to be quite different. In particular poly(LA-*co-rac*-*i*PrGL) should be a somewhat “blocky” copolymer.

The kinetic rate constants derived from Fineman-Ross and Kelen-Tudos analyses of the data are shown in **Tables 9** and **10**. Both methods gave similar results. As would be expected from simple steric arguments, the homopolymerization of LA is 8 times faster than that of *i*PrGL. Steric effects also provide a plausible argument for the higher reactivity of lactide chain ends. Chains ending in isopropylglycolide should be the least stable (most reactive) and add lactide faster than chains terminated with lactide. Adding the sterically

hindered isopropylglycolide to a chain ending in isopropylglycolide should be the slowest process. Therefore rates decrease in the order  $k_{22} > k_{11} > k_{12} > k_{21}$ .

One way to understand the kinetics of these two copolymerizations is to think in terms of the rate-determining step of the polymerization. According to Yin,<sup>1</sup> two steps in the chain propagation need to be considered (**Scheme 17**), nucleophilic attack ( $k_{p1}$ ) and ring opening ( $k_{p2}$ ). For chains ending in hindered monomers such as isopropylglycolide, the intermediate is relatively unstable and the activation energy to form products is decreased. Such chains should react rapidly, especially with reactive monomers like lactide. Chains ending in lactide units are more stable, and their reaction with hindered monomers is slow. This process is analogous to that seen for the copolymerization of vinyl monomers such as styrene (stable chain end) and vinyl acetate (unstable chain end).

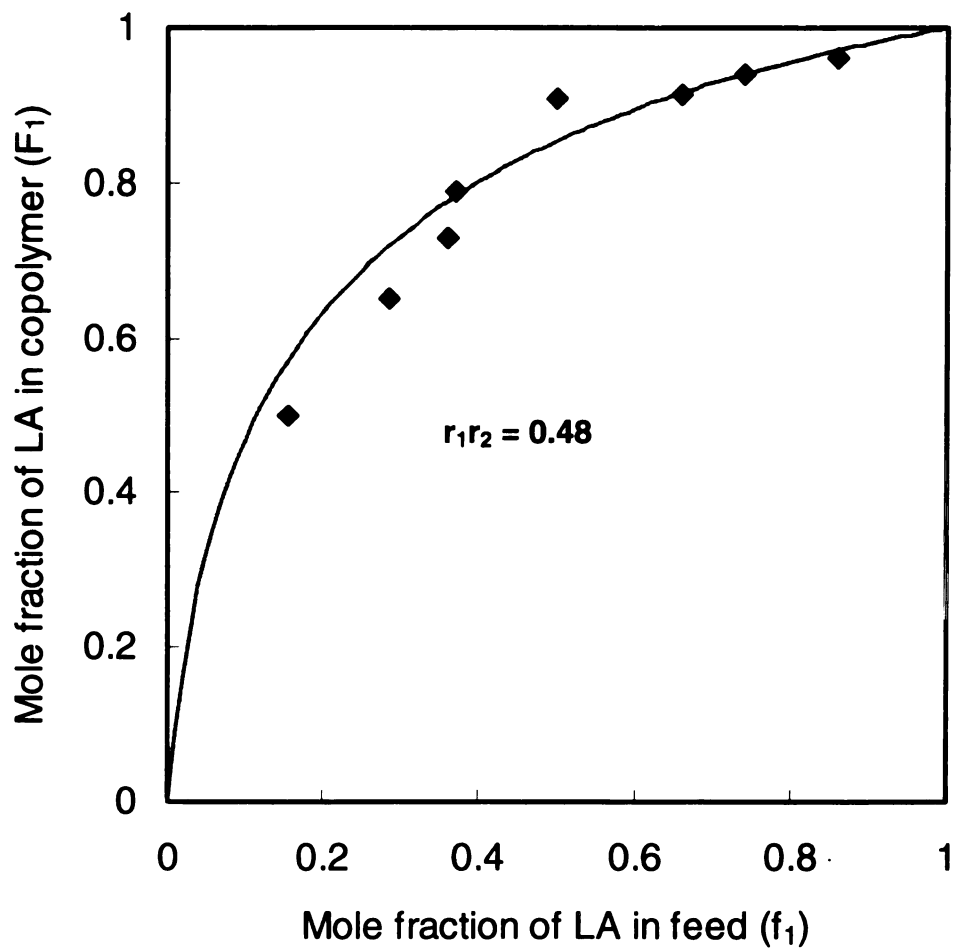


**Figure 12.** Mole fraction of lactide in the copolymer ( $F_1$ ) as a function of the feed ratio ( $f_1$ ) during the copolymerization of lactide with poly(lactide-co-rac-isopropylglycolide)

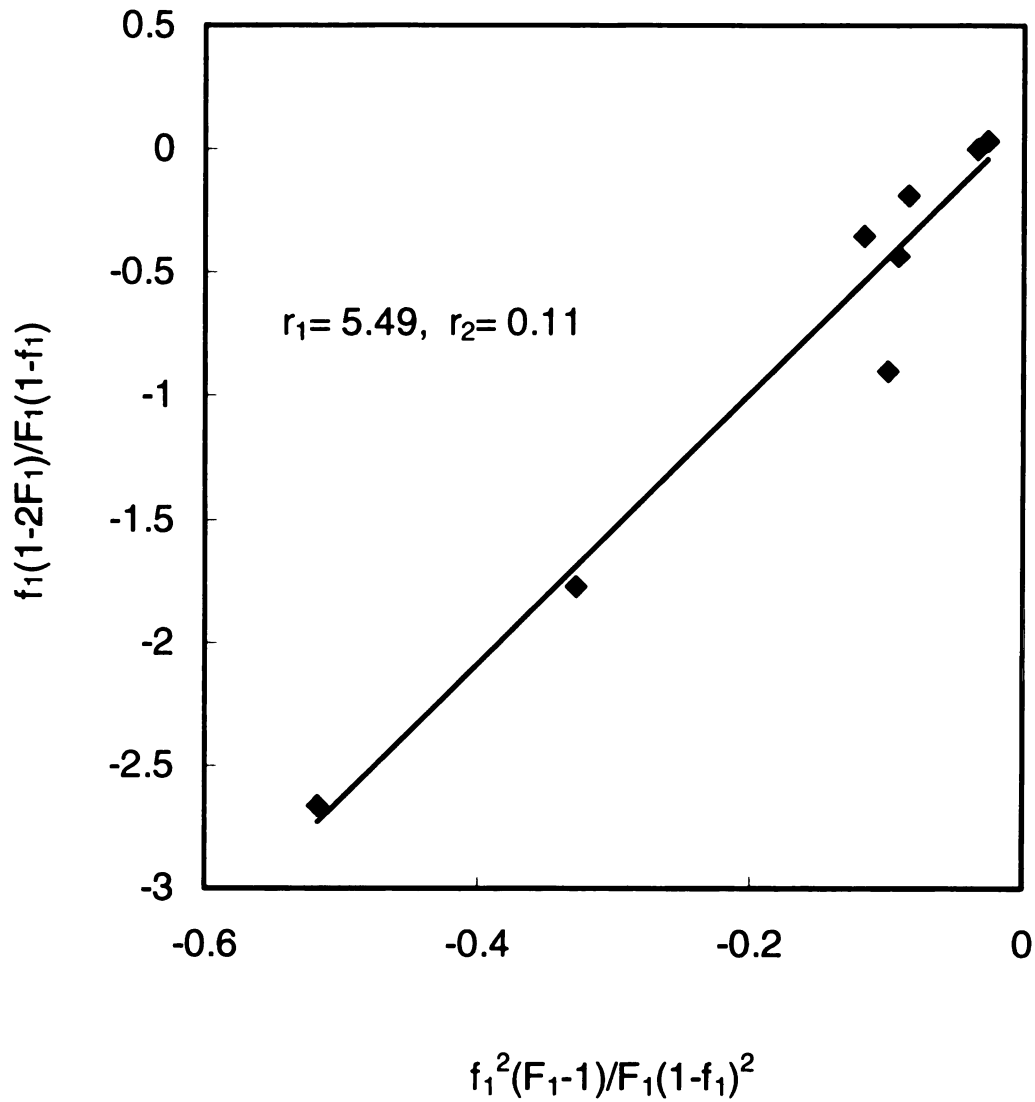


**Figure 13.**  $r_1$   $r_2$  determination using the Fineman-Ross method

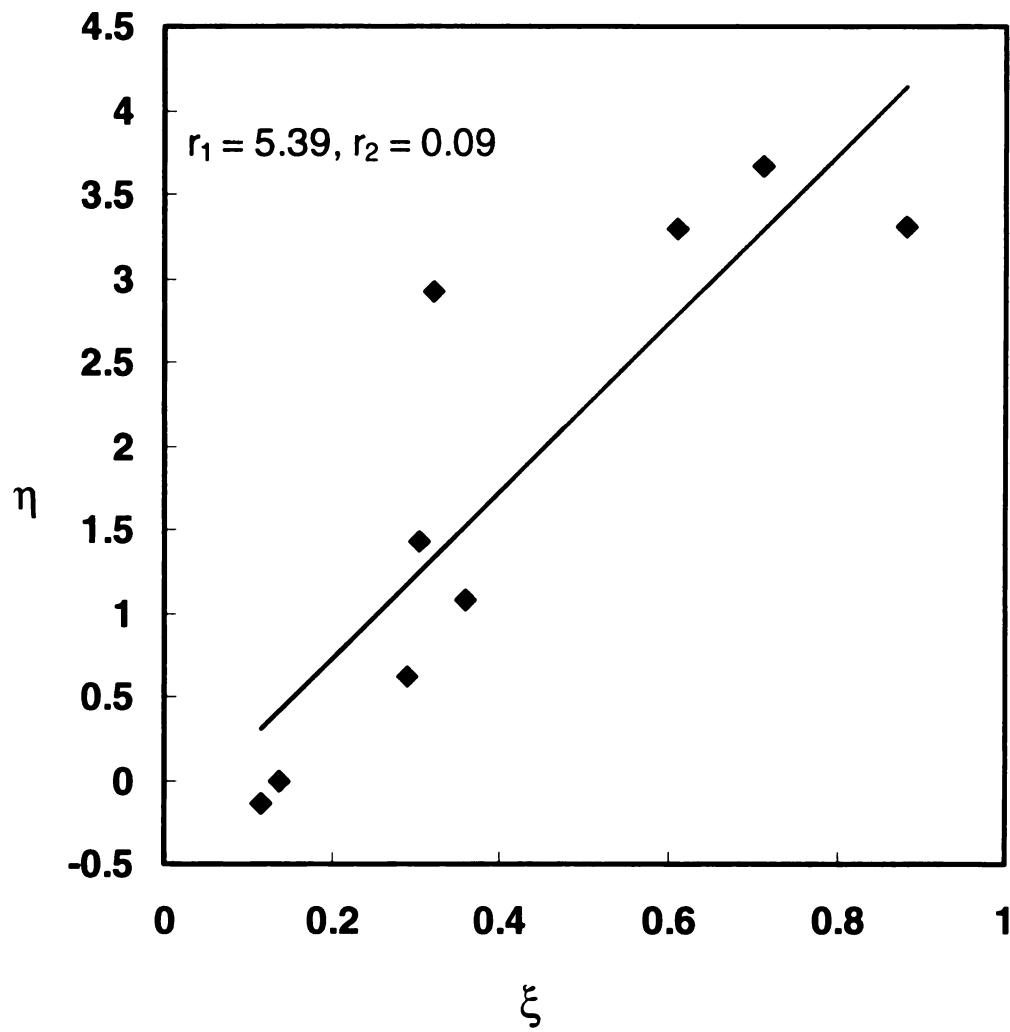


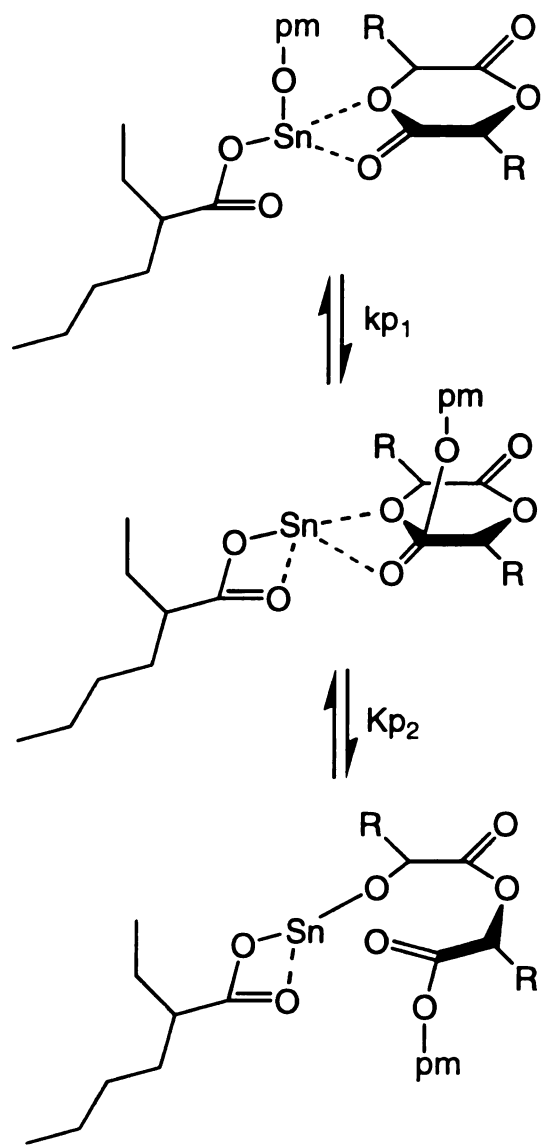
**Figure 14.**  $r_1, r_2$  Determination using the Kelen-Tudos method

**Table 9.** Copolymerization behavior from Fineman-Ross method

	$K_p[I] (\text{sec}^{-1}) \times 10^3$	
<b>monomer</b>	<b>lactide</b>	<b>isopropylglycolide</b>
<b>lactide</b>	40.3 ( $k_{11}$ )	7.3( $k_{12}$ )
<b>isopropylglycolide</b>	53.6( $k_{21}$ )	4.8 ( $k_{22}$ )

**Table 10.** Copolymerization behavior from Kelen-Tudos method

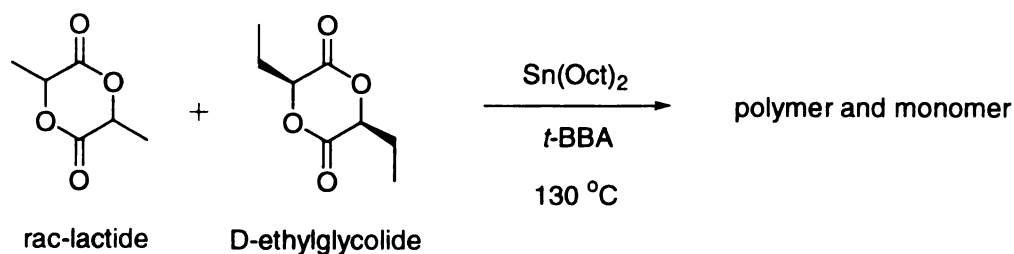
	$K_p[I] (\text{sec}^{-1}) \times 10^3$	
<b>monomer</b>	<b>lactide</b>	<b>isopropylglycolide</b>
<b>lactide</b>	40.3 ( $k_{11}$ )	7.5( $k_{12}$ )
<b>isopropylglycolide</b>	58.8 ( $k_{21}$ )	4.8 ( $k_{22}$ )



**Scheme 17.** Chain propagation mechanism for lactide copolymerization.

#### 6.4. Copolymerization of Lactide with R-ethylglycolide

Our results show that steric factors play an important role in determining the microstructure of lactide copolymers, and it would be interesting to explicitly add another complication to the copolymerization, stereochemistry. Ethylglycolide has been obtained as a single diastereomer, D-ethylglycolide (R,R). The physical properties of D-ethylglycolide are quite different from the ethylglycolide monomer mixture used earlier, which was composed of a 1:1 mixture of *meso* and *rac*-ethylglycolide. For example, the melting point of D-ethylglycolide is 122 °C, while the monomer mixture used previously melts at room temperature.



**Scheme 18.** Copolymerization of lactide with R-ethylglycolide

The homopolymerization rate for D-ethylglycolide has not been reported, so to obtain  $k_{22}$ , D-ethylglycolide was polymerized at 130 °C. Judging from the propagation rate constant  $k_p[I]$  (**Figure 15**), the polymerization rate of the pure diastereomer is slower than that of the ethylglycolide mixture (3.2 vs 4.8), which is consistent with literature.<sup>95,96</sup> Yin's study of the polymerization of *rac*-lactide with L-lactide showed that depending on the polymerization

conditions, *rac*-lactide polymerized 1.7 to 3 times faster than L-lactide.<sup>1</sup> This phenomena is termed “syndiotactic preference”, a bias toward adding a monomer of opposite stereochemistry to the end of the growing chain. The difference in the activation energies for these two copolymerizations was ascribed to chain end control, where differences in the steric hindrance for the addition of monomers of different stereochemistry lead to preferential insertion of one stereoisomer.

The study of the copolymerization of lactide with D-ethylglycolide followed that used for poly(lactide-*co*-ethylglycolide) except that the

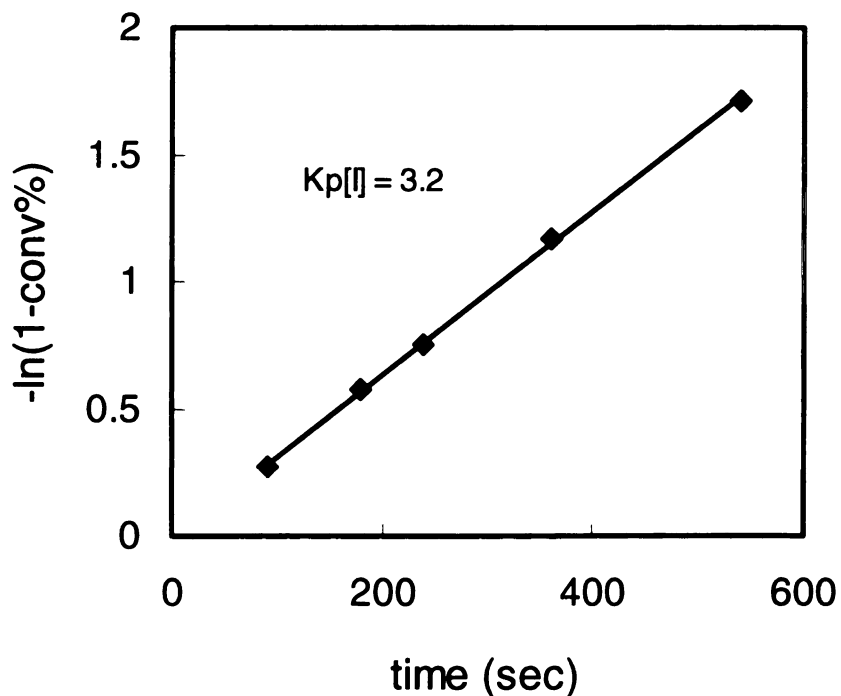


**Figure 15.** Melt polymerization of D-ethylglycolide at 130 °C catalyzed by  $\text{Sn}(\text{Oct})_2 + t\text{-BBA}$

transesterification time was increased from two to three days. The copolymerization behavior of lactide with D-ethylglycolide is summarized in **Figures 16, 17 and 18**. In the  $f_1$  vs  $F_1$  plot, most data are consistent with the theoretical curve (generated from the  $r_1$  and  $r_2$  values derived from the Kelen-Tudos method). As expected, lactide is the more reactive monomer, and therefore we observed  $k_{11} > k_{12}$  and  $k_{21} > k_{22}$ . As to the chain end reactivity, we observed the same trend as seen in the copolymerization of lactide with isopropylglycolide; lactide adds faster to an isopropylglycolide chain end than to a lactide chain end ( $k_{21} > k_{11}$ ). When the incoming monomer is D-ethylglycolide, it is the lactide chain end that is more reactive ( $k_{12} > k_{22}$ ). Therefore, we conclude that effect of stereochemistry on the copolymerization can largely be explained by steric arguments.

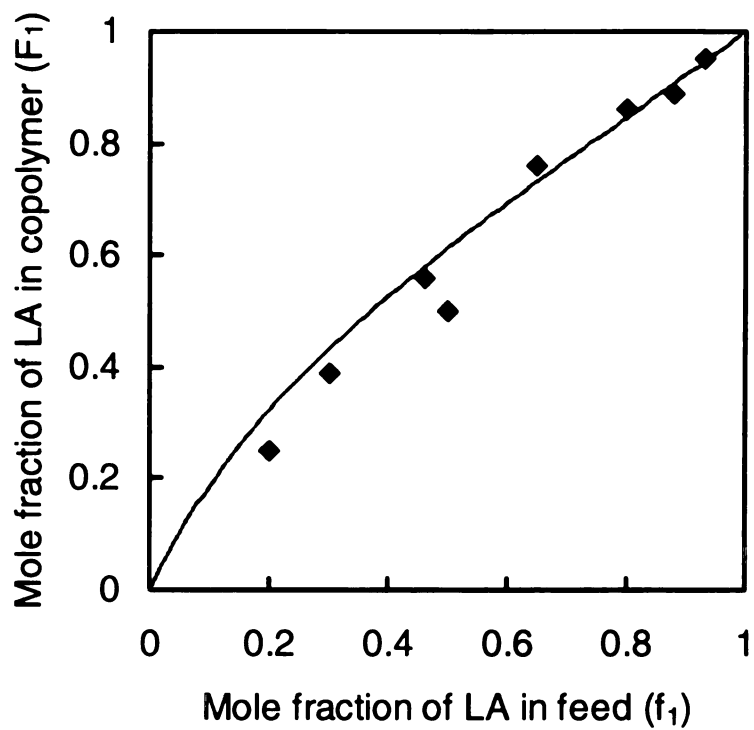


**Figure 16.** Mole fraction of lactide in the copolymer ( $F_1$ ) as a function of the feed ratio ( $f_1$ ) during the copolymerization of lactide with D-ethylglycolide

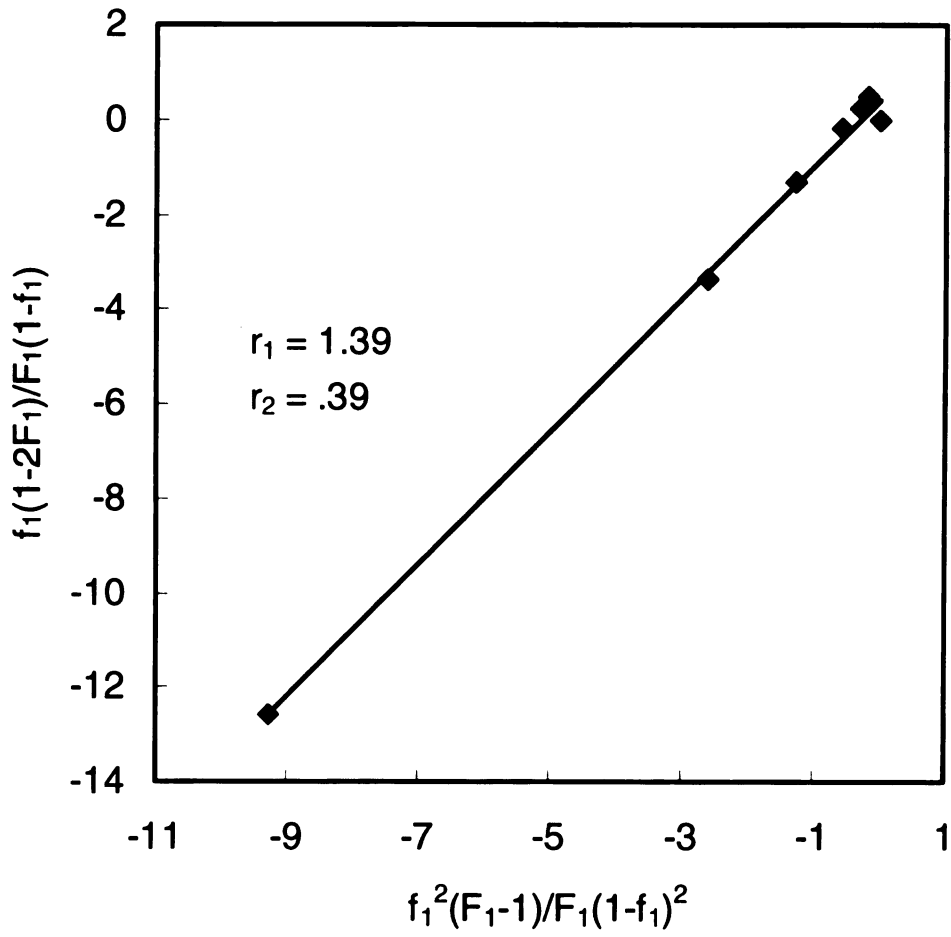


**Figure 17.**  $r_1, r_2$  determination by Fineman-Ross method

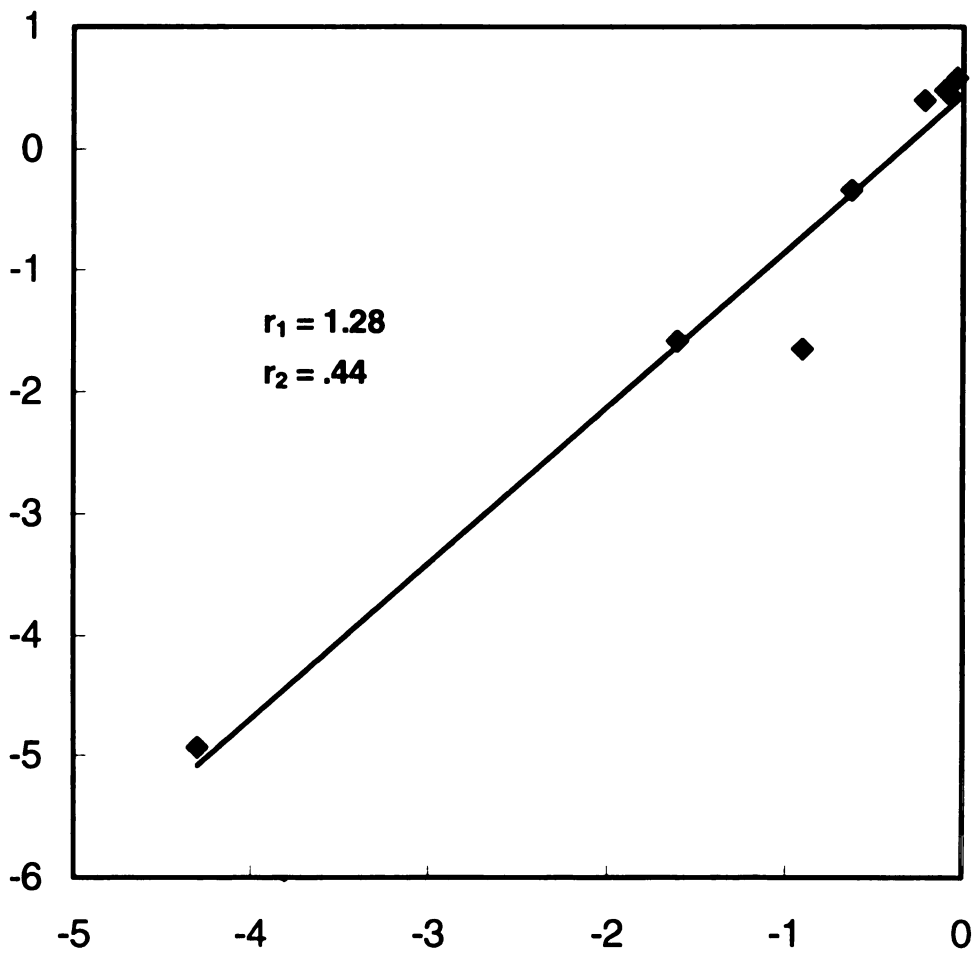


**Figure 18.**  $r_1, r_2$  determination by Kelen-Tudos method

**Table 11.** Copolymerization behavior from Fineman-Ross method

	$K_p[I] \text{ (sec}^{-1}) \times 10^3$	
<b>monomer</b>	<b>lactide</b>	<b>D-ethylglycolide</b>
<b>lactide</b>	6.2 ( $k_{11}$ )	4.3 ( $k_{12}$ )
<b>ethylglycolide</b>	8.0 ( $k_{21}$ )	3.2 ( $k_{22}$ )

**Table 12.** Copolymerization behavior from Kelen-Tudos method

	$K_p[I] \text{ (sec}^{-1}) \times 10^3$	
<b>monomer</b>	<b>lactide</b>	<b>D-ethylglycolide</b>
<b>lactide</b>	6.2 ( $k_{11}$ )	4.8 ( $k_{12}$ )
<b>ethylglycolide</b>	7.3 ( $k_{21}$ )	3.2 ( $k_{22}$ )

## 6.5. Physical Properties and Structure of Copolymers

Prior work suggested that poly(lactide-*co*-ethylglycolide)s were homogeneous materials with the two comonomers distributed randomly along the polymer chain. Differential scanning calorimetry (DSC) analyses of the poly(lactide-*co*-isopropylglycolide)s (Table 13) show that these polymers also are single-phase materials, since all of the copolymers exhibit one  $T_g$  that falls between that of the polylactide and poly(isopropylglycolide) homopolymers. The change in the  $T_g$  of random copolymers with composition can be predicted by the Fox equation (Figure 19). The good fit to the Fox equation ( $\pm 2$  °C deviation) is consistent with the poly(LA-*co*-*rac*-iPrGL)s being homogeneous. However, this is not a rigorous test in that the  $T_g$ s of the two homopolymers are similar, making it hard to detect deviations from the behavior expected for a random copolymer.

**Table 13.** Properties of P(LA-*co*-iPrGL)

Polymers	$M_n \cdot 10^{-3}$ <sup>a</sup>	$M_w/M_n$	$T_g$ °C <sup>b</sup>
Polylactide	35.4	1.78	56
LA/iPrGL = 3/1	27.8	1.82	48
LA/iPrGL = 1/1	25.7	1.76	48
LA/iPrGL = 1/3	28.2	1.90	43
Poly (isopropylglycolide)	32.6	1.74	42

a. measured by GPC in THF using polystyrene as standard

b. measured by DSC under He at a rate of 10 °C/min

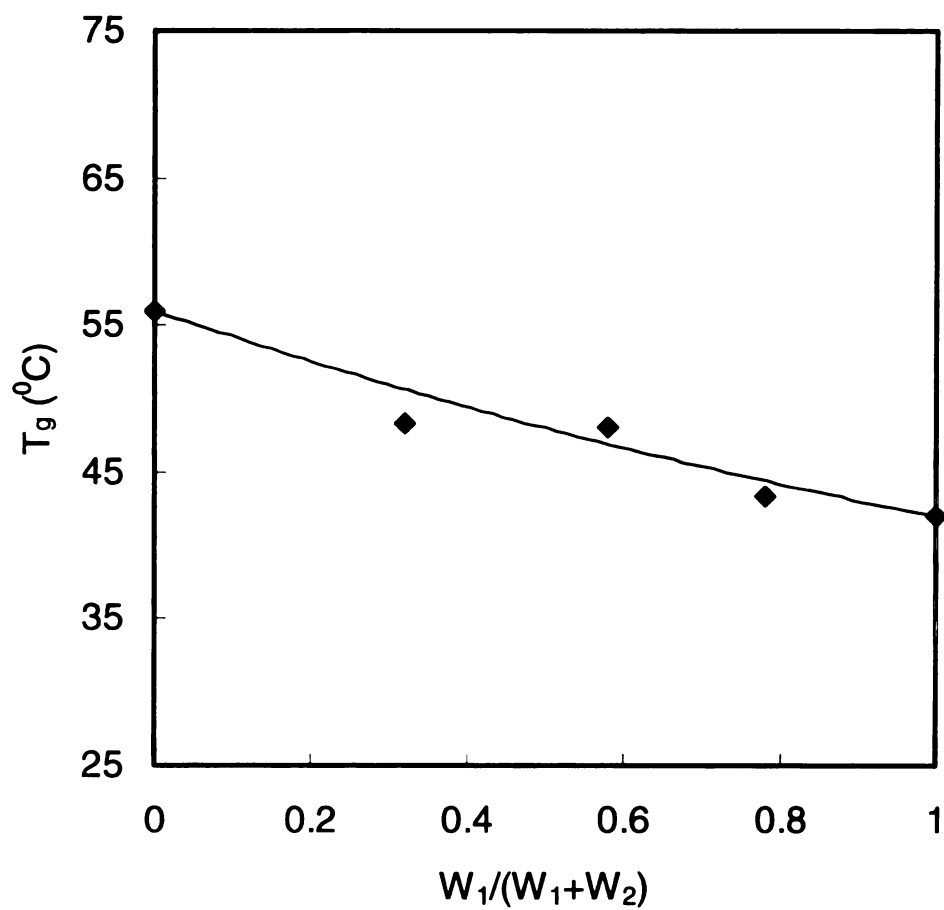


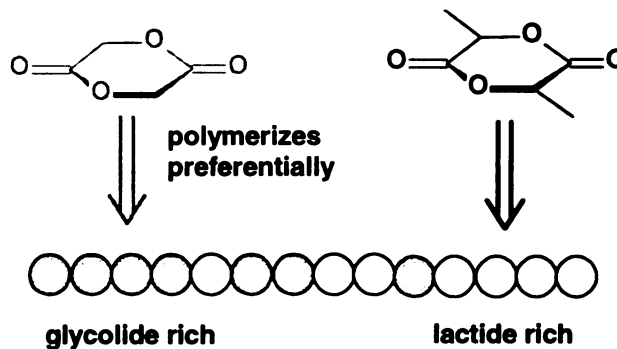
**Figure 19.** Glass transition temperature of lactide and isopropylglycolide copolymers.

Although the kinetic data indicate that both poly(LA-co-EG) and poly(LA-co-rac-PrGL) are random copolymers, there are differences in the extent of “randomness” of these two copolymers. When lactide copolymerizes with ethylglycolide, the reactivities of these two monomers are very close due their structural similarity ( $r_1 = 1.53$ ,  $r_2 = .69$ ). Therefore, even though lactide is more reactive than ethylglycolide, these two monomers have nearly the same opportunity to be added to the copolymer. As seen from the results of the kinetic study (**Figure 9**), the  $r_1r_2$  product is 1.06, very close to unity, and thus is a random copolymer. On the other hand, the reactivity difference in the copolymerization of lactide with isopropylglycolide ( $r_1 = 5.39$ ,  $r_2 = .09$ ,  $r_1r_2 = 0.48$ ) results in a strong preference for the polymerization of lactide. Therefore, lactide would be consumed first during the copolymerization, and as the concentration of lactide decreases in the monomer feed pool, isopropylglycolide enters the polymer chain at an increasing rate. The  $r_1r_2$  product is a signature that this copolymerization is less random than poly(LA-co-EG), and there may be small blocks of polylactide and poly(isopropylglycolide) randomly distributed along the polymer chain. However, these blocks are apparently not long enough to generate phase separation. Thus, this copolymerization resembles the copolymerization of lactide with glycolide.<sup>94</sup> Although the physical properties of the poly(lactide-co-D-ethylglycolide)s were not studied, the kinetic parameters of this copolymerization indicate this copolymer is a random copolymer similar to poly(LA-co-EG) rather than a “blocky” random copolymer, such as poly(LA-co-

GL) and poly(LA-co-*ipr*GL). Nevertheless, kinetic evaluation and the study of the physical properties of copolymers provide only a partial analysis of the copolymerization. A full characterization of the polymer microstructure would require a full sequence analysis by NMR. The relationship between the monomer reactivity difference and the copolymer structure is illustrated in **Scheme 19**.

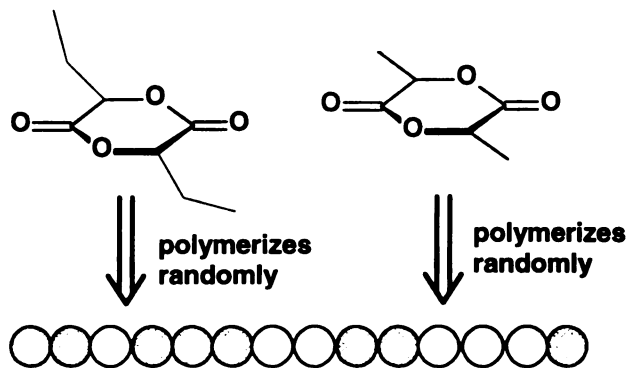
P (LA-co-GL)  
 $r_1 = 3.4, r_2 = .22$   
 $r_1 r_2 = .75$

“blocky” random



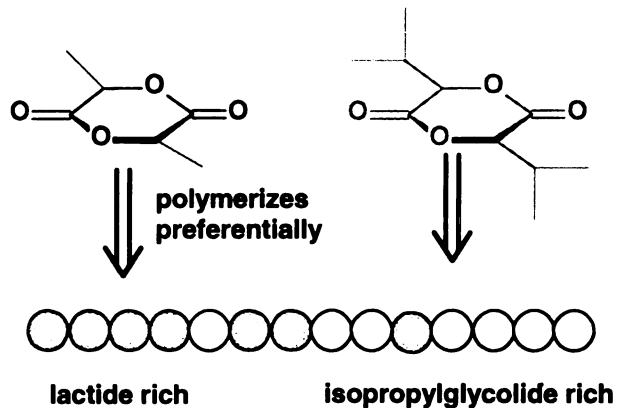
P (LA-co-EG)  
 $r_1 = 1.53, r_2 = .69$   
 $r_1 r_2 = 1.06$

“ideal” random



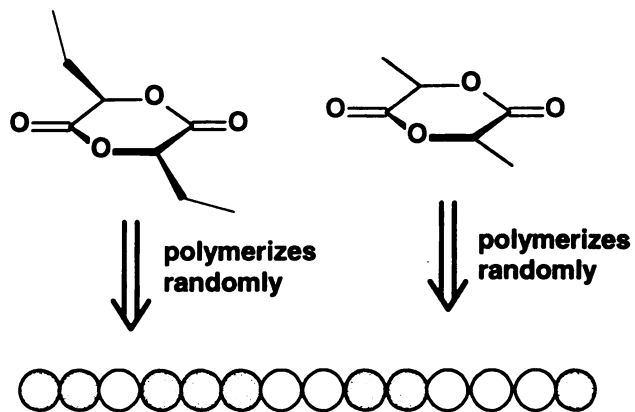
P (LA-co-*i*PrGL)  
 $r_1 = 5.29, r_2 = .09$   
 $r_1 r_2 = .48$

“blocky” random



P (LA-co-DEG)  
 $r_1 = 1.39, r_2 = .39$   
 $r_1 r_2 = 1.06$

“ideal” random



**Scheme 19.** The relationship between monomer reactivity ratio and the structure of copolymers.

## 6.6. Biodegradation of the Copolymers

We studied the hydrolytic degradation of a series of lactide and isopropylglycolide copolymers at pH 7.4 at 55 °C. The samples were 1 mm by 1 mm pieces of polymer, and at predetermined times, samples were removed from the degradation experiment and analyzed for loss in mass and molecular weight. The size of the polymer samples must be small to avoid the autocatalytic effects. Because the degradation product is acidic (carboxyl group formed by ester hydrolysis), acid groups localized in large samples cause an increase in the local degradation rate. For small samples, the diffusion rate of the aqueous buffer solution in the polymer will be higher than the polymer chain scission and the hydrolytic degradation proceeds uniformly.

The two most characteristic features of polymer hydrolytic degradation are mass loss and a decrease in molecular weight during degradation process. The weight loss process is associated with the formation of short polymer chains that are soluble in the buffer solution. The degradation data are summarized in **Figures 20** and **21**. For all samples, there was an initial drop in molecular weight, but the mass remained constant, and then declined. This behavior is consistent with a bulk degradation mechanism. It is also clear that the composition of the copolymer strongly influences the degradation profile. Since lactide is more hydrophilic than isopropylglycolide, the higher the lactide content in a copolymer, the faster the degradation rate in terms of both mass and molecular weight loss. The extreme case is that the polylactide

homopolymer totally degrades in 30 days, whereas poly(isopropylglycolide) samples under the same conditions lost only 2% of their weight in 60 days.

To further understand the degradation of these copolymer samples, we tried to fit a random chain scission model to the data in **Figure 21**. In the random scission model, the average number of bond cleavages per polymer molecule ( $N$ ) was calculated according to:

$$N = [M_n(0)/M_n(t) - 1] = k_d P_n(0)t$$

where  $M_n(0)$  and  $M_n(t)$  are the number-average molecular weights of polyesters at time 0 and time  $t$ ,  $k_d$  is the rate constant for hydrolytic degradation, and  $P_n(0)$  is the number-average of degree of polymerization at time 0.  $k_d$  was obtained from the slope from **Figure 22**. As expected, polylactide degrades the fastest, as the lactide content decreases, the degradation rate slows. Poly(isopropylglycolide) has the lowest degradation rate.

In an earlier study, we found that alkyl substituted lactide showed constant weight<sup>1</sup> until the degree of polymerization ( $P_n$ ) dropped to 30. The data for the copolymers show a similar trend (**Figure 23**); all of the polymer samples started to lose weight when the  $P_n$  drop to 30-40. This “turning point” in the degradation process must be related to the structure of the polylactide backbone, and perhaps corresponds to the entanglement limit for these polymers. Solubility arguments cannot explain the data since the same phenomena is seen for polymers of different degrees of hydrophobicity.

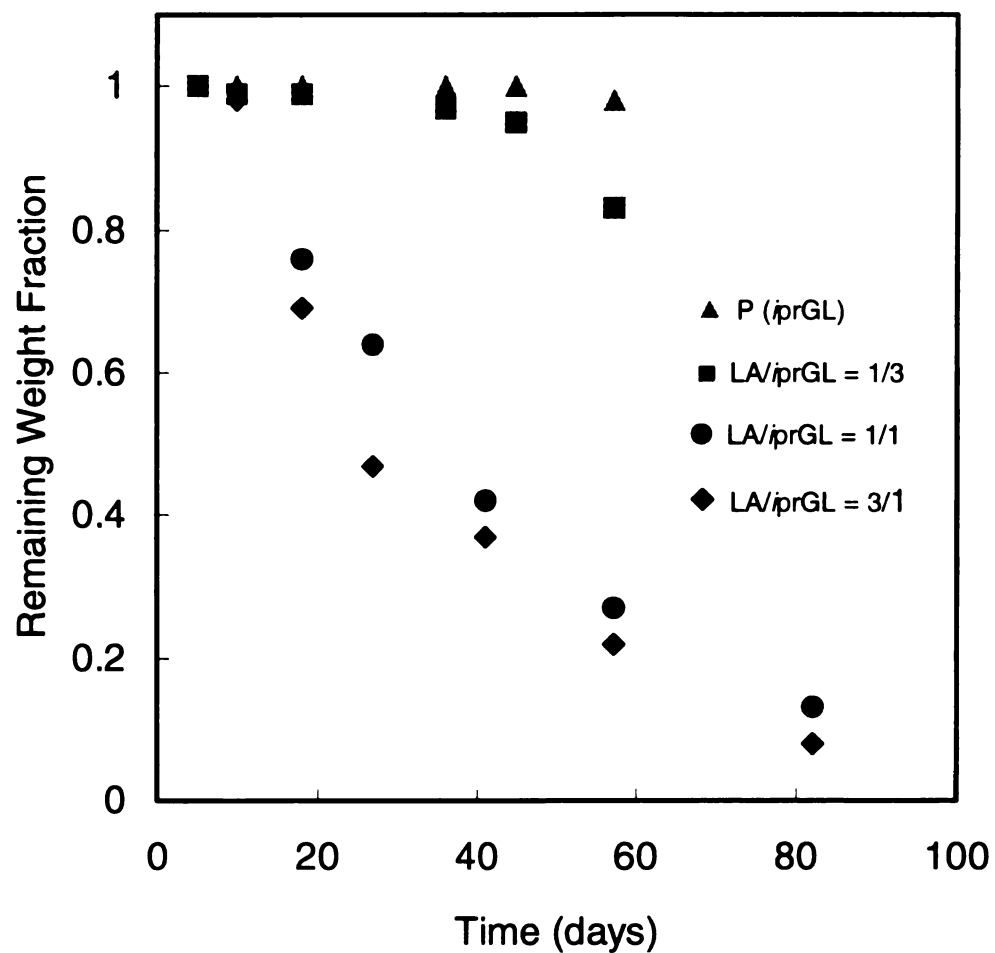


**Figure 20.** The weight loss of polymer samples during hydrolytic degradation

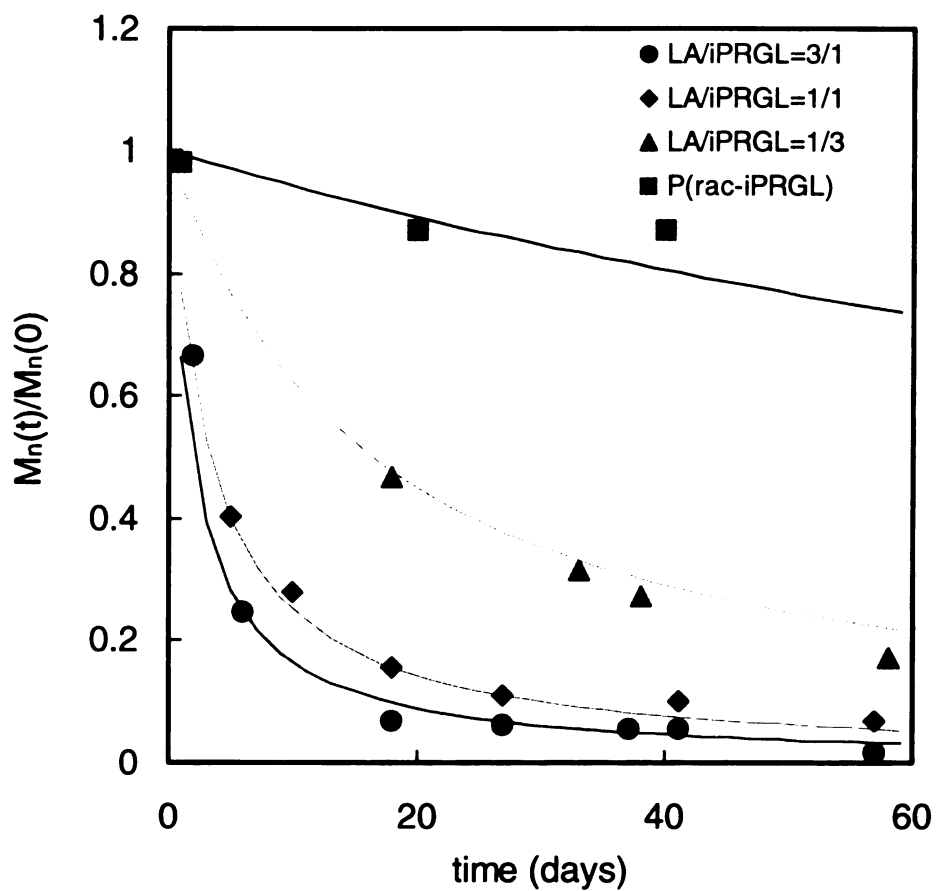


**Figure 21.** The molecular weight loss of poly(LA-co-iPRGL) during hydrolytic degradation.

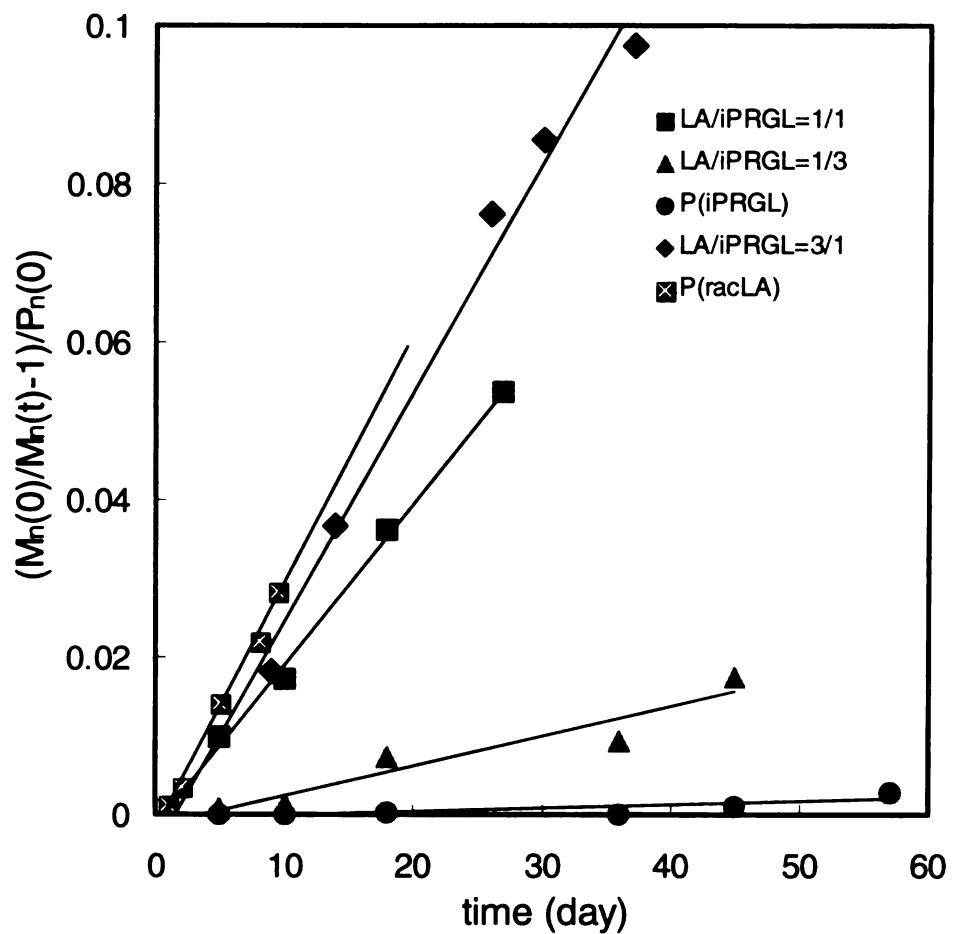


**Figure 22.** Decrease in the molecular weight of P(LA-co-iPRGL) during hydrolytic degradation fitted to the random chain scission model

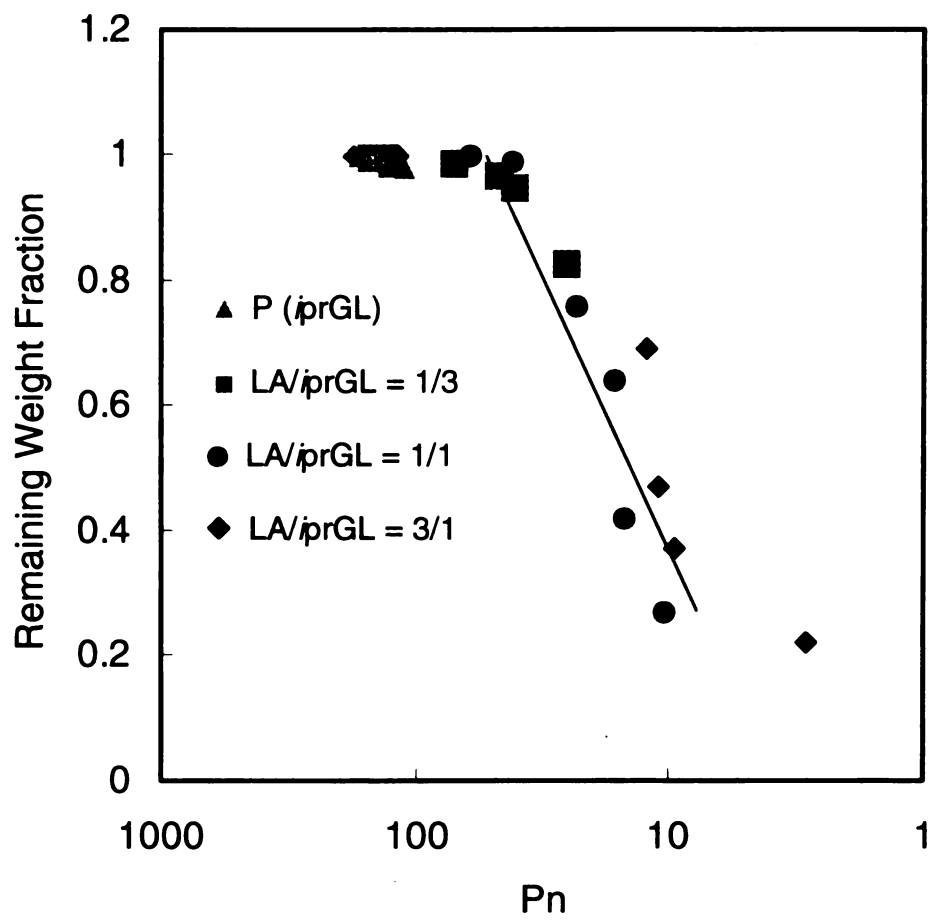


**Figure 23.** The decrease in the degree of polymerization of polymer samples during hydrolytic degradation.

## BIBLIOGRAPHY

- 1 Yin, M. *Synthesis and Characterization of Substituted Polylactides*, Michigan State University, 2000.
- 2 Gilding, D. K.; Reed, A. M. *Polymer* **1979**, *20*, 1459-1464.
- 3 Jamshidi, K.; Hyon, S. H.; Ikada, Y. *Polymer* **1988**, *29*, 2229-2234.
- 4 Varmanair, M.; Pan, R.; Wunderlich, B. *J. Polym. Sci. Pt. B-Polym. Phys.* **1991**, *29*, 1107-1115.
- 5 Helder, J.; Feijen, J.; Lee, S. J.; Kim, S. W. *Makrom. Chem.-Rapid Commun.* **1986**, *7*, 193-198.
- 6 Starkweather, H. W.; Avakian, P.; Fontanella, J. J.; Wintersgill, M. C. *Macromolecules* **1993**, *26*, 5084-5087.
- 7 Nijenhuis, A. J.; Grijpma, D. W.; Pennings, A. J. *Polym. Bull.* **1991**, *26*, 71-77.
- 8 Migliaresi, C.; Cohn, D.; Delollis, A.; Fambri, L. *J. Appl. Polym. Sci.* **1991**, *43*, 83-95.
- 9 Bendix, D. *Polym. Degrad. Stabil.* **1998**, *59*, 129-135.
- 10 Scott, G.; Gilead, D.; Editors *Degradable Polymers: Principles and Applications*, 1995.
- 11 Pitt, C. G.; Gratzl, M. M.; Kimmel, G. L.; Surles, J.; Schindler, A. *Biomaterials* **1981**, *2*, 215-220.
- 12 Williams, D. F.; Mort, E. J. *Bioeng.* **1977**, *1*, 231-238.
- 13 Williams, D. F. *Eng. Med.* **1981**, *10*, 5-7.
- 14 Holland, S. J.; Tighe, B. J. *Adv. Pharm. Sci.* **1992**, *6*, 101-64.
- 15 Joziassse, C. A. P.; Veenstra, H.; Topp, M. D. C.; Grijpma, D. W.; Pennings, A. J. *Polymer* **1998**, *39*, 467-474.
- 16 Mooney, D. J.; Baldwin, D. F.; Suh, N. P.; Vacanti, L. P.; Langer, R. *Biomaterials* **1996**, *17*, 1417-1422.
- 17 Chaput, C.; Yahia, L. H.; Landry, D.; Rivard, C. H.; Selmani, A. *Biomat.-Living Syst. Interact.* **1995**, *3*, 19-27.

- 18 Freed, L. E.; Marquis, J. C.; Nohria, A.; Emmanuel, J.; Mikos, A. G.; Langer, R. *J. Biomed. Mater. Res.* **1993**, *27*, 11-23.
- 19 Organ, G. M.; Mooney, D. J.; Hansen, L. K.; Schloo, B.; Vacanti, J. P. *Transplant. Proc.* **1992**, *24*, 3009-3011.
- 20 Bergsma, J. E.; Rozema, F. R.; Bos, R. R. M.; Boering, G.; Debruijn, W. C.; Pennings, A. J. *Biomaterials* **1995**, *16*, 267-274.
- 21 Cordewener, F. W.; Rozema, F. R.; Joziase, C. A. P.; Bos, R. R. M.; Boering, G.; Pennings, A. J. *J. Mater. Sci.-Mater. Med.* **1995**, *6*, 561-568.
- 22 Arvanitoyannis, I.; Nakayama, A.; Kawasaki, N.; Yamamoto, N. *Polymer* **1995**, *36*, 2271-2279.
- 23 Roper, H.; Koch, H. *Starch-Starke* **1990**, *42*, 123-130.
- 24 Lindsay, K. F. *Mod. Plast. Int.* **1989**, *19*, 110.
- 25 Chiellini, E.; Solaro, R. *Adv. Mater.* **1996**, *8*, 305-313.
- 26 Odian, G. *Principles of Polymerization*; 3rd ed.; Wiley-Interscience: New York, 1991.
- 27 Deng, X. M.; Yuan, M. L.; Xiong, C. D.; Li, X. H. *J. Appl. Polym. Sci.* **1999**, *71*, 1941-1948.
- 28 HiljanenVainio, M. P.; Orava, P. A.; Seppala, J. V. *J. Biomed. Mater. Res.* **1997**, *34*, 39-46.
- 29 Vion, J. M.; Jerome, R.; Teyssie, P.; Aubin, M.; Prudhomme, R. E. *Macromolecules* **1986**, *19*, 1828-1838.
- 30 Sawhney, A. S.; Hubbell, J. A. *J. Biomed. Mater. Res.* **1990**, *24*, 1397-1411.
- 31 Vanhoome, P.; Dubois, P.; Jerome, R.; Teyssie, P. *Macromolecules* **1992**, *25*, 37-44.
- 32 Deng, X. M.; Zhu, Z. X.; Xiong, C. D.; Zhang, L. L. *J. Polym. Sci. Pol. Chem.* **1997**, *35*, 703-708.
- 33 Kricheldorf, H. R.; KreiserSaunders, I. *Macromol. Symp.* **1996**, *103*, 85-102.
- 34 Song, C. X.; Feng, X. D. *Macromolecules* **1984**, *17*, 2764-2767.

- 35 Veld, P.; Velner, E. M.; VanDeWitte, P.; Hamhuis, J.; Dijkstra, P. J.; Feijen, J. *J. Polym. Sci. Pol. Chem.* **1997**, *35*, 219-226.
- 36 Apokan, N. K.; Yilmaz, O. K.; Baysal, K.; Baysal, B. M. *Polymer* **2001**, *42*, 4109-4116.
- 37 Gruvegard, M.; Lindberg, T.; Albertsson, A. C. *J. Macromol. Sci.-Pure Appl. Chem.* **1998**, *A35*, 885-902.
- 38 Stridsberg, K.; Albertsson, A. C. *Polymer* **2000**, *41*, 7321-7330.
- 39 Yamaoka, T.; Takahashi, Y.; Fujisato, T.; Lee, C. W.; Tsuji, T.; Ohta, T.; Murakami, A.; Kimura, Y. *J. Biomed. Mater. Res.* **2001**, *54*, 470-479.
- 40 Abe, H.; Doi, Y.; Hori, Y.; Hagiwara, T. *Polymer* **1998**, *39*, 59-67.
- 41 Hiki, S.; Miyamoto, M.; Kimura, Y. *Polymer* **2000**, *41*, 7369-7379.
- 42 Matsumura, S.; Tsukada, K.; Toshima, K. *Int. J. Biol. Macromol.* **1999**, *25*, 161-167.
- 43 Schmidt, P.; Keul, H.; Hocker, H. *Macromolecules* **1996**, *29*, 3674-3680.
- 44 Li, Y. X.; Kissel, T. *Polymer* **1998**, *39*, 4421-4427.
- 45 Kricheldorf, H. R.; Jonte, J. M.; Berl, M. *Makromol. Chem. Phys.* **1985**, *25*-38.
- 46 Dong, C. M.; Qiu, K. Y.; Gu, Z. W.; Feng, X. D. *J. Polym. Sci. Pol. Chem.* **2000**, *38*, 4179-4184.
- 47 Li, Y. X.; Nothnagel, J.; T., K. *Polymer* **1997**, *38*, 6197-6206.
- 48 Agrawal, C. M.; Athanasiou, K. A.; Heckman, J. D. In *Porous Materials For Tissue Engineering* 1997; Vol. 250, p 115-128.
- 49 Jain, R.; Shah, N. H.; Malick, A. W.; Rhodes, C. T. *Drug Dev. Ind. Pharm.* **1998**, *24*, 703-727.
- 50 Yin, M.; Baker, G. L. *Macromolecules* **1999**, *32*, 7711-7718.
- 51 Simmons, T. *Synthesis and Characterization of Aromatic Substituted Poly lactides*, Michigan State University, 2000.
- 52 Imasaka, K.; Yoshida, M.; Fukuzaki, H.; Asano, M.; Kumakura, M.; Mashimo, T.; Yamanaka, H.; Nagai, T. *Int. J. Pharm.* **1992**, *81*, 31-38.
- 53 Hrkach, J. S.; Ou, J.; Lotan, N.; Langer, R. *Macromolecules* **1995**, *28*, 4736-4739.

- 54 Barrera, D. A.; Zylstra, E.; Lansbury, P. T.; Langer, R. *Macromolecules* **1995**, *28*, 425-432.
- 55 Lee, R. S.; Yang, J. M. *J. Polym. Sci. Pol. Chem.* **2001**, *39*, 724-731.
- 56 Fujiwara, T.; Miyamoto, M.; Kimura, Y. *Macromolecules* **2000**, *33*, 2782-2785.
- 57 Fujiwara, T.; Miyamoto, M.; Kimura, Y.; Sakurai, S. *Polymer* **2001**, *42*, 1515-1523.
- 58 Chen, X. H.; McCarthy, S. P.; Gross, R. A. *Macromolecules* **1997**, *30*, 4295-4301.
- 59 Nagasaki, Y.; Okada, T.; Scholz, C.; Iijima, M.; Kato, M.; Kataoka, K. *Macromolecules* **1998**, *31*, 1473-1479.
- 60 Han, D. K.; Hubbell, J. A. *Macromolecules* **1997**, *30*, 6077-6083.
- 61 Otsuka, H.; Nagasaki, Y.; Kataoka, K. *Curr. Opin. Colloid Interface Sci.* **2001**, *6*, 3-10.
- 62 Dunn, R. L.; English, J. P.; Strobel, J. D.; Cowsar, D. R.; Tice, T. R. *Prog. Biomed. Eng.* **1988**, *5*, 149-60.
- 63 Han, D. K.; Hubbell, J. A. *Macromolecules* **1996**, *29*, 5233-5235.
- 64 Yoshioka, M.; Hagiwara, N.; Shiraishi, N. *Cellulose* **1999**, *6*, 193-212.
- 65 Chen, D. P.; Sun, B. Q. *Mater. Sci. Eng. C-Biomimetic Supramol. Syst.* **2000**, *11*, 57-60.
- 66 Bennis, J. M.; Kim, S. W. *J. Drug Target.* **2000**, *8*, 1-12.
- 67 Chen, X. H.; Gross, R. A. *Macromolecules* **1999**, *32*, 308-314.
- 68 Arvanitoyannis, I.; Nakayama, A.; Psomiadou, E.; Kawasaki, N.; Yamamoto, N. *Polymer* **1996**, *37*, 651-660.
- 69 Dittrich, M.; Hampl, J.; Soukup, F. *J. Microencapsul.* **2000**, *17*, 587-598.
- 70 Wang, Y. B.; Hillmyer, M. A. *Macromolecules* **2000**, *33*, 7395-7403.
- 71 Frick, E. M.; Hillmyer, M. A. *Macromol. Rapid Commun.* **2000**, *21*, 1317-1322.
- 72 Zalusky, A. S.; Olayo-Valles, R.; Taylor, C. J.; Hillmyer, M. A. *J. Am. Chem. Soc.* **2001**, *123*, 1519-1520.

- 73 Lim, D. W.; Choi, S. H.; Park, T. G. *Macromol. Rapid Commun.* **2000**, *21*, 464-471.
- 74 Barakat, I.; Dubois, P.; Grandfils, C.; Jerome, R. *J. Polym. Sci. Pol. Chem.* **1999**, *37*, 2401-2411.
- 75 Cadee, J. A.; De Kerf, M.; De Groot, C. J.; Den Otter, W.; Hennink, W. E. *Polymer* **1999**, *40*, 6877-6881.
- 76 D'Angelo, S.; Galletti, P.; Maglio, G.; Malinconico, M.; Morelli, P.; Palumbo, R.; Vignola, M. C. *Polymer* **2001**, *42*, 3383-3392.
- 77 Kohori, F.; Sakai, K.; Aoyagi, T.; Yokoyama, M.; Yamato, M.; Sakurai, Y.; Okano, T. *Colloid Surf. B-Biointerfaces* **1999**, *16*, 195-205.
- 78 Thakur, K. A. M.; Kean, R. T.; Hall, E. S.; Doscotch, M. A.; Munson, E. *J. Anal. Chem.* **1997**, *69*, 4303-4309.
- 79 Thosar, S. S.; Forbess, R. A.; Kemper, M.; Shukla, A. J. *J. Pharm. Biomed. Anal.* **1999**, *20*, 107-114.
- 80 Kister, G.; Cassanas, G.; Bergounhon, M.; Hoarau, D.; Vert, M. *Polymer* **1999**, *41*, 925-932.
- 81 Lee, H.; Lee, W.; Chang, T.; Choi, S.; Lee, D.; Ji, H.; Nonidez, W. K.; Mays, J. W. *Macromolecules* **1999**, *32*, 4143-4146.
- 82 Kreiser-Saunders, I.; Kricheldorf, H. R. *Macromol. Chem. Phys.* **1998**, *199*, 1081-1087.
- 83 Nieuwenhuis, J. *Clin. Mater.* **1992**, *10*, 59.
- 84 Fineman, M.; Ross, S. D., . *J. Polymer Sci.* **1950**, *5*, 259-62.
- 85 Kelen, T.; Tudos, F. *J. Macromol. Sci., Chem.* **1975**, *A9(1)*, 1-27.
- 86 Kelen, T.; Tudos, F.; Braun, D.; Czerwinski, W. K. **1990**, *191*, 1863-1869.
- 87 Bataille, P.; Bourassa, H. *J. Polym. Sci. Pol. Chem.* **1989**, *27*, 357-365.
- 88 Polic, A. L.; Duever, T. A.; Penlidis, A. *J. Polym. Sci. Pol. Chem.* **1998**, *36*, 813-822.
- 89 Leicht, R.; Fuhrmann, J. *J. Polym. Sci. Pol. Chem.* **1983**, *21*, 2215-2224.
- 90 Dong, C. M.; Qiu, K. Y.; Gu, Z. W.; Feng, X. D. *Chin. Chem. Lett.* **2000**, *11*, 815-818.

- 91 Schmidt, E.; Sachtleben, R. *Justus Liebigs Ann. Chem.* **1878**, *193*, 112.
- 92 Sinclair, R. G. *J. Macromol. Sci.-Pure Appl. Chem.* **1996**, *A33*, 585-597.
- 93 Breitenbach, A.; Kissel, T. *Polymer* **1998**, *39*, 3261-3271.
- 94 Liu, G.; Fang, Y. E.; Shi, T. Y. *Chem. J. Chin. Univ.-Chin.* **1997**, *18*, 486-488.
- 95 Thakur, K. A. M.; Kean, R. T.; Hall, E. S.; Kolstad, J. J.; Munson, E. J. *Macromolecules* **1998**, *31*, 1487-1494.
- 96 Kasperczyk, J. E. *Macromolecules* **1995**, *28*, 3937-3939.

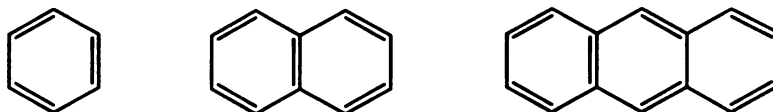
## **II. SYNTHESIS AND CHARACTERIZATION OF POLYACENES**

## INTRODUCTION

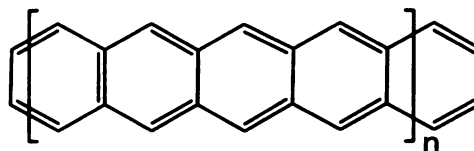
### 1. Structure of Polyacene

#### 1.1. Chemical Structure

Polyacenes are the long chain members of the family of edge-fused aromatic compounds that includes benzene, naphthalene, anthracene, and higher homologs. As shown in **Figure 1**, acenes can also be viewed as one-dimensional analogs of graphite, a ribbon taken from a single graphene sheet. The valence bond structure of true acenes is ladder-like with the rungs of the



Edge Fused Aromatic Compounds



Polyacene

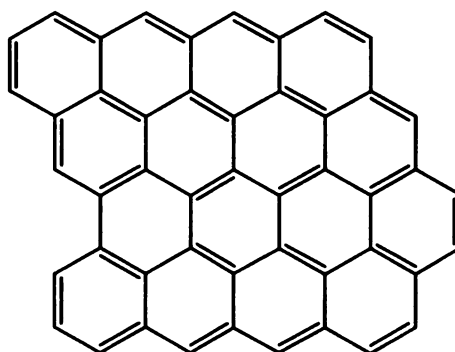


**Figure 1.** Chemical structure of polyacene.

ladder connecting two trans-polyene chains. Theory predicts that these planar polyacenes should have small band gaps ( $E_g$ ), about 0.4 eV.<sup>1</sup>

## **1.2. Electronic Structure and Properties**

### **1.2.1. Electronic structure of unsubstituted polyacene**

Long chain polyacenes have not yet been synthesized, but the electronic structure of the infinite polyacene has long been the object of theoretical interest. There are four possible configurations for polyacene<sup>2</sup> as shown in **Figure 2**. In each unit cell, there are four  $sp^2$  carbon atoms, each contributing one  $\pi$  electron and one hydrogen, thus giving rise to four  $\pi$  bands, two of which are filled, which are termed valence bands, and two unfilled bands, denoted as conduction bands. One of the most important features of the electronic structure is the band gap, the difference in energy gap between the highest energy valence band or highest occupied molecular level (HOMO) and the lowest energy conduction band or lowest unoccupied molecular level (LUMO).

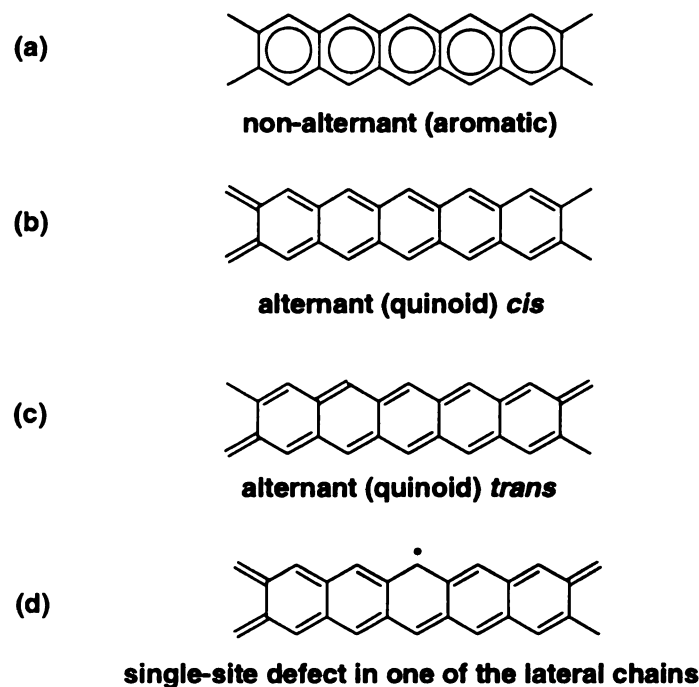


**Figure 2.** Four possible double bond configurations for polyacene.

Configuration **a** is a non-alternant structure; there is no alternation of single and double bonds and all of the bonds has the same bond length and bond energy. The band gap of this configuration is zero, the same as that of a metal. However structure **a** is not the most stable configuration because it is susceptible to a Peierls distortion that lowers the overall energy of the system by forming alternating single and double bonds. There are two principal ways for non-alternant polyacenes to undergo a periodic distortion. One leads to the *cis* conformation **b** while the other leads to *trans* conformation **c**. Configurations **b** and **c**, are termed “quinonoid” structures, and both have a larger band gap than the nonalternant polyacene. Structure **d** results from a defect breaking the pattern of alternation between the single and double bonds

in one of the lateral chains, dividing the polyacene into a *cis* structure to the left, and a *trans* structure to the right. According to our knowledge, there has been no work on such defects, which should be involved in the conduction process at low doping levels.<sup>3-6</sup>

The first group to study the electronic structure of polyacene was Salem and Longuett-Higgins in 1960.<sup>7</sup> In their pioneering tight-binding study of the electronic structure of polyacene, they concluded that the ground-state configuration of the polymer should correspond to the non-alternate structure **a**. Later, using the same calculational method, Boon pointed out that Salem and Longuett-Higgins failed to take into account the plane of symmetry that corresponds to the molecular plane. Inclusion of that symmetry gave the *trans* form **c** as the most stable structure.<sup>8</sup> Whangbho *et al.* included long-range interactions through an extended-Hückel-crystalline-orbital (EHCO) method to compute the band structure of polyacene,<sup>9</sup> and their results also pointed to the alternate *trans* form as the most stable configuration with a band gap on the order of 0.45 eV. Based on *ab initio* calculations, Cioslowski also concluded that the *trans*-distorted structure has the lowest energy per unit cell, and therefore was the most favored.<sup>10</sup> A Complete-Neglect-of-Differential-Overlap-Crystalline-Orbital (CNDO CO) study by Tanaka *et al.* agreed,<sup>11</sup> with the band gap estimated to be 0.504 eV for **c**. He also suggested that because of the small band gap, polyacene should be a promising electrical conductor.

There is no experimental data for the band gap of polyacene. The next best data are extrapolations of  $E_g$  obtained from the electron absorption

spectra of finite polyacenes. Similar plots of polyenes and polyaryls give reasonably good estimates of  $E_g$ .<sup>12</sup> A plot of the  $E_g$  for polyacene oligomers up to hexacene vs. the reciprocal of the number of rings ( $1/n$ ) in the acene is shown in **Figure 3**. The intercept with y-axis is 0.32 eV, close to the band gap predicted for the *trans* form, providing circumstantial evidence that the *trans* form is the most stable polyacene configuration.

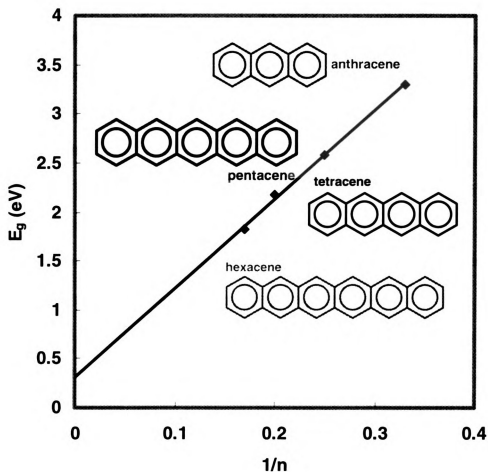


**Figure 3.** Empirical determination of the band gap ( $E_g$ ) of polyacene.

Polyacene is structurally related to polyacetylene in that it can be regarded as resulting from the lateral interaction between two parallel *trans*-polyacetylene chains. Studies of the electronic structure of polyacene and polyacetylene within a first-neighbor tight-binding Hamiltonian model led to the conclusion that the electronic structure of polyacene closely resembles that of two interacting polyacetylene chains.<sup>7</sup> However, the band gap of *trans*-polyacetylene is about 1.4 eV, much larger than that of polyacene. The fused

ring structure of polyacenes force the top and bottom polyacetylene strands to be in the same plane. Therefore the  $\pi$ -band of the top strand interacts with that of the bottom strand, decreasing  $E_g$ . Defects on a single strand polymer, such polyacetylene, degrade the conductivity. However, for a ladder or double stranded polymer such as polyacene, charge carriers have the opportunity to bypass a defect on the other polyene chain. In fact, polyacene meets simultaneously the four criteria recently enumerated by Bredas for a polymer to have a high conductivity at low voltages,<sup>13</sup> since it possesses 1) a high degree of  $\pi$ -electron conjugation, 2) a very simple structure, 3) a planar  $\pi$ -system, and 4) is expected to have a very low ionization potential associated with a very large bandwidth. Besides a high conductivity, polyacene should have a higher thermostability and mechanical strength due to its ladder structure.

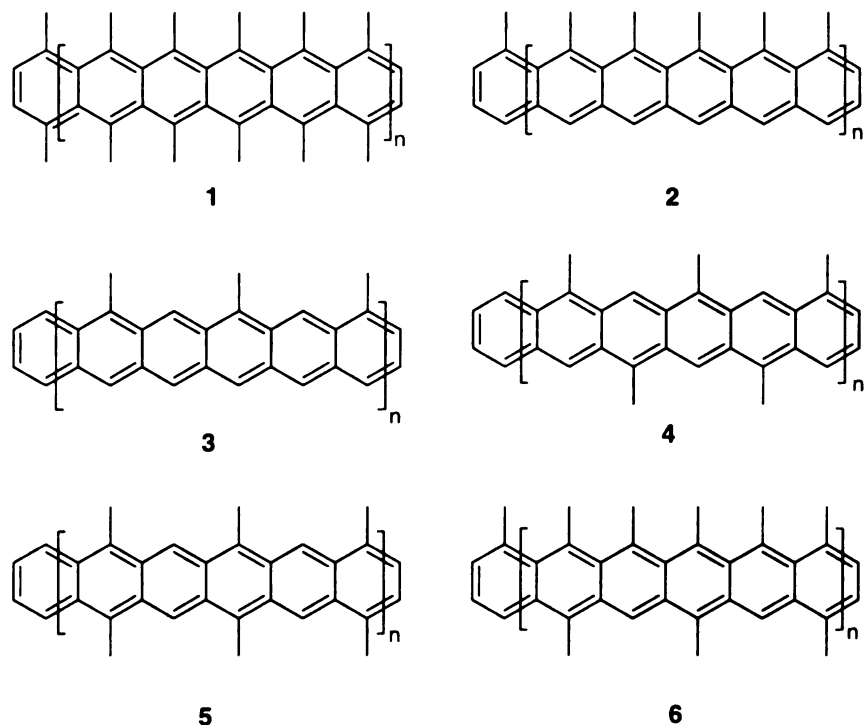


**Figure 4.** Six methyl-substituted polyacenes studied by Wang and Hou

Band gap largely determines whether the polymer is intrinsically a metal, a semiconductor or insulating material. Besides band gap, there are two other important properties that related to the electronic structure: the ionization potential (IP) and electron affinity (EA). For intrinsically semi-conducting polymers, IP and EA are measures of the ease that the polymers can be oxidized and reduced, respectively.<sup>14</sup> The theoretical value of the IP of polyacene is about 4.71 eV,<sup>11</sup> which is rather low, suggesting that polyacene can easily be doped with electron acceptors such as I<sub>2</sub> or AsF<sub>5</sub>. The EA of polyacene is predicted to be about 4.21 eV, signifying that polyacene can be readily doped with electron donors such as alkali metals.<sup>15,16</sup> As a whole, although polyacene is particularly stable, it is still very interesting as a

conductive material either by itself or after doping with electron acceptors or donors.

### 1.2.2. Electronic structures of alkyl substituted polyacene

The preparation of polyacenes is difficult, partially due to the low solubility of linear acenes. We are interested in alkylated polyacenes and how the alkyl group will affect the electronic structure and conductivity of polyacene. There are few studies on this subject. Wang and Hou<sup>17</sup> studied the electronic structure of three of the possible isomers of six different methyl substituted polyacenes (**Figures 4, 5**). Their calculation, using a one-dimensional tight-binding SCF-CO method at the CNDO/2 level, predicted that the most stable configuration of all six methyl-substituted polyacenes is either structures **b** or **c** of **Figure 2**, or in another words, like the unsubstituted polyacene, the quinoid structure is a more stable structure than the non-alternant form. Some electronic properties from their calculations are listed in **Table 1**. The band gaps of structures **2, 3**, and **6** are the largest because of the unsymmetric substitution pattern of the methyl groups in these three derivatives. From the values of ionization potential and electron affinity, both n-type and p-type doping are expected to be effective for these three methyl derivatives. The

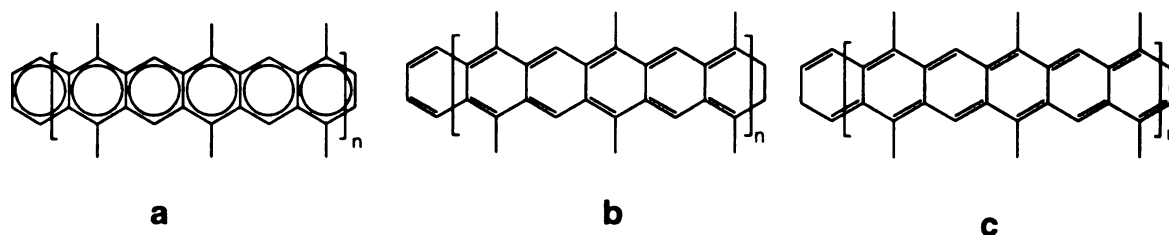


**Figure 5.** Three possible isomers of structure 5.

band gap of structure 1 is the smallest (highest symmetry) and therefore its conductivity is expected to be the highest. The band gaps of 4 and 5 are small, and therefore they too should be conductive materials, especially when n or p-doped. Thus, to achieve both structural stability and good electrical conductivity, synthetic efforts should be aimed at molecules with structures 4 or 5.

**Table 1.** Electronic properties of structures 1-6

	1	2	3	4	5	6
<b>E<sub>g</sub> (eV)</b>	1.77	4.32	2.80	2.45	2.48	3.04
<b>IP<sup>a</sup> (eV)</b>	4.75	6.11	5.61	5.23	5.23	5.41
<b>EA<sup>b</sup> (eV)</b>	2.80	1.79	2.81	2.79	2.76	2.37

a: ionization potential; b: electron affinity.

### **1.2.3. Properties of polyacenes**

The most interesting feature of polyacene is its narrow band gap, estimated at  $\sim 0.4$  eV from theory and by experimental approximation. In terms of their electronic properties, materials are usually classified as insulators (band gap  $> 5$  eV), semiconductors (band gap of 3 - 5 eV), and conductors (band gap = 0) (**Figure 6**). The most conductive materials are metals (no gap between the valence band and conducting band), where there are many free unbound electrons that make metal conductive.<sup>18</sup> Most conductive polymers can be considered to be semiconductors. For example, the  $E_g$  of polypyrrole is 3 eV,<sup>19</sup> that of polythiophene is 2 eV,<sup>19</sup> and polyacetylene, one of the first conducting polymers, has an  $E_g$  of 1.2 eV.<sup>19</sup>

## **1.3. Applications**

### **1.3.1. Electronically conductive materials**

Conducting polymers have attracted considerable attention since the 1960s due to the wide range of possible applications for these materials. In principle, conducting polymers offer two potential advantages over the traditional inorganic materials used as conductors. First, the processing of conducting polymers by molding and other plastics processing techniques is easy compared to the metallurgical processes used for inorganic materials. Second, the low densities of polymeric materials would make certain types of applications more practical and economical. Polyacenes are promising conductors due to their low band gap energy and are predicted to be highly

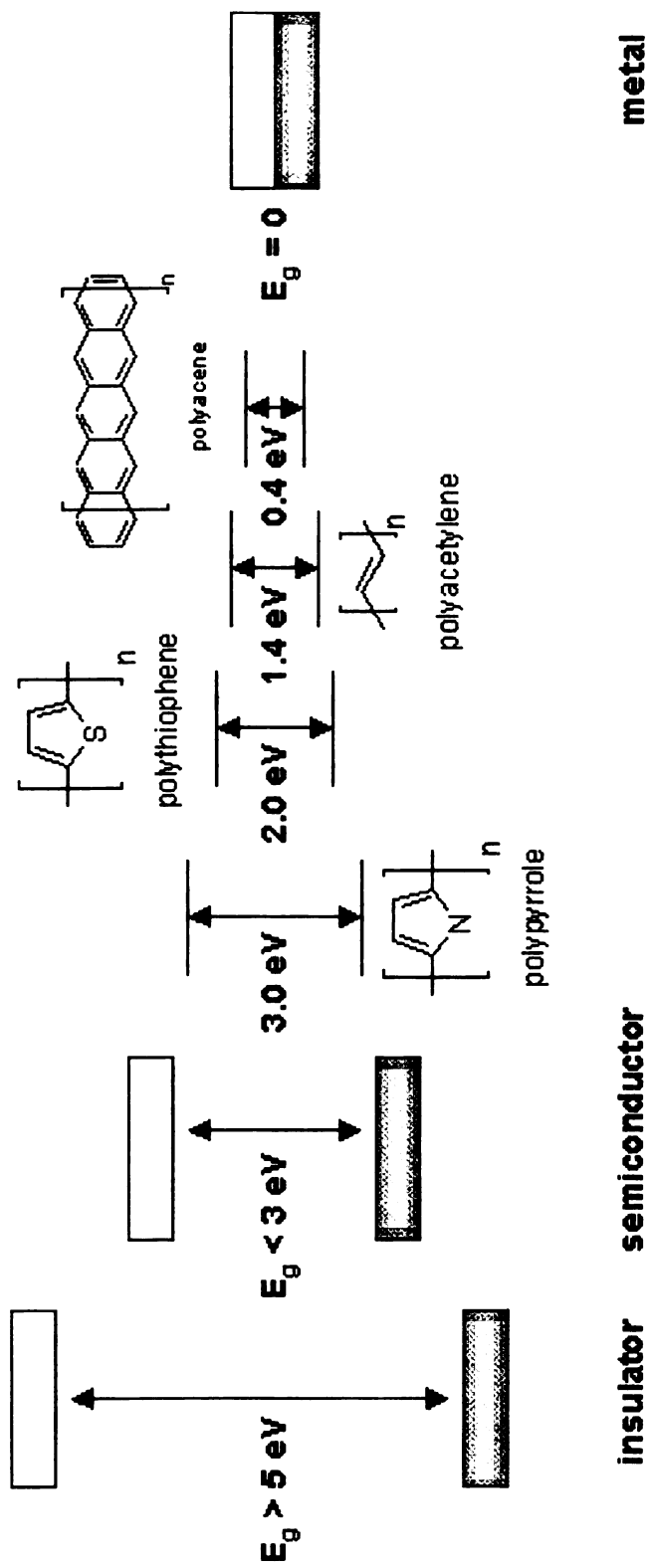


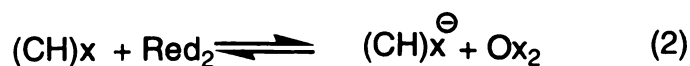
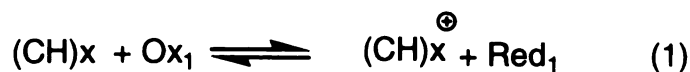
Figure 6. Band gaps of conductive materials.

have not yet been prepared,

although low molecular weight oligomers can be obtained by thermal or photo induced polymerization.<sup>20</sup>

Acene-like materials, often termed PAS (polyacenic semiconductive material), are prepared from pyrolytic treatment of phenol-formaldehyde resin,<sup>21</sup> styrene-divinyl benzene copolymer<sup>22</sup> and polyphenylene.<sup>23</sup> Most studies of the applications of acenes use PAS since it is easy to prepare from low cost starting materials. PAS has some of the attributes of graphite. It is air stable, and its electrical conductivity ranges from  $10^{-11}$ - $10^0$  S cm<sup>-1</sup>, depending on the degree of graphitization. The properties of PAS can be controlled by the pyrolysis temperature.<sup>24</sup> According to Tanaka, as the pyrolysis temperature increases, the H/C molar ratio decreases and at the same time the conductivity increases. Similar to most other conductive polymers, PAS can be readily doped and its conductivity increases by up to 11 orders of magnitude.<sup>24,25</sup> The highest reported conductivity after doping is around  $10^3$  S/cm.<sup>24</sup>

“Doping” is an important method used to improve the conductivity of a material. Doping can be accomplished through chemical and electrochemical processes. Chemical doping can be considered as a redox reaction in which neutral PAS is oxidized or reduced to polycations or polyanions.



where  $ox_1$  and  $red_2$  denote the oxidizing and reducing agents, respectively, while  $red_1$  and  $ox_2$  are their conjugates formed as a result of the charge transfer reaction.

In electrochemical doping, the doping process corresponds to the removal or addition of electrons at electrodes. Positively charged polyacene molecules are said to be p-doped, and negatively charged polyacenes are n-doped. The oxidation or reduction of polyacene requires the inclusion of an oppositely charged counter ion in the polyacene. These so-called dopant ions may be formed during the electron transfer reaction or they may be an original component of the system. In the case of electrochemical doping, the dopant ions correspond to the ions of the supporting electrolyte.

The obvious result of successful doping is an increase in the electrical conductivity. In conjugated materials, there is a finite energy that separates the HOMO (valence band) and LUMO levels (conducting band). This energy gap,



$E_g$ , corresponds to the energy that must be applied to the system to observe conductivity. Since  $E_g$  is usually  $\gg kT$ , the gap must be decreased for there to be appreciable conductivity at ambient temperatures. As shown in **Figure 7**, oxidation of polyacene (p-doping) removes an electron from the HOMO, and thus the energy of that level increases and  $E_g$  decreases. Similarly, adding an

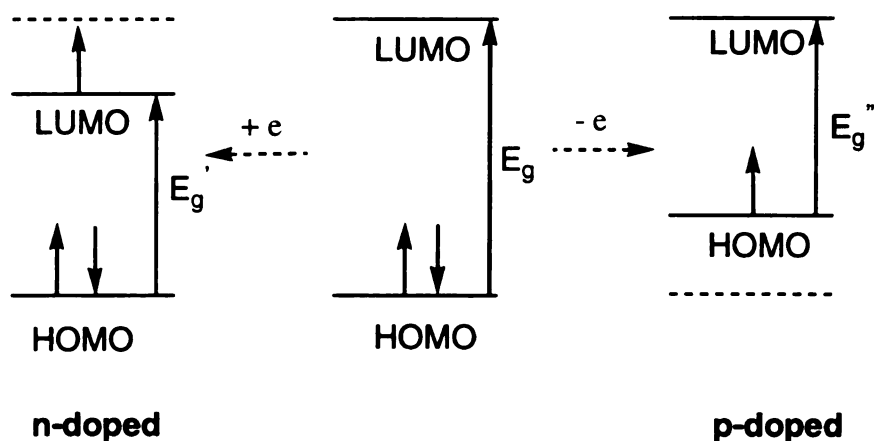


**Figure 7.** Molecular orbital energy diagram of polyacene and doped polyacene

electron to the LUMO (n-doping) lowers its energy and decreases  $E_g$ . Thus, both p and n-doping decrease  $E_g$  and increase the conductivity.

PAS can be readily doped because both structural and electrical transport studies have shown that PAS has a porous, amorphous structure.<sup>26</sup> This enables PAS to be heavily doped with high stability. Porous PAS samples have macropores and micropores.<sup>27</sup> The dimensions of the macropore is around  $10^4 \text{ \AA}$ , suggest that it may play a role in promoting the transport and diffusion of electrolyte during electrochemical doping, while the dimensions of the micropores is about  $10 \text{ \AA}$ , roughly the same as that of the dopant molecules and hence is considered to be closely related to the chemical doping and undoping processes. The pores can be reduced to around  $5 \text{ \AA}$  by controlling the specific pyrolysis temperature.<sup>27</sup> The high porosity of PAS opens the possibility of using PAS in rechargeable batteries. A detailed examination of the electrochemical doping-undoping processes in PAS samples showed that p and n-doping were reversible, a requirement for rechargeable batteries.<sup>28</sup>

### 1.3.2. Optical limiters

Optical limiters are devices that strongly attenuate intense optical beams while exhibiting high transmittance for ambient low-intensity light. These nonlinear optical devices are of significant interest for the protection of human eyes and optical sensors from intense laser pulses, which can pose considerable hazards in laboratory and field environments. The simplest limiters use materials whose optical transmittance decreases at high light levels. Molecules with weak ground-state absorptions that form strongly absorbing excited states can be used in optical limiters.<sup>29</sup>

At low fluences, the absorption of the light passing through materials follows the Beer-Lambert law:  $\log(I_0/I) = \epsilon cl$ , where  $I_0$  is the input fluence,  $I$  is

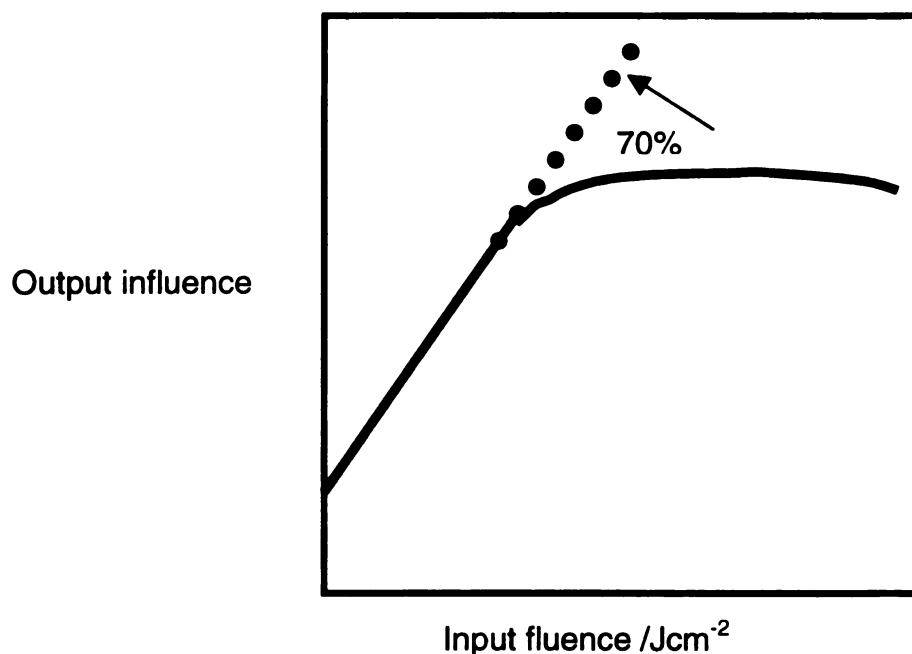


**Figure 8.** Relationship between output fluence and input fluence of a 70% transmitting solution of a polyacene-based oligomer in toluene

the output fluence, and  $\log(I_0/I)$  is the absorption. This law implies that the transmittance ( $I/I_0$ ) is independent of the input fluence. **Figure 8** shows the input-output response of a solution of a polyacene-based oligomer in toluene. At low input fluence, the transmittance obeys the Beer-Lambert law, but at high input fluence, the transmittance decreases with input fluence, an effect termed “optical limiting”. Optical limiting was first observed by Giuliano and Hess for indanthrone compounds.<sup>30</sup> Since then, many compounds were shown to exhibit optical limiting, especially conjugated  $\pi$ -electron systems such as metallophthalocyanines,<sup>31,32</sup> diphenylpolyenes,<sup>33</sup>  $C_{60}$ ,<sup>34</sup>  $C_{70}$ ,<sup>34</sup> and polyacene-based materials.<sup>35</sup> Mechanisms proposed for optical limiting include reverse saturable absorption<sup>36</sup> (non-linear absorption such as sequential single photon absorption), nonlinear scattering,<sup>37</sup> thermal blooming,<sup>38</sup> and multi-photon absorption.<sup>35</sup>

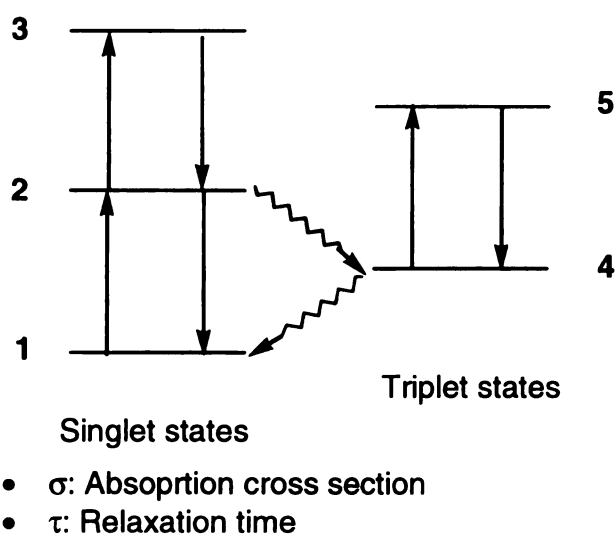


**Figure 9.** Five-level energy diagram of polyacene

The reverse saturable absorption mechanism, shown in **Figure 9**, yields a reasonable explanation for optical limiting of conjugated  $\pi$ -electron systems such as  $C_{60}$  at low input fluences ( $1\text{J}/\text{cm}^2$ ). As polyacenes also are conjugated  $\pi$ -electron systems, the optical limiting behavior of polyacenes might also be described using the five-level energy diagram shown in **Figure 9**. The initial absorption is from a ground state (level 1), typically a singlet, to an excited singlet state (level 2). This excited state can relax to its original ground state, be excited to a higher singlet state (level 3), or transfer to the lower level of a triplet state (level 4) by intersystem crossing. Triplet state absorption involves excitation from level 4 to level 5. To obtain optical limiting, the upper singlet and lower triplet must have larger absorption cross-sections ( $\sigma_s$  and  $\sigma_t$ ) than the ground state ( $\sigma_g$ ). The relaxation times between levels 3 and levels 2,  $\tau_{32}$ , and between level 5 and level 4,  $\tau_{54}$ , are extremely fast. The upper singlet level and lower triplet level should have large relaxation times ( $\tau_{21}$  and  $\tau_{41}$ ) compared with relaxation times  $\tau_{32}$  and  $\tau_{54}$ .

### **1.3.3. Electrodes for lithium ion batteries**

In 1982, a rechargeable (secondary) polymer battery was proposed in which the charge-discharge cycle corresponds to the electrochemical doping-undoping process of an electrically conductive polymer.<sup>11</sup> Since then, investigations of polymers as electrodes have shown that a serious limitation of polymer batteries stems from the chemical instability of most conductive polymers.<sup>39</sup>

Perhaps the most important application of acene-like materials is their use as anodes in lithium ion batteries. Porous PAS can be electrochemically and reversibly doped with both electron acceptor and donors, and can be used to store electrical energy.<sup>40</sup> Since porous PAS can serve as both the cathode and the anode in a rechargeable battery, two types of PAS-containing batteries

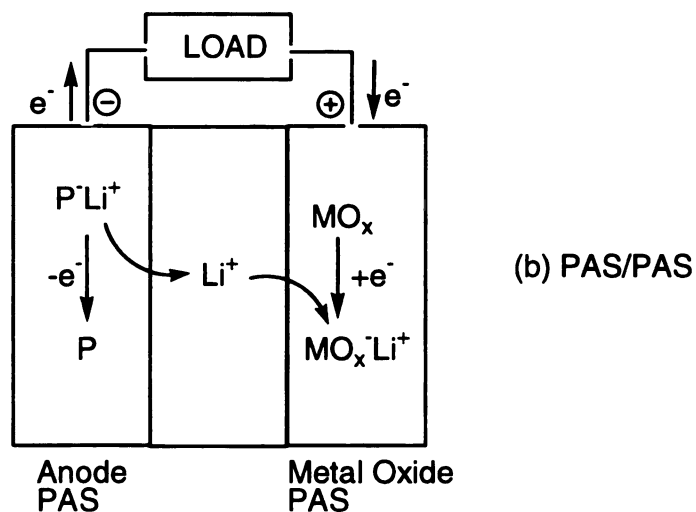
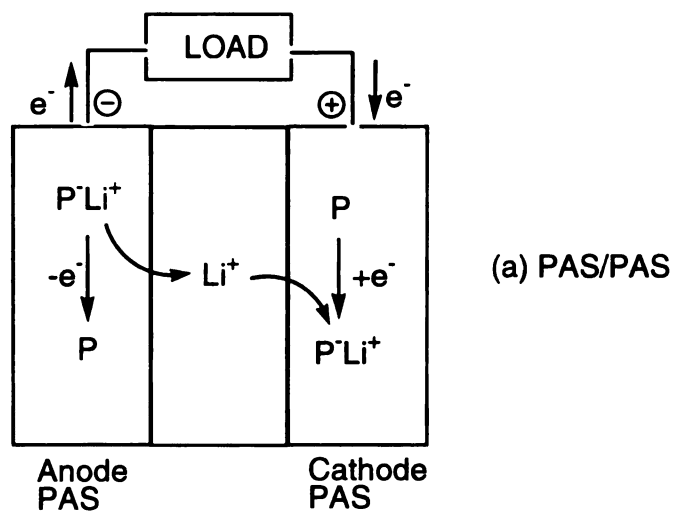


**Figure 10.** Cell structure and electrochemistry of electrodes in PAS batteries

were developed, PAS/PAS<sup>41,42</sup> and PAS/metal oxide cells.<sup>43</sup> Both types of batteries cycle well. The cell structure and electrochemistry of electrodes of these two types of batteries are shown in **Figure 10**. In the PAS/metal oxide battery, the charged cell corresponds to lithium intercalated in the carbon, and the discharge reaction is the transfer of lithium ions from the PAS anode and intercalation of the ions in the metal oxide structure. Rechargeable batteries function by repeatedly cycling Li<sup>+</sup> between the metal oxide and the PAS anode. Fully charged batteries have potentials of 3.5-4.5 volts, depending on the chemical potential of the host materials.

An important parameter of these lithium cells is their capacity, usually expressed as Ah/g, which is limited by the moles of lithium that can be inserted reversibly into the carbon. For highly crystalline graphite, the interlayer distance of graphite is 3.35 Å and it can be doped with lithium only up to the C<sub>6</sub>Li stage<sup>44</sup> with expansion of the interlayer distance to 3.70 Å as indicated in

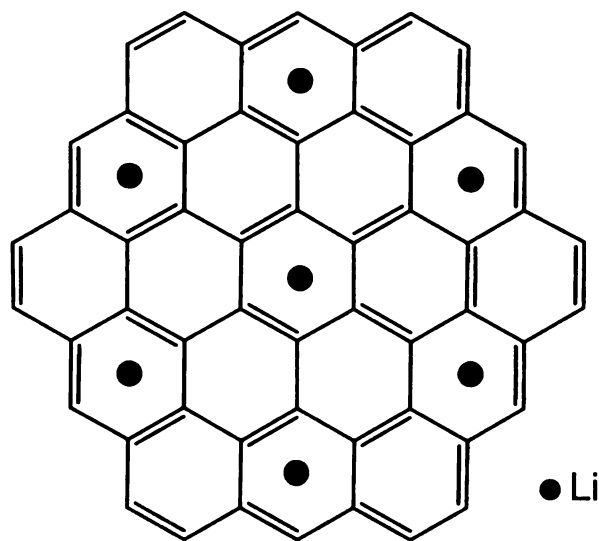


**Figure 11.** The C<sub>6</sub>Li configuration observed in the first stage Li-graphite intercalation compound (Li-GIC)

**Figure 11.**<sup>25</sup> The strong electrostatic repulsions prevent occupation at nearest neighbor sites, therefore in this state, Li atoms are located over every three benzene rings. The theoretical capacity of the fully intercalated graphite is 372 mAh/g.

Recent work by Dahn *et al.*<sup>45</sup> and Sawada *et al.*<sup>46</sup> using carbon heat-treated at low temperatures show that the C<sub>6</sub>Li ratio can be exceeded. The key to the increase in capacity seems to be the high degree of disorder found in carbon pyrolyzed at low temperature. PAS materials are one some of the most promising amorphous carbons. PAS materials have a larger interlayer distance ( $d_c = 3.7\text{-}4.0 \text{ \AA}$ ) than that of graphite ( $d_c = 3.5 \text{ \AA}$ ), and the results of electron spin resonance (ESR),<sup>47</sup> X-ray diffraction (XRD),<sup>48</sup> and <sup>13</sup>C-NMR<sup>49</sup> have been rationalized to provide the illustrative model of PAS shown in **Figure 12**.

Owing to such a loose structure, PAS materials have been intensively examined as anodes for Li-rechargeable batteries.<sup>50,51</sup> Yata reported that PAS electrodes have capacities as high as 850 mAh/g with good stability and reversibility.<sup>52</sup> Moreover, an extraordinary high capacity of 1100 mAh/g, corresponding to the molar ratio [Li]/[C] = 1/2, was reported in 1993.<sup>44</sup> The C<sub>2</sub>Li stage is obviously much more highly doped than the C<sub>6</sub>Li stage of graphite, and has an energy density on a volume basis almost equal to Li metal.

The Li storage mechanism of PAS materials has been studied extensively, but is still controversial, due to their disordered structures. A model with Li atoms located over every benzene ring (C<sub>2</sub>Li) was proposed on the basis of Li NMR measurement by Sato *et al.*<sup>53</sup> proposed at the excess

capacity corresponds to cluster-like lithium doping that fills the void space in the disordered carbon,<sup>54</sup> while Dahn *et al.* argued that lithium can also be located at the edges of the graphite sheets.<sup>55</sup> The latter view is supported by experiments that show that the increased capacity is correlated with the hydrogen content of the electrode,<sup>45</sup> as well as by recent calculations.<sup>56</sup> Yata *et al.* studied the electronic and geometrical structures of Li-doped PAS using a semiempirical molecular orbital (MO) method and studied the Li storage mechanism and capacity in detail. According to their calculation, Li can edge intercalate between carbon layers of PAS, as well as absorb on the surface and planes of carbon substrates. Since the maximum ratio of intercalating Li is only C<sub>6</sub>Li, it is the Li absorbed on the surface and peripheral edges that push the capacity to as great as C<sub>2</sub>Li.

Since the charge-storing capacity is highest when the residual hydrogen content is between 0.15 and 0.30 H atoms per C atom, it is important to be able to prepare acene-like structures with a substantial fraction of edges. Current routes to carbons use petroleum pitches or phenolic resins as the base material, and when pyrolyzed, these materials give partially graphitized structures. However, the high temperatures needed for the pyrolysis allows little control of the acene-like structural elements that are the precursors to graphite. In contrast, if elements of the acene structure can be designed into the starting material, it should be possible to obtain partially graphitized structures at low temperatures that retain some memory of the chemical

structure before pyrolysis. In principle, PAS could be prepared that requires no thermal treatment for it to be useful electrode materials.

However, one disadvantage of PAS materials is that there often is a large capacity loss in the first charge-discharge cycle in rechargeable Li ion batteries, and there is a large hysteresis in charge-discharge potentials.<sup>50</sup> PAS materials with higher hydrogen contents usually have higher capacities but show larger hysteresis. This suggests that the hysteresis is caused by Li binding at the hydrogen terminated edges of graphene fragments. Bonding changes in the host have been previously shown to cause hysteresis in electrochemical measurements.<sup>57</sup> If the inserted Li binds to an edge carbon atom, then the carbon-carbon bond changes from  $sp^2$  to  $sp^3$ , which would in turn, cause the hysteresis.

Besides hysteresis, PAS materials usually exhibit capacity loss on the first charging cycle. The irreversible capacity observed in the first discharge step is defined as the difference in capacity between the first discharge and the subsequent charge. The irreversible capacity is usually ascribed to the formation of a solid electrolyte interface (SEI) layer on the carbon surface due to the decomposition of electrolyte. Lithium can also irreversibly react with surface functional groups such as hydroxyl and carboxyl groups. Since PAS materials are highly disordered, the samples likely have many defect sites where surface oxides may form. Thus PAS or polyacene-like materials offer the highest capacities found thus far in anode materials, but more work is

needed to verify the reported values of specific energy, improve the discharge curves, and reduce the irreversible capacity lost on first charging.

### **1.3.3. Capacitors**

The high capacities and deep-discharge cycle of PAS makes it an attractive material for capacitors.<sup>58,59</sup> Yata *et al.* studied PAS-based capacitors and found that their capacities were much higher than that of conventional electric double-layer capacitors (EDLCs) which uses activated carbon as the electrode.<sup>60</sup> A PAS capacitor can maintain more than 70% of the initial capacity even after 100,000 cycles. Moreover, this capacitor can be charged and discharged in a few minutes as well as at lower rates. PAS capacitors are produce in coin-type and cyclindrical geometries, the coin-type capacitors are currently used for memory back-up in electrical and communications equipment, while the cyclindrical geometry provides higher power densities and is used as back-up power for starting the drive parts of electric equipment.

### **1.4. Synthetic Approaches to Polyacenes**

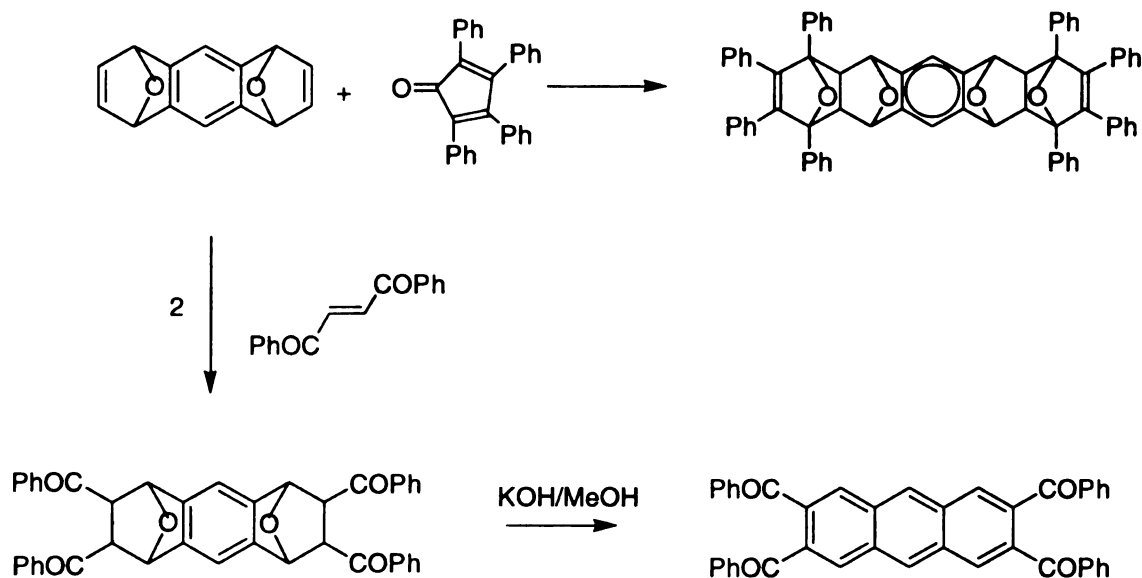
Efficient methods for the preparation of well-defined polyacenes are not yet known. Problems with stability and solubility have stymied the synthesis of long chain acenes, although oligomers containing several rings have been synthesized. Efforts to synthesize polyacenes have been reported,<sup>61,62</sup> however insolubility, low purity, and crystallinity prevent these materials from being directly compared to the theoretical work on idealized infinite polyacene chains.

Unsubstituted linear polyacenes up to heptacene have been synthesized.<sup>63</sup> As the length of the polyacene chain increases, the chemical reactivity also increases. Materials become so sensitive toward photooxidation that polyacenes higher than pentacene and hexacene must be handled under nitrogen. Heptacene has never been obtained in a pure state. The high reactivity of acenes shows up in acene oligomers such as anthracene, where oxidation and halogenation at the 9,10-positions is facile. Similarly, an infinite polyacene becomes unstable toward formation of two  $sp^3$  carbons flanked by two polyacene chains. Not surprisingly, the higher acenes have proved too reactive to isolate under ordinary conditions, and only derivatives of octacene,<sup>64,65</sup> nonacene,<sup>66</sup> and undecacene<sup>67</sup> have been prepared.

There are two general synthetic routes to polyacenes: “topochemical polymerization”, and “Diels-Alder polyadduction.

### 1.4.1. The Diels-Alder approach

Diels-Alder reactions have been employed in the stepwise construction of compounds with molecular architectures that resemble ladders, such as polyacenes.<sup>68-74</sup> An example of this strategy that of Clardy,<sup>72</sup> shown in **Scheme 1**, is the reaction of a dienophile with an electron rich diene. Changing the nature of the olefin changes the end groups of the acene oligomer (**Figure 13**). Although the reported yields are very high, these reactions cap the acene, and do not allow for further extension of the polyacene chain. Thus, only anthracene derivatives were prepared. As shown in **Scheme 2**, Mullen *et al.* used benzyne (generated with 1,2-dibromobenzene and *n*-butyllithium at -40 °C) as the dienophile to synthesize higher acenes.<sup>75</sup> The key to the synthesis is to mask the center ring using a group that can be later eliminated via a retro Diels-Alder reaction to give the fully conjugated acene. Due to the driving force



**Scheme 1.** Polyacene oligomer synthesized by via Diels-Alder adduction

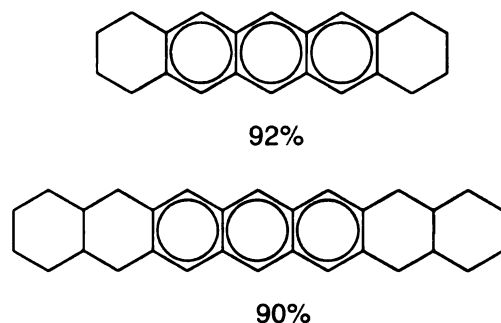
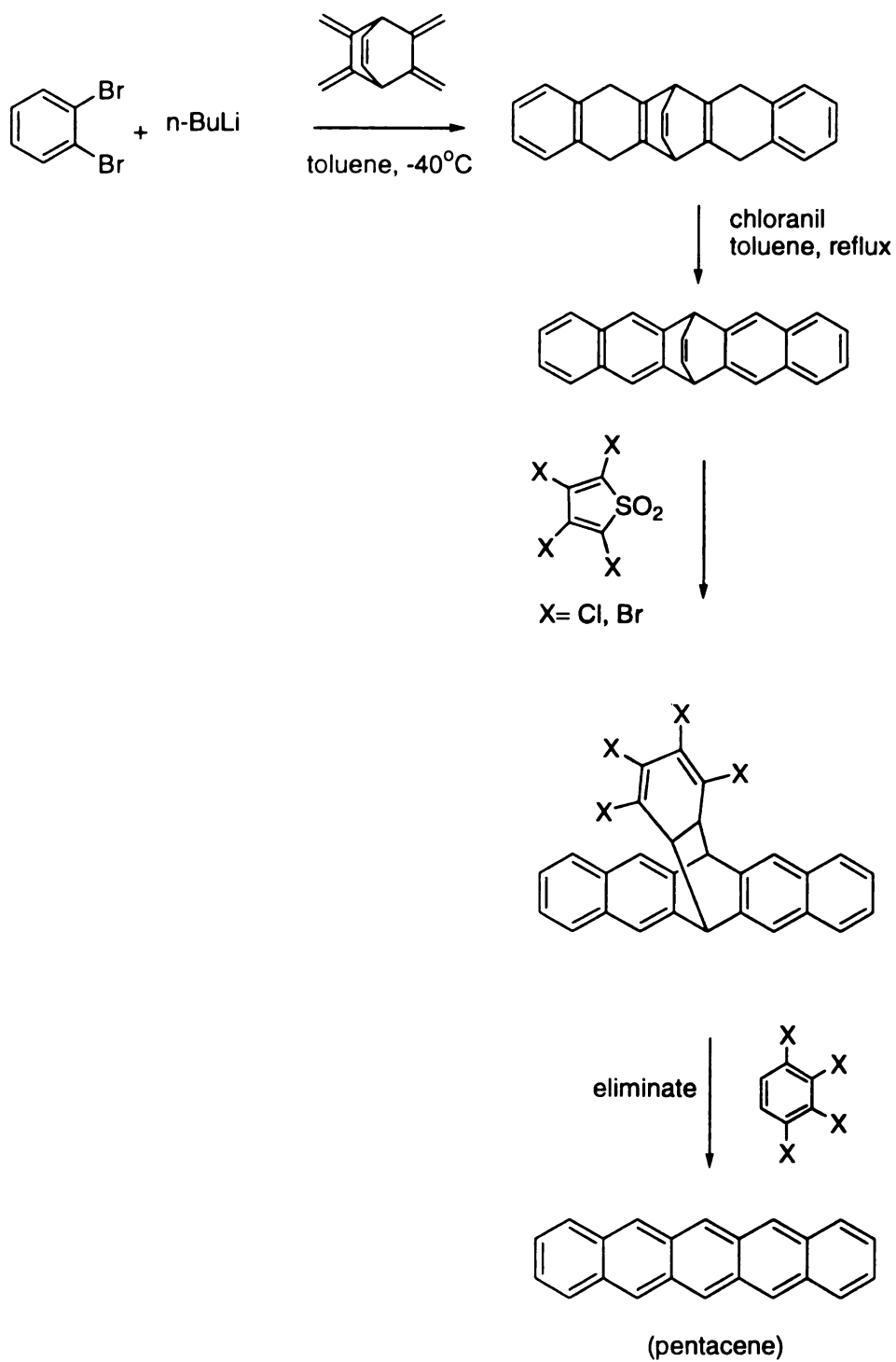


**Figure 13.** Other acene derivatives made by Clardy's group

of forming benzene derivatives, this reaction takes place at low temperatures (70 °C) to give the pentacene product in 90 % yield. However, the same approach failed when applied to nonacene. Because the anthracene unit in the nonacene precursor itself can act as a diene, the reaction of the nonacene precursor and tetrachlorothiophenedioxide and its bromo homolog turned out to be very complicated.

Diels-Alder reactions have also played an important role in the synthesis of various acene-related species, such as cyclacene<sup>73,76</sup> and spiro acenes.<sup>68</sup> Thus, we see that while the Diels-Alder reaction, in principle, allows for the stepwise growth of polyacenes, its use has been limited to heptacene and shorter acenes. This approach is probably not a practical method for synthesizing long chain linear polyacenes.



**Scheme 2.** Polyacene oligomer synthesized via Diels-Alder addition and retro Diels-Alder elimination.

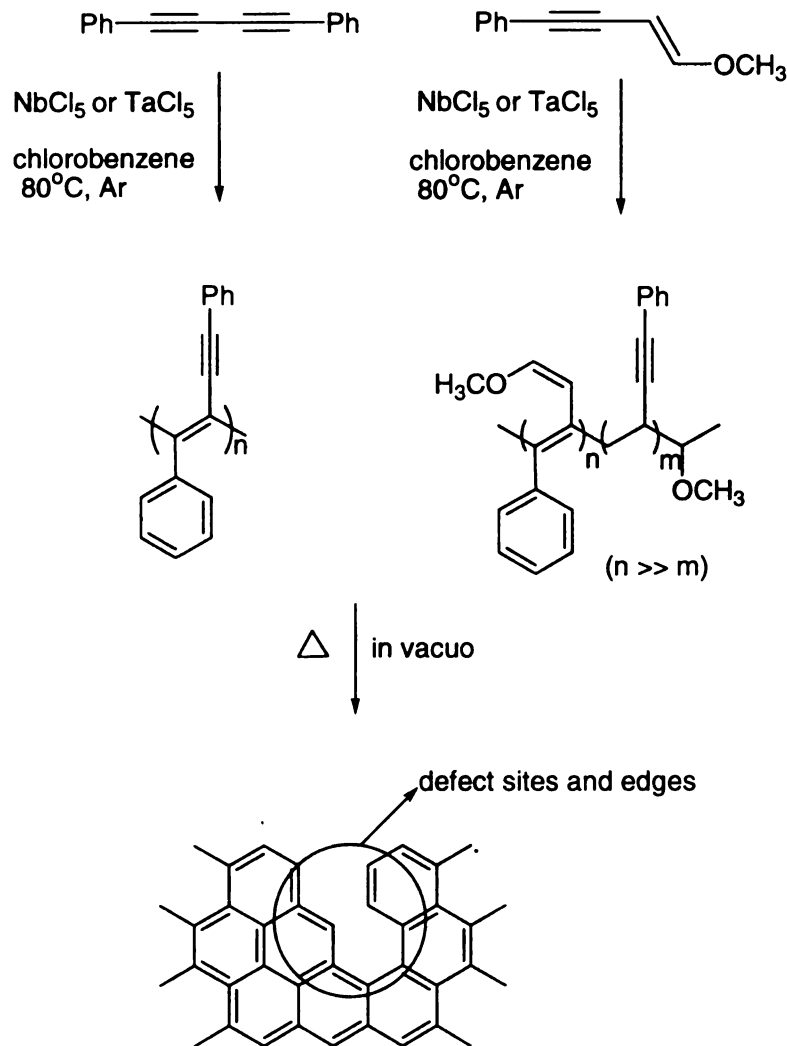
### 1.4.2. Topochemical polymerizations

Besides sequential Diels-Alder reactions, the other common approach to polyacene synthesis is through topochemical polymerization of butadiyne<sup>77-79</sup> or 1-buten-3-yne<sup>70,78,79</sup> derivatives followed by pyrolysis. As shown in **Scheme 3**, metathesis polymerization of the diyne is selective for the 1,2 pathway. Triple bonds are more reactive than the double bonds in coordination polymerization<sup>80</sup>, and thus the acetylene is the major reaction site during metathesis polymerization of 1-buten-3-yne derivatives. The pyrolysis step is a high-temperature polycondensation that yields graphite-like pyropolymers. The pendant substituents on the pre-polymers not only suppress the gasification of the polymer itself, they also control the morphology of the final pyropolymers. Bulky substituents, such as phenyl group, are thought to hinder the development of polymer order during pyrolysis, and therefore cause the final graphite-like polymer to contain defect sites.

Compared to the Diels-Alder approach, topochemical polymerization provides much higher molecular weight polyacenes, but with poor control over the configuration and morphology of the final product. More important, most of the pyrolysis products resemble two-dimensional graphite rather than the one-dimensional linear polyacenes.

### 1.4.3. Acene-like materials

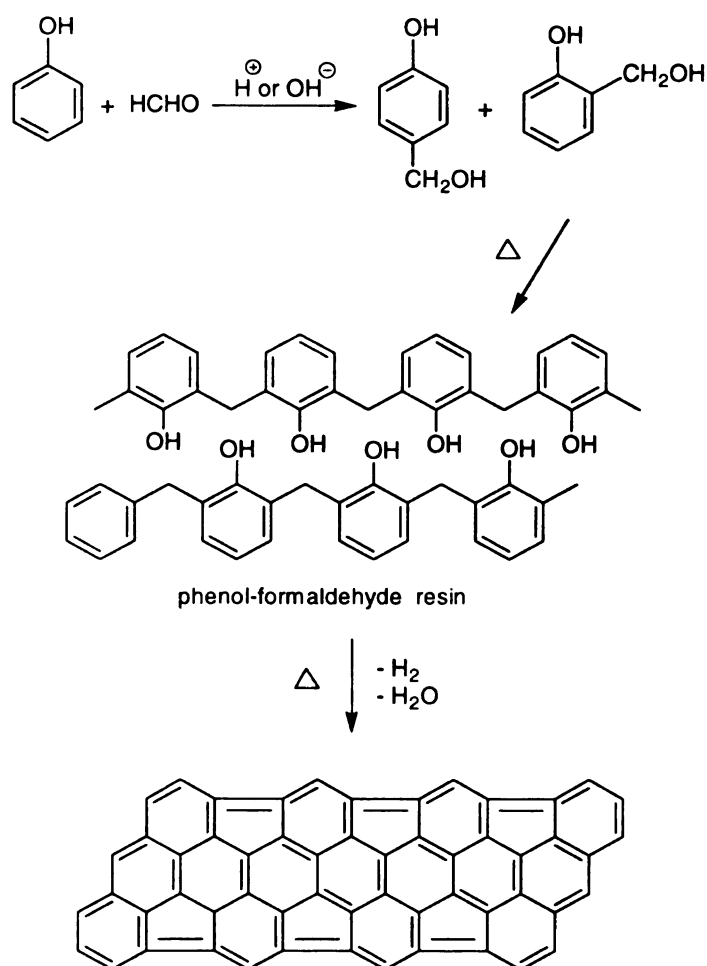
Although polyacene has promising properties, the synthesis of perfect linear polyacenes is very difficult. Despite various attempts to synthesize polyacenes, this intriguing, fully unsaturated ribbon polymer is still unknown. One solution to this problem is the preparation of acene-like products from well-commercialized starting materials. These materials are termed “polyacenic semiconductors” or PAS, and are the materials that are studied in most



**Scheme 3.** Topochemical polymerization of butadiyne and 1-buten-3-yne to prepare polyacene

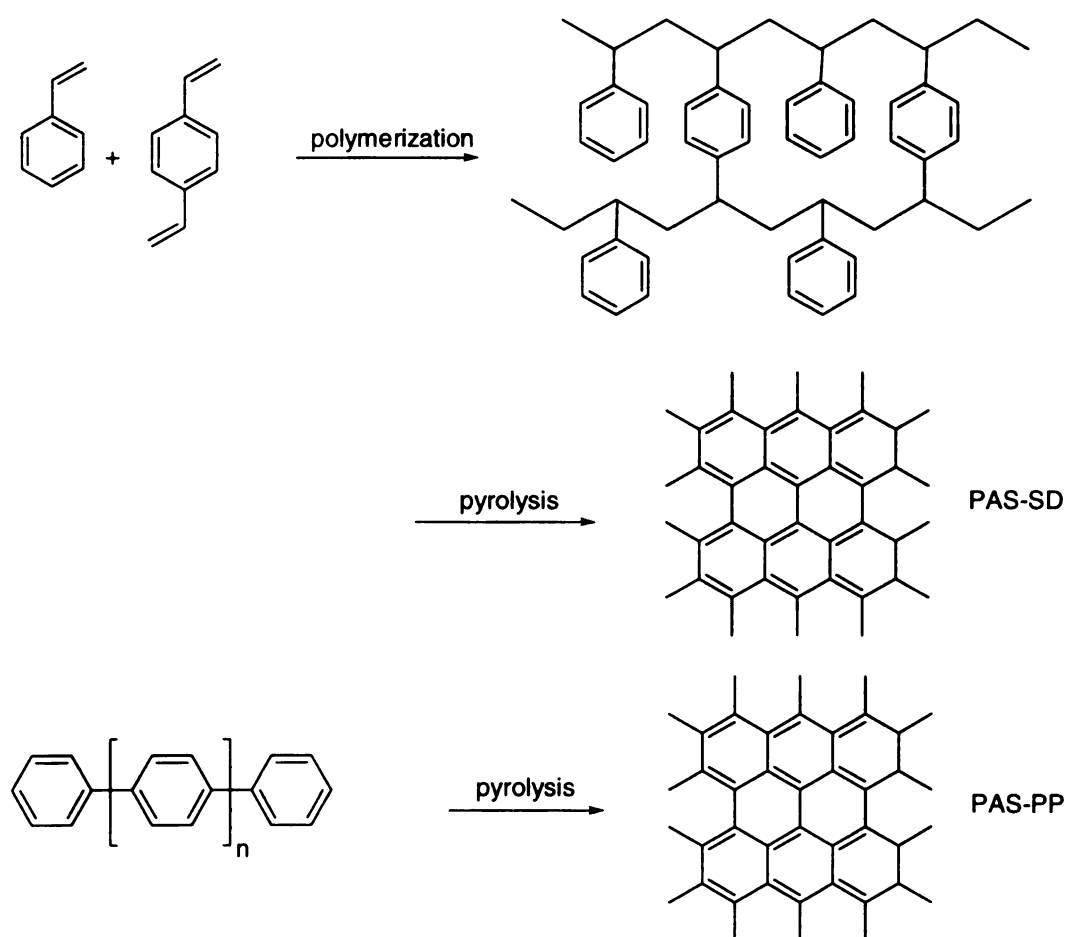
application-based research.

Among the acene-like materials, the most well-studied and broadly-utilized is the pyrolyzed product from phenol-formaldehyde resin, which is named "PAS-PF". As shown in **Scheme 4**, porous PAS-PF is prepared by the pyrolysis of phenol-formaldehyde resin molded with  $\text{ZnCl}_2$ .<sup>24</sup> The  $\text{ZnCl}_2$  serves as the pore-forming agent, resulting in open pores that grow into a three-dimensional network structure in the cured material. This leads to a loose structure that can be easily



**Scheme 4.** Preparation acene-like material from phenol-formaldehyde resin.

doped with bulky dopants. To prepare PAS-PF, a mixture of resole-type phenolic resin,  $\text{ZnCl}_2$  and water was heated to  $100\text{ }^\circ\text{C}$  for 1 hr. The cured resin was further heat-treated at  $500\text{-}800\text{ }^\circ\text{C}$  in a non-oxidative atmosphere. The reaction is essentially a carbonization process consisting of dehydration and dehydrogenation, the degree of which can be controlled by the temperature applied.  $\text{ZnCl}_2$  was removed by washing with water at the last step. As shown in **Scheme 5**, similar acene-like materials can be produced by pyrolysis of styrene-divinylbenzene copolymers (PAS-SD) and poly(*p*-phenylene) (PAS-



**Scheme 5.** Acene-like material synthesized from styrene-divinylbenzene copolymers and poly(*p*-phenylene)



materials.

One common approach to solve the solubility problem is by use of soluble precursors of acenes, which can be converted to the desired acenes after processing.<sup>75,82</sup> **Scheme 2** shows an example of this approach, the synthesis of pentacene. A retro Diels-Alder reaction is an appropriate step for the solid state transformation of a precursor to the product because a small, volatile molecule (benzene in this case) is eliminated and can be easily removed from the reaction medium.

It is well known that solubility problems can be solved by introducing alkyl substituents to  $\pi$ -conjugated aromatic compounds,<sup>75</sup> and a similar strategy can be applied to improve the solubility of polyacene. However, there is no general method for the synthesis of highly substituted alkyl-acenes<sup>83-86</sup> Nakajima *et al.*<sup>71</sup> recently reported a general method for the synthesis of alkyl-substituted pentacenes and naphthacenes by the homologation scheme shown in **Scheme 6**.

## 1.6. Characterization of Polyacenes

The intractability of polyacenes severely limits the ability to accurately determine structures of polyacenes. UV/VIS, near IR, elemental analysis, X-ray diffraction, Raman, and other spectroscopic methods have been used to analyze the polyacene network.

### 1.6.1. X-ray diffraction

There are several X-ray diffraction studies of polyacenes, with most of the analyses performed on polyacenic semiconductive materials derived from PAS-PF, a pyrolyzed phenol-formaldehyde resin. Sugawara *et al.* studied the graphitization of these materials<sup>86</sup> and Ban *et al.* reported X-ray studies of alkali metal intercalation in amorphous carbon.<sup>87</sup> Tanaka *et al.* studied porous PAS-PF,<sup>48,52</sup> and the X-Ray results from pristine samples pyrolyzed from 25 to 935 °C show two broad peaks in all samples, indicating that the PAS-PF samples are essentially amorphous. As the pyrolysis temperature ( $T_p$ ) increases, peaks around  $2\theta = 20-24^\circ$  shift to larger angles and appear to evolve toward the (002) peak of graphite. Thus the samples have a layered structure that becomes increasingly graphitized as  $T_p$  increases. The interlayer distances,  $d_c$ , and the crystallite size,  $L_c$ , were derived from the (002) band. The range of  $d_c$  values for PAS (4.42 Å to 3.76 Å) is considerably larger than that of graphite (3.35 Å), and  $L_c$  remains small (8-9 Å) for all the pristine samples, indicating that PAS lacks long range order.

### 1.6.2. <sup>13</sup>C NMR

Solid state NMR has also been used to characterize undoped and doped PAS-PF derived from pyrolyzed phenol-formaldehyde resin. The NMR spectra clearly indicate that heat-treatment converts the resin from a phenolic resin to a polyacenic material by the decrease in peaks at 150 ppm, assigned to aromatic carbons bonded to the hydroxy group, and at 40 ppm which corresponds to the methylene carbons. Ando *et al.*<sup>88</sup> obtained dipolar-

dispersion (DDPh)/MAS NMR spectra of PAS-PF. From an analysis of the data and decomposition of overlapping peaks by computer-aided curve fitting, they assigned each peak to different carbons of the polymer. These experiments are hampered by the complexity of the pyrolyzed structure, making it difficult to make more than basic structural assignments.

### **1.6.3. ESR (Electron Spin Resonance)**

The ESR studies of PAS-PF mainly focus on the doping and undoping processes.<sup>89,90</sup> The ESR peak seen in pristine samples is believed to result from carbon-centered radicals associated with structural defects. When acenes are oxidized or reduced, the ESR spectral lines broaden, probably due to the formation of charged sites on the polyacene structure.<sup>90</sup> Ando *et al.*<sup>89</sup> studied Li-doped PAS-PF which was used as an anode of the Li rechargeable batteries. Initially, the line width increased, but a narrow spike showed up in the ESR spectrum of heavily doped PAS (Li doping amount  $x > 50\%$ , for  $C_2Li$ ,  $x = 50\%$ ). This spike is due to the formation of  $Li^\circ$  clusters, which is consistent with  $C_2Li$  being the highest doped stage for PAS.

### **1.6.4. UV and fluorescence**

Among all the analytical methods, UV/VIS and fluorescence studies should provide the most straightforward characterization of the electronic structure of polyacenes. The presence of polyacene units can be detected by their strong absorbance through the visible region and into the near IR. The absorbance of a perfectly linear polyacene is expected to tail into the IR region. For soluble acene materials, the distribution of the length of acene segments

can be estimated by comparing the UV and fluorescence spectra<sup>91</sup> with those of known linear oligomers. For PAS materials, UV and fluorescence are not applicable due to the poor solubility of these materials.

#### **1.6.5. Raman spectroscopy**

Raman spectroscopy is an important technique for the characterization of polyacene networks. Although no Raman spectra of authentic linear acenes have been reported, Raman spectroscopy is widely used to characterize polyacene-like material such as PAS-PF.<sup>92</sup> Two peaks in the Raman spectrum are used for diagnostic purposes, one at  $1575\text{ cm}^{-1}$  assigned to the  $E_{2g}$  vibration mode of the crystalline graphite, and a second at  $1355\text{ cm}^{-1}$  from the  $A_{1g}$  vibration from amorphous portions of graphite. The intensity of the latter band is inversely proportional to the crystallite size and also allows an estimation of the crystallite size in the surface layer of any carbon sample.

## **EXPERIMENTAL**

### **2.1. General**

Tetrahydrofuran (THF) and toluene were first distilled from powdered calcium hydride under nitrogen, then from sodium benzophenone ketyl under nitrogen. Unless otherwise specified, ACS reagent grade starting materials and solvents were used as received from commercial suppliers without further purification.  $^1\text{H}$  and  $^{13}\text{C}$  NMR spectra were measured using a Varian Gemini-300 spectrometer at 300 MHz. All samples were run at room temperature in  $\text{CDCl}_3$ . The chemical shifts were calibrated using residual  $\text{CHCl}_3$  and reported in ppm ( $\delta$ ) relative to tetramethylsilane. Infrared spectra were obtained from KBr pellets under nitrogen at room temperature on a Nicolet Magna-IR 550 Fourier Transform IR spectrometer. A Hitachi U-4001 UV-visible spectrometer was used to obtain the UV-visible spectra of cyclohexane solutions of the polymers. The spectra of Raman was taken by exciting the sample at 633nm on a Holoprobe Raman Spectrometer. Polymer molecular weights were determined by gel permeation chromatography (GPC) using a PLgel 20 $\mu$  Mixed A column with THF as the eluting solvent at a flow rate of 1 mL/min, a Waters R401 Differential Refractometer detector at room temperature, and a Varian 2050 Variable Wavelength detector set at 254 nm. Monodisperse polystyrene standards were used to calibrate the molecular weights. The concentration of the polymer solutions used for GPC measurements was 1 mg/mL. Thermogravimetric analyses (TGA) were performed in nitrogen and air atmospheres at a heating rate of 10  $^\circ\text{C}/\text{min}$  on a Perkin-Elmer TGA 7 instrument.

## 2.2. Synthesis

***bis(methoxymethyl)benzenes.*** A mixture of hexanes/MeOH (1:1, 50 mL) was added drop-wise to a slurry of sodium hydride (NaH, 1.4 g, 57 mmol) that had been rendered oil-free by washing with hexanes. The solution was stirred at room temperature until all of the NaH reacted. The sodium methoxide solution was transferred *via* cannula to a solution of the *bis(bromomethyl)benzene* (6.0 g, 23 mmol) in hexanes (100 mL). The mixture was gently refluxed for 3 hr, during which the color of the solution turned slightly tan. After cooling, the solution was washed with water (3 x 50 mL). The organic layer was passed through a short pad of Celite, and dried with MgSO<sub>4</sub>. The solvent was removed under reduced pressure and the products were purified by vacuum distillation to yield clear oils.

**1,2-*bis(methoxymethyl)benzene.*** Prepared in 91% yield (3.45 g); bp 98 °C/25 mm Hg (lit.<sup>93</sup> 40-45 °C/2 mm Hg). <sup>1</sup>H NMR (CDCl<sub>3</sub>) δ 3.35 (s, 6H), 4.5 (s, 4H), 7.2-7.35 (m, 4H).

**1,3-*bis(methoxymethyl)benzene.*** Prepared in 85% yield (3.21 g); bp 110 °C/25 mm Hg (lit.<sup>93</sup> 25-130 °C/2 mm Hg). <sup>1</sup>H NMR (CDCl<sub>3</sub>) δ 3.35 (s, 6H), 4.4 (s, 4H), 7.25-7.4 (m, 4H).

**1,4-*bis(methoxymethyl)benzene.*** Prepared in 89% yield (3.36 g); bp 105 °C/25 mm Hg (lit.<sup>93</sup> 55-60 °C/2 mm Hg). <sup>1</sup>H NMR (CDCl<sub>3</sub>) δ 3.35 (s, 6H), 4.4 (s, 4H), 7.4 (s, 4H).

**Polymerization of the *bis(methoxymethyl)benzenes.*** A 100 mL round bottomed flask was charged with the *bis(methoxymethyl)benzene* (1.0 g)

and cooled in an ice bath. Concentrated sulfuric acid (3 mL) was added, and the mixture was stirred at 0 °C for 36 hr. The resulting suspension was washed with 20 % (w/w) sodium hydroxide solution (3 x 25 mL), water (3 x 25 mL), and rinsed with ether (3 x 50 mL). The collected solid was dried overnight at 120 °C under vacuum to yield 0.44 g (72%) of a finely powdered, tan solid.

**Chemical dehydrogenation of polyacenic networks.** The tan powder (0.270 g) from the acid catalyzed polymerization of the *bis*(methoxymethyl) benzene, 2,3-dichloro-5, 6-dicyano-1, 4-benzoquinone (DDQ, 1.20 g, 5.3 mmol), and xylenes (60 mL) were added to a 100 mL round bottomed flask. The yellow DDQ immediately turned dark violet. The flask was fitted with a water condenser and purged with nitrogen. After refluxing for 48 hr, the suspension was collected *via* filtration and the solid was repeatedly washed with benzene, ethanol, water, and acetone until the filtrate was colorless. The solid was dried at 120 °C under vacuum for 3 hr to give 0.25 g of a tan powder.

**1,4-*bis*(bromomethyl)-2,5-dibromobenzene.** Into a 500 mL round-bottom flask was added 2,5-dibromo-*p*-xylene (20.0 g, 0.076 mol), N-bromosuccinimide (28.4 g, 0.160 mol), a catalytic amount of benzoyl peroxide (10 mg), and carbon tetrachloride (CCl<sub>4</sub>, 250 mL). The flask was fitted with a water condenser and the system was flushed with argon. The reaction was initiated by a 250 W sunlamp. The solution was gently refluxed until the succinimide floated atop the mixture (1-2 hours). Upon cooling, the succinimide was removed by filtration and rinsed thoroughly with CCl<sub>4</sub>. The combined organic layers were washed with water (3 x 50 mL) and dried with

MgSO<sub>4</sub>. Filtration and evaporation of the solvent *in vacuo* resulted in a slightly yellow solid. Repeated recrystallization from ethanol yielded 10.6 g (33%) of 1,4-*bis*(bromomethyl)-2,5-dibromobenzene as a fine white powder. mp 156-157 °C (lit.<sup>94</sup> 161-162 °C). <sup>1</sup>H NMR (CDCl<sub>3</sub>) δ 7.65 (s, 2H), 4.50 (s, 4H).

**1,4-*bis*(methoxymethyl)-2,5-dibromobenzene.** Over a period of one hour, anhydrous methanol (5 mL) and hexanes (10 mL) were added drop-wise *via* a pressure equalizing addition funnel to an argon filled 100 mL round bottomed flask containing a stirred solution of oil-free sodium hydride (2.1 eq, 0.051 mol) in 25 mL hexane. After the addition was complete, the flask was fitted with a reflux condenser and the solution was gently refluxed for an additional hour until all of the sodium hydride reacted. Upon cooling, the solution was transferred *via* cannula to argon filled 250 mL round bottomed flask containing 1,4-*bis*(bromomethyl)-2,5-dibromobenzene (10.30 g, 0.024 mol) dissolved in warm hexanes (150 mL). The mixture was gently refluxed for 3-4 hours. The cooled reaction mixture was poured into a separatory funnel containing 100 mL dilute HCl (1N) and extracted with dichloromethane (CH<sub>2</sub>Cl<sub>2</sub>). The combined organic layers were dried with magnesium sulfate, filtered, and the solvent evaporated under reduced pressure to yield the crude product as a yellow solid. Recrystallization from ethanol yielded 6.64 g (84%) of 1,4-*bis*-(methoxymethyl)-2,5-dibromobenzene as a pale yellow crystalline solid. mp 68.5-70 °C (lit.<sup>94</sup> 71-72 °C). <sup>1</sup>H NMR (CDCl<sub>3</sub>) δ 7.61 (s, 2H), 4.44 (s, 4H), 3.45 (s, 6H).

**1,4-bis(methoxymethyl)-2,5-dialkylated-benzenes.** To a round bottom flask were added an alkene (5.5 mmol), dry THF (5 mL) and then a solution of 9-BBN (0.5 M solution in THF, 5.5 mmol). The solution was warmed slowly to room temperature and then stirred for 4-6 h to give a solution of the alkyl-9-BBN derivative. To the above solution were added PdCl<sub>2</sub> (dppf) (0.15 mmol), the 1,4-bis(methoxymethyl)-2,5-dialkylated-benzene (5 mmol), an additional 12 mL THF and aqueous NaOH (5 mL of 3 M solution) at room temperature. The mixture was refluxed overnight. After the reaction was complete, the reaction mixture was diluted with dichloromethane (20 mL), and the residual borane was oxidized by addition of H<sub>2</sub>O<sub>2</sub> (30%, 2 mL) at room temperature. The product was extracted, washed with brine, and dried over magnesium sulfate. The crude product was purified by recrystallization from ethyl alcohol.

**1,4-bis(methoxymethyl)-2,5-dioctylated-benzene.** Prepared with a yield of 64%. <sup>1</sup>H NMR (CDCl<sub>3</sub>) δ 7.46 (s, 2H), 4.34 (s, 4H), 3.42 (s, 6H), 2.84(t, 4H), 1.94(m, 4H), 0.82-1.40 (m, 26H).

**1,4-bis(methoxymethyl)-2,5-dioctylated-benzene.** Prepared with a yield of 57%. <sup>1</sup>H NMR (CDCl<sub>3</sub>) δ 7.42 (s, 2H), 4.32 (s, 4H), 3.452(s, 6H), 2.86(t,4H), 1.95 (m,4H), 0.80-1.48 (m, 34H).

**Polymerization of bis(methoxymethyl)benzenes.** To a 25 mL Schlenk flask containing 10 mL of CH<sub>2</sub>Cl<sub>2</sub> was added the 1,4-bis(methoxymethyl)-2,5-dialkylated-benzene (0.26 mmol). Following 3 freeze-pump-thaw cycles, BF<sub>3</sub>.H<sub>3</sub>PO<sub>4</sub> (0.8 mL, 9 mmol) was added slowly to the solution. The mixture was purged by argon for four days under room

temperature, quenched with H<sub>2</sub>O, and extracted with CH<sub>2</sub>Cl<sub>2</sub>. Evaporation of the solvent gave the polyacene precursor as a brown solid.

**Dehydrogenation.** To 10 mg of the above polyacene precursors was added a deoxygenated solution of DDQ (20 mg, 0.088 mmol) in 10 mL of toluene. The reaction was refluxed under argon overnight, and then the DDQ was removed by an Al<sub>2</sub>O<sub>3</sub> column.

**2-Benzoylbenzoic acid.** A mixture of 5 g of phthalic anhydride, 9 g of AlCl<sub>3</sub> and 80 mL of benzene were shaken for 30 min. at room temperature. The temperature was then raised to the reflux temperature, and after heating for 2 hr, the reaction mixture was hydrolyzed with 1N HCl. A grayish-white solid was removed by filtration, and the filtrate was extracted three times with diethyl ether. The combined ethereal extracts were washed with 5% aqueous sodium bicarbonate and then were acidified with conc. HCl. A milky suspension formed, and after storing the product overnight in a refrigerator, white crystals were obtained. A 98% yield of the product was obtained after collecting the crystals by filtration. m.p. 96°C.<sup>95</sup> <sup>1</sup>H NMR (CDCl<sub>3</sub>) δ 11.6 (s, 1H), 8.00-7.27 (m, 9H).

**2-Benzylbenzoic acid.** 2-Benzoylbenzoic acid (7.6 g) was reduced at approximately 65 °C in 20 mL of acetic acid and 1.2 g of 10% Pd on carbon. After 2 hr, the catalyst was removed by filtration and the solution was poured into 100 mL of water. After the mixture was chilled for 12 hr, the product was collected by filtration and dried under in vacuum to yield 4.5 g (65%) of

colorless 2-benzylbenzoic acid. m.p. 111-113°C.<sup>96</sup> <sup>1</sup>H NMR (CDCl<sub>3</sub>) δ 11.6 (s, 1H), 7.33-8.00 (m, 9H), 4.46 (s, 2H).

**2-Benzylbenzyl alcohol.** To a stirred suspension of 1.1 g of LiAlH<sub>4</sub> in 50 mL of anhydrous ether was added a solution of 4 g of 2-benzylbenzoic acid in 20 mL of anhydrous ether. The resulting mixture was stirred and refluxed for one hour, and the excess hydride was destroyed by addition of 2 mL of ethyl acetate. The ether solution, after washing with 10 % sulfuric acid and 10% sodium bicarbonate, was dried over magnesium sulfate and the solvent was later removed. The oily residue was crystallized from 30-60 °C petroleum ether to give 3.2 g of 2-benzylbenzyl alcohol, in 53% yield. m.p. 40-41 °C.<sup>97</sup> <sup>1</sup>H NMR, (CDCl<sub>3</sub>) δ 7.40-7.07 (m, 9H), 4.58 (s, 2H), 4.04 (s, 2H), 1.80 (br s, 1H).

**2-Benzylbenzyl methyl ether.** To a round bottom flask containing a stirred solution of NaH in anhydrous THF under argon, was added drop-wise a solution of methyl iodide in THF. After the addition was complete, the mixture was refluxed gently for 1hr. Upon cooling, a solution of 2-benzylbenzyl alcohol in dry THF was added drop wise, and the mixture was refluxed overnight. The mixture was cooled and the suspension was filtered. The collected solid was rinsed with dichloromethane, and the the combined organic layers were washed with water, dried over magnesium sulfate, filtered and evaporated to dryness. The product was purified by column chromatography to give a pale yellow liquid in 68% yield. <sup>1</sup>H NMR (CDCl<sub>3</sub>) δ 3.42 (s, 3H), 4.15 (s, 2H), 4.49 (s, 2H), 7.0-7.6 (m, 9H).<sup>98</sup>

**Cyclization of model compound in CH<sub>2</sub>Cl<sub>2</sub>.** A solution of 25 mg of 2-benzylbenzyl methyl ether in 40 mL of CH<sub>2</sub>Cl<sub>2</sub> was degassed via 3 freeze-pump-thaw cycles, and then 0.5 mL of BF<sub>3</sub>/PA was added drop-wise. The reaction was stirred for 12 hr at room temperature and was quenched by adding 30 mL of water. The organic layer was washed with water until it was no longer acidic, dried over magnesium sulfate and the solvent removed. A white solid was obtained in 95% yield. <sup>1</sup>H NMR (CDCl<sub>3</sub>) δ 3.9 (s, 2H), 7.14 (dd, 4H), 7.36 (dd, 4H).

**Nickel catalyzed polymerization of 1,4-bis (methoxymethyl)-2,5-dibromobenzene.** Inside a helium atmosphere dry box, NiCl<sub>2</sub> (8.6 mg, 0.067 mmol), bipyridine (10.4 mg, 0.067 mmol), and zinc powder (0.27 g, 4.12 mmol) were added into a 100 mL round bottomed flask fitted with a reflux condenser capped by a rubber septum. After removal from the dry box, the system was connected to an argon bubbler through the rubber septum and placed in an oil bath. DMF (1 mL) was added to the flask and the solution was stirred magnetically. The mixture was then heated to 80 °C. The green solution became brown after 10 minutes, eventually turning deep red-brown after 30 minutes. The 1,4-bis(methoxymethyl)-2,5-dibromobenzene (0.43 g, 1.33 mmol) was dissolved in DMF (4 mL) in an argon filled 50 mL round bottomed flask and transferred via cannula to the catalyst mixture. The solution returned to its original green color upon addition of the monomer but turned deep red-brown after 15 minutes. The mixture was refluxed overnight. Upon cooling, the solution was poured into a flask containing 200 mL of 2N HCl/MeOH (1:1)

and stirred until the excess zinc dissolved. The yellow precipitate was collected by filtration and was repeatedly washed with distilled water and methanol. The polymer was dried under vacuum at 110 °C overnight to yield 0.194 g (88%) of a fine, pale yellow powder that was insoluble in common organic solvents. Anal. Calcd. for  $(C_{10}H_{12}O_2)_n$ : C, 73.17; H, 7.32; O, 19.51. Found: C, 69.85; H, 7.19; O, not determined.

**Cross-linking of methoxymethyl substituted PPP.** The bis (methoxymethyl) substituted PPP 6 (0.035 g) and concentrated sulfuric acid (3 mL) were mixed in a scintillation vial and cooled in an ice bath. Stirring at 0 °C was continued for 36 hr. The suspension was washed with 20 %(w/w) sodium hydroxide solution (3 x 25 mL), water (3 x 25 mL), and rinsed with ether (3 x 50 mL). The collected solid was dried overnight at 120 °C under vacuum to give 0.009 g (30%) of the cross-linked polymer as a tacky, black solid.

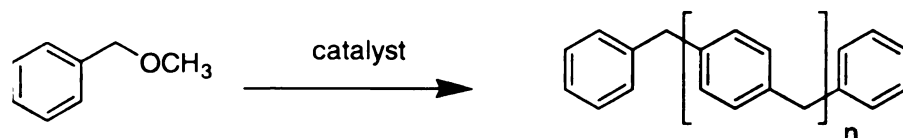
## RESULTS AND DISCUSSION

Realization of the many applications of polyacenes is limited by their instability (facile oxidation in air) and poor solubility.<sup>99</sup> Thus the longest acene synthesized to date is heptacene.<sup>100</sup> The primary goal of this work was to devise and execute the synthesis of well-defined polyacenes and acene-like materials. We investigated two types of polyacene syntheses based on acid-catalyzed electrophilic aromatic substitution reactions. The first targets simple routes to acene-like materials that contain a substantial fraction of acene subunits. Materials resulting from this approach are relevant to applications such as electrical conductors, anti-static agents, and carbon electrodes, where it is important to be able to supply large amounts of material at relatively low cost. The second target is to develop a synthetic scheme for the preparation of soluble well-defined polyacenes that would enable characterization of the structure-property relationships of polyacenes and comparisons of the experimental data with theoretical predictions.<sup>9,101</sup>

### 3.1. Polyacenic materials.

#### 3.1.1. Simple routes to acene-like materials

It is well-known that methoxymethyl benzenes condense via acid-catalyzed electrophilic aromatic substitution reactions to give polybenzyl networks (**Scheme 7**).<sup>44</sup> While most reported syntheses of polybenzyls are polycondensations utilizing benzyl halides and various Lewis acids ( $\text{AlCl}_3$ ,  $\text{TiCl}_4$ , and  $\text{SnCl}_4$ ), we found that we could obtain a product with a similar structure by adding concentrated sulfuric acid to neat methoxymethyl benzene.



**Scheme 7.** Acid catalyzed polymerization of methoxymethylbenzene.

The polymerization yielded a poorly soluble tan solid with a glass transition at 180 °C. When cooled from above that temperature, the polybenzyl product formed a glassy resin. Thermal gravimetric analysis runs at 10°C/min (**Figure 14**) indicate that the polymer is stable in nitrogen to 400 °C, but then the benzyl linkages that connect the aromatic rings degrade and the polymer converts to volatile products and evaporates. The material is completely decomposed before it reaches 600 °C.

If we apply similar chemistry to bis(methoxymethyl)benzenes, the resulting networks should contain a large fraction of fused ring aromatic compounds that upon elimination of hydrogen would yield materials with a large proportion of acene-like structures. To test this idea, we prepared 1,2-*bis*(methoxymethyl) benzene, 1,3-*bis*(methoxymethyl benzene), and 1,4-*bis*(methoxymethyl)benzene and used sulfuric acid to catalyze their condensation (**Scheme 8**). Compared to the condensation of methoxymethyl benzene, instead of forming two benzyl bridges per ring to give a linear polymer, having two methoxymethyl groups per ring should result in formation of four benzyl bridges per ring. These starting materials have the potential to form polymeric edge-fused ring compounds where alternate rings are aromatic.

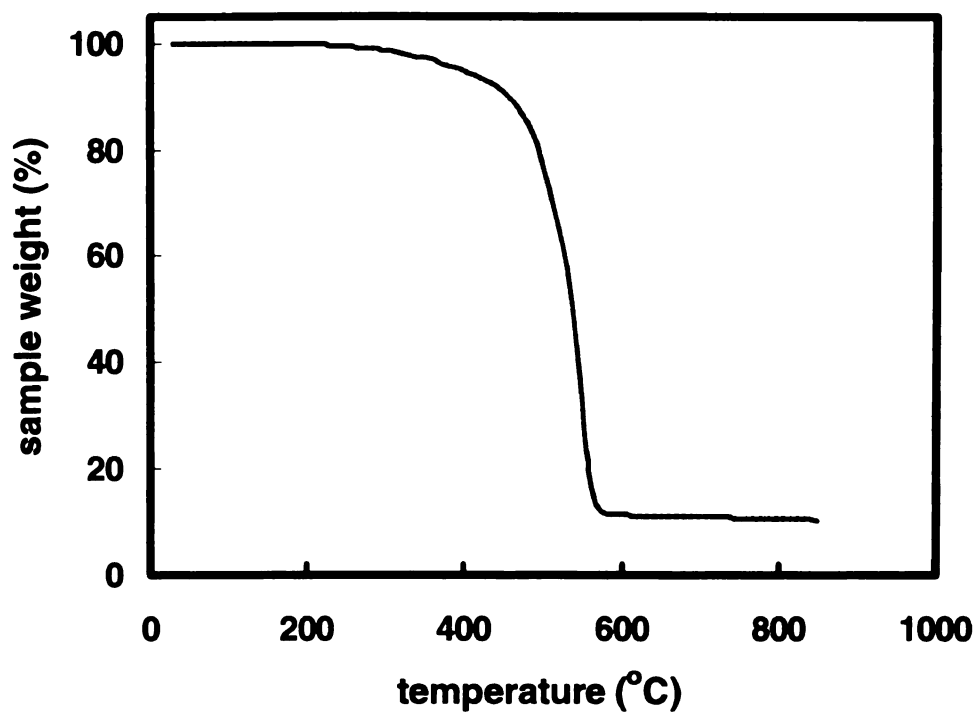
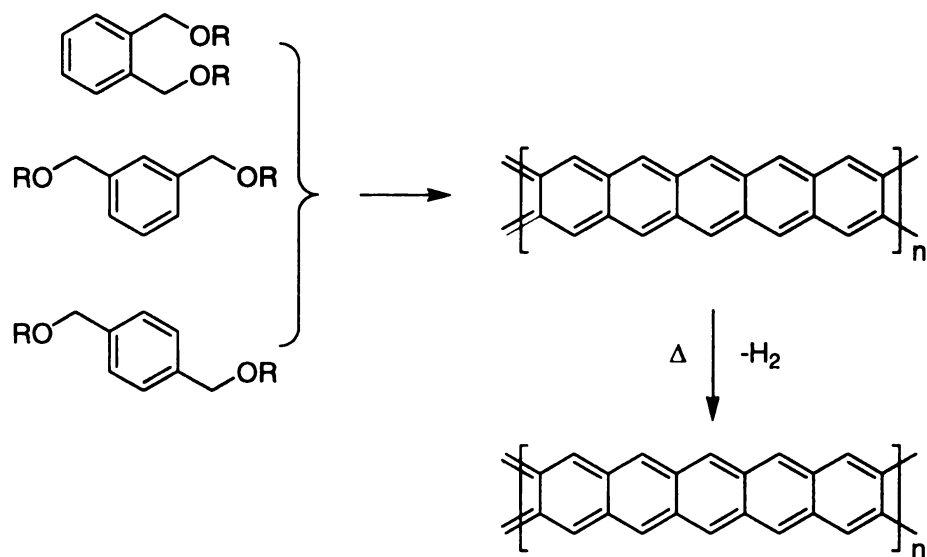


**Figure 14.** Thermogravimetric analysis results for poly(methoxymethylbenzene). Heating rate: 10 °C/min.



**Scheme 8.** Acid-catalyzed polymerization of bis(methoxymethyl)benzenes.

Dehydrogenation of these “polyacene precursors” should yield polyacenes. In all three cases, we observed rapid formation and precipitation of brown solids. Characterization of these materials is difficult. Not only are they insoluble, but also the structural differences between polybenzyl and the polyacene precursor are subtle and not easily detected by IR, NMR, and other standard spectroscopic techniques.

Thermal gravimetric analyses of the products showed that the networks formed from the acid-catalyzed polymerization from each of the methoxymethyl

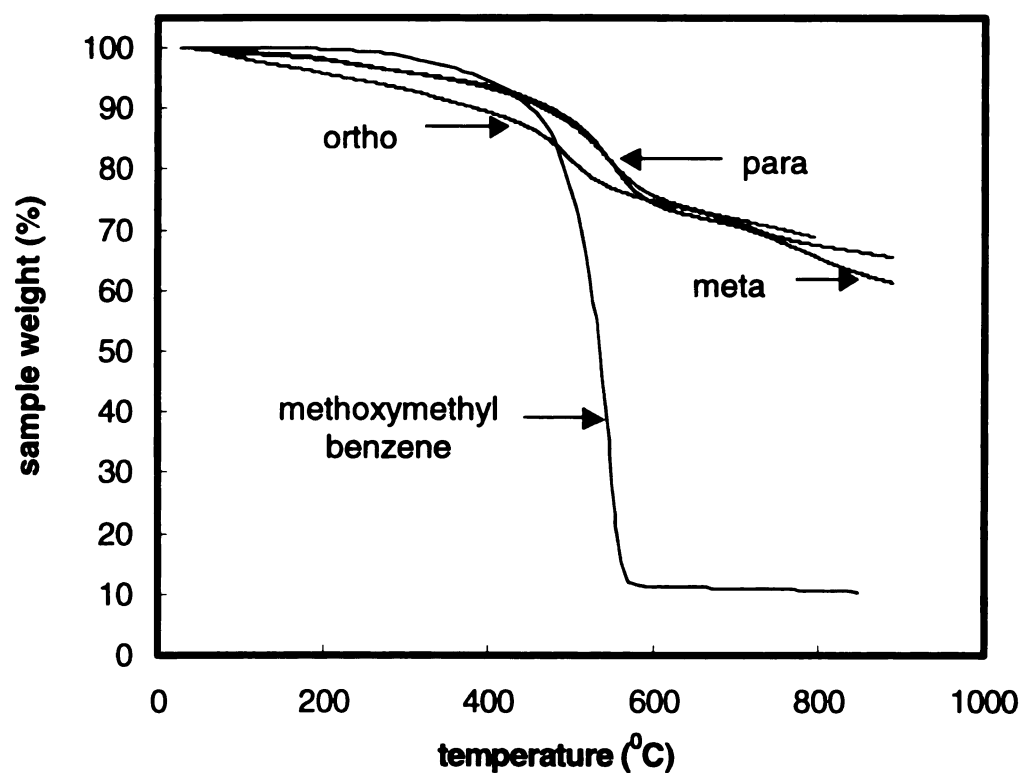


**Figure 15** Thermogravimetric analysis results for poly(methoxybenzene) and poly(bis(methoxymethyl)benzene) when O<sub>2</sub> is rigorously excluded. Heating rate: 10 °C/min.

benzenes exhibit surprising thermal stability in nitrogen. As shown in **Figure 15**, after losing a small weight fraction near 400 °C, presumably due to the loss of a low molecular weight fraction or residual unreacted methoxymethyl groups, the polymers derived from the di-substituted monomers were thermally stable to >700 °C and resulted in 70% char yields.

We made an interesting observation from a series of thermal gravimetric analysis runs where the nitrogen atmosphere was not continuously purged, and thus was contaminated with a slight amount of oxygen (**Figure 16**). Under these conditions, the sample prepared from the *ortho* bis(methoxymethyl) benzene retained high thermal stability with a 60% char yield at 700 °C. In contrast, the *para* and *meta* derivatives degraded more rapidly, with the *para* derivative completely degrading before reaching 500 °C.

These results imply that the three materials are structurally different. As shown in **Scheme 9**, there are two limiting structures that can be obtained from bis(methoxymethyl) benzenes. The desired polyacene precursor (top) forms when the polymerization is exclusively intramolecular, i.e. both methoxymethyl groups react to give linear chains. The other extreme is a hyperbranched polybenzyl structure (bottom), highly cross-linked but connected via thermally labile benzyl bridges. The acene structure is particularly stable thermally because of its ladder-like architecture. Unlike a single stranded polybenzyl, two chains must be severed to form volatile products. Based on the thermal gravimetric analysis runs, the *ortho* derivative presumably contains

a higher fraction of thermally stable rings, while the thermal behavior of the

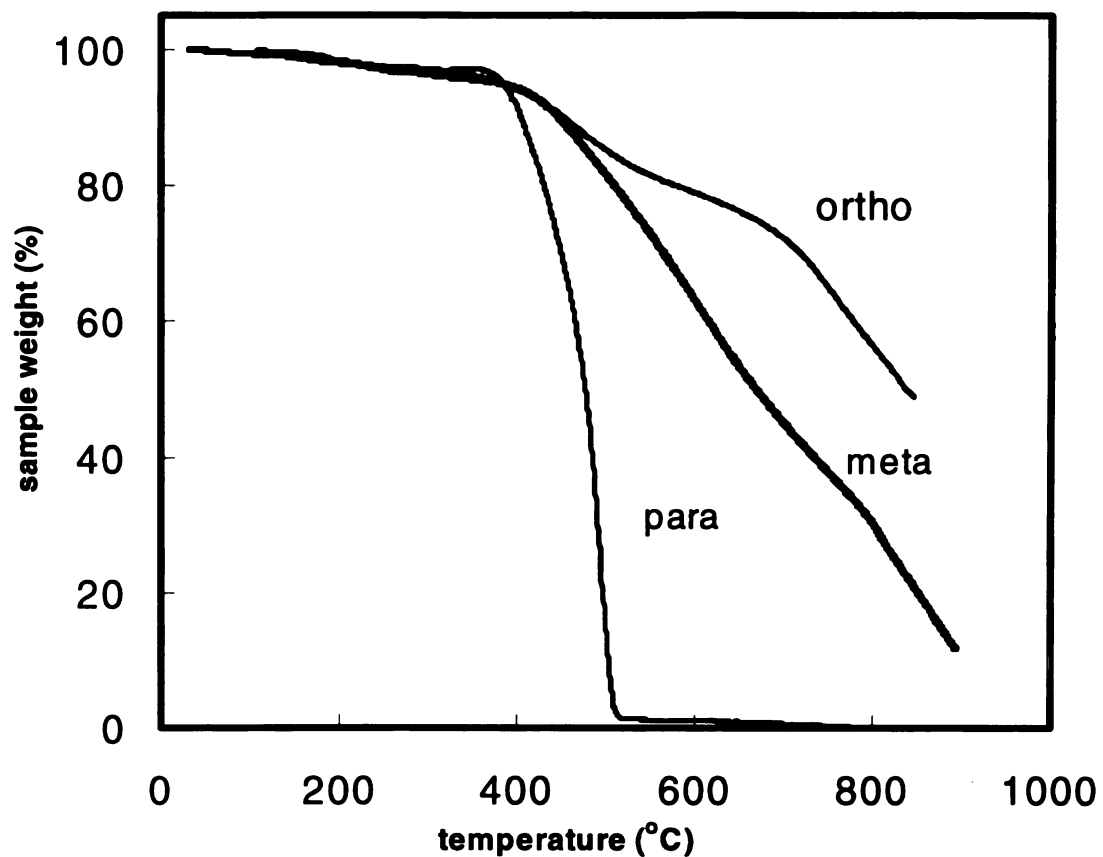


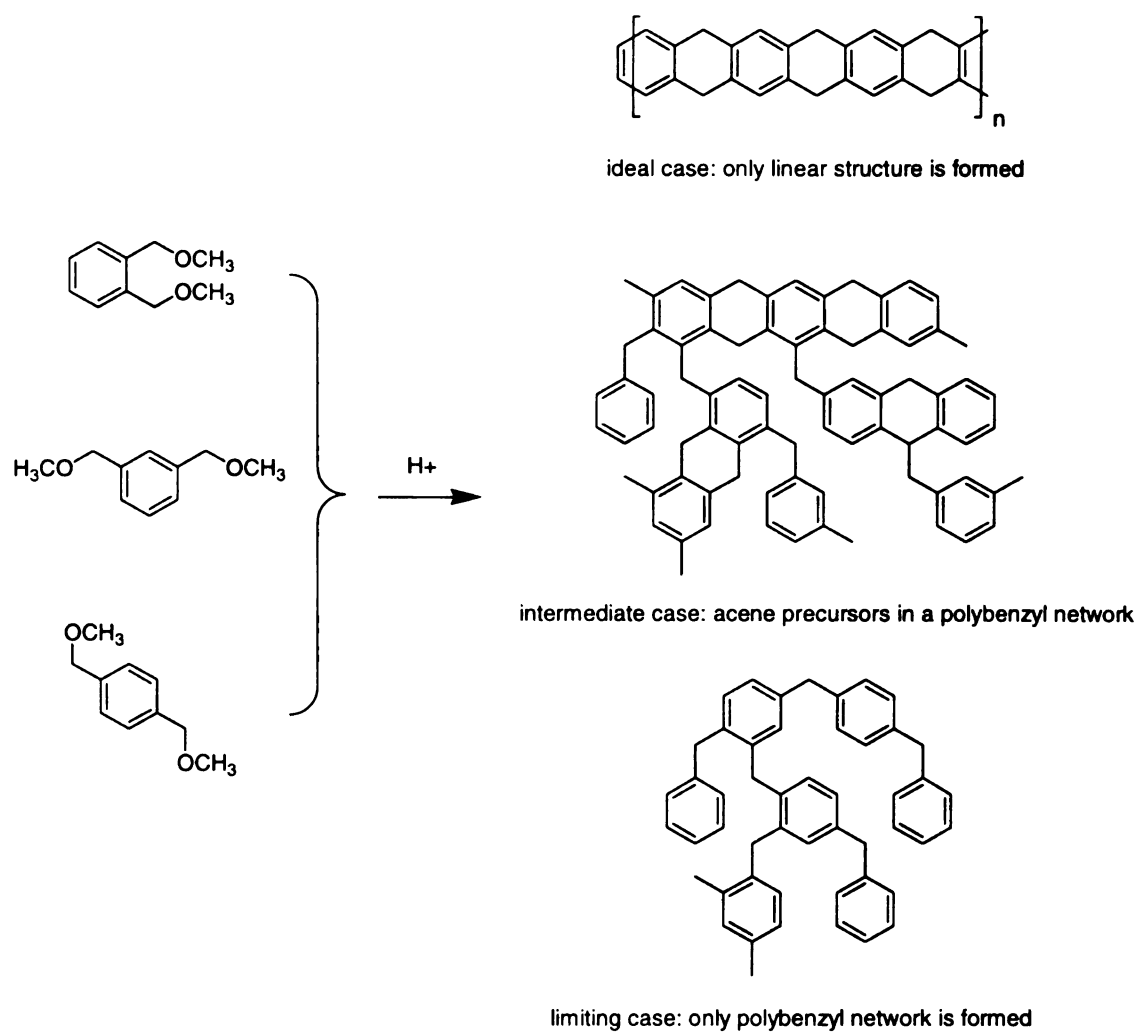
**Figure 16.** Thermogravimetric analysis results for poly(methoxymethylbenzene) and poly(bis(methoxymethyl)benzene) run under nitrogen contaminated with 10% oxygen. Heating rate: 10 °C/min.

least stable

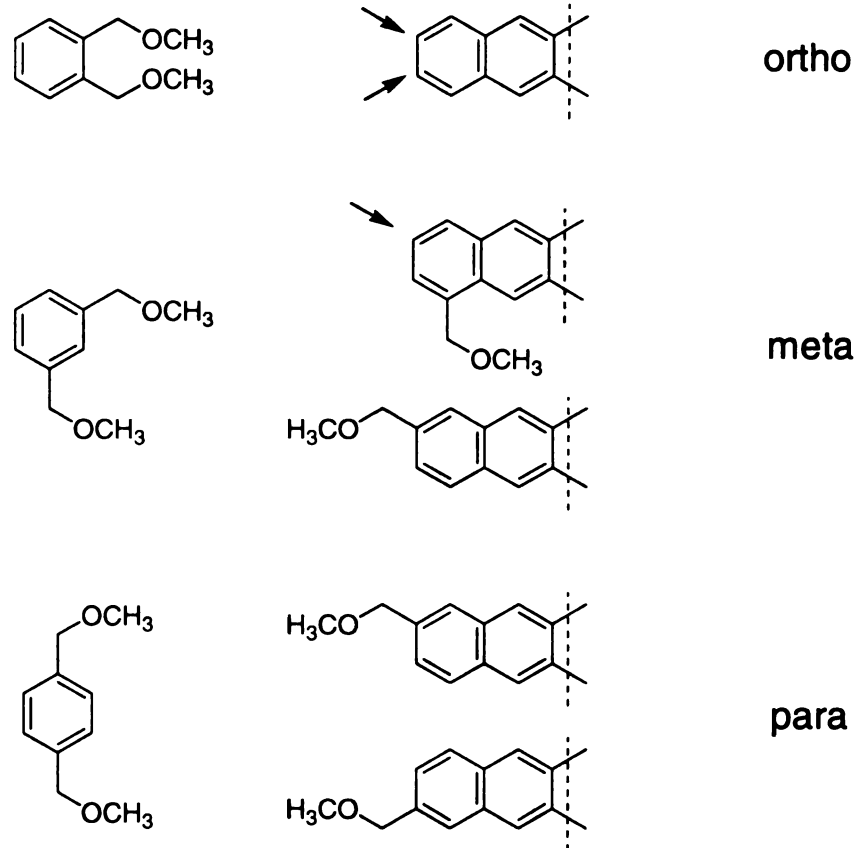
product, the *para* derivative, resembles that of a linear polybenzyl. Thus it appears that *ortho* substitution favors cyclization, *para* substitution leads to a polybenzyl structure, and *meta* substitution represents an intermediate case.

A plausible argument for explaining the differences in the structures obtained from the three monomers can be developed from considering steric factors during the substitution reactions. As shown in **Scheme 10**, the growing polyacene chain ends for the *ortho*, *para*, and *meta* methoxymethyl benzenes are structurally different. The *ortho* case is unique in that in forming the first connection to the growing chain, it can add to two sites without having to form a bond *ortho* to either a ring juncture or a methoxymethyl group on the chain end. Both the *meta* and *para* cases require at least one such interaction.

We note that in a rigorously inert atmosphere, the *ortho*, *para*, and *meta* methoxymethyl benzene products have similar thermal stabilities. Linear polyacene precursors eliminate hydrogen to give acenes, while polybenzyl networks rearrange and graphitize as commonly seen in phenol-formaldehyde resins. Elimination of oxygen is critical for limiting oxidation of the benzyl linkages and formation of volatile hydrocarbon products.



**Scheme 9.** Possible outcomes from the polymerization of bis(methoxymethyl)benzenes.



**Scheme 10.** The substitution pattern on the benzene ring leads to different condensation products.

### 3.1.2. Chemical dehydrogenation

The dihydroanthracene units of polyacene precursors dehydrogenate thermally, but the high temperatures involved probably cause rearrangement of the carbon skeleton. An alternative method is to use a chemical agent such as 2,3-dichloro-5,6-dicyano-1,4-benzoquinone (DDQ). DDQ was refluxed with suspensions of the polyacenic materials in refluxing xylenes for 2 days. The product was collected by filtration, washed and dried. Neither IR spectroscopy nor TGA runs showed changes in the materials (**Figures 17 and 18**), not surprising given the insolubility of the materials.

### 3.1.3. Polymerization in solution

The synthesis of a perfectly linear polyacene is difficult due to the lack of synthetic control over the electrophilic aromatic substitution reaction used to prepare the polyacenic materials. Instead of a bulk polymerization, which tends to favor the intermolecular reaction, we briefly considered the use of different solvents, including ethanol, ethyl ether, and ethyl acetate. 10 wt% of the 1,2-*bis*(methoxymethyl)benzene was added to a 1:1 mixture of sulfuric acid and the solvent. The usual brown precipitate formed, was washed and dried under vacuum. The char yields from these polymerizations (**Figure 19**) were less than the yields from bulk polymerizations. It is likely that the solvent reacted under these conditions.

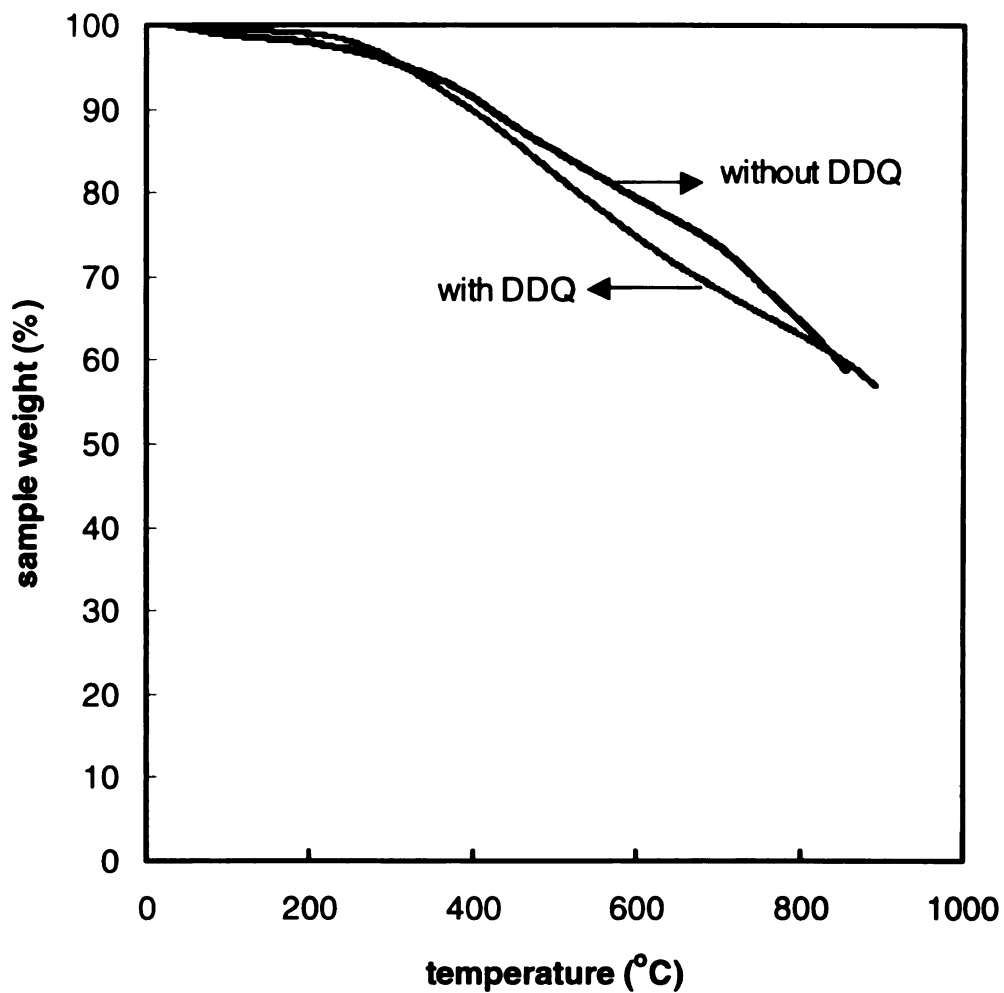


**Figure 17.** Thermogravimetric analysis results for poly (bis 1,2-(methoxymethyl)benzene) in nitrogen. Heating rate: 10 °C/min.

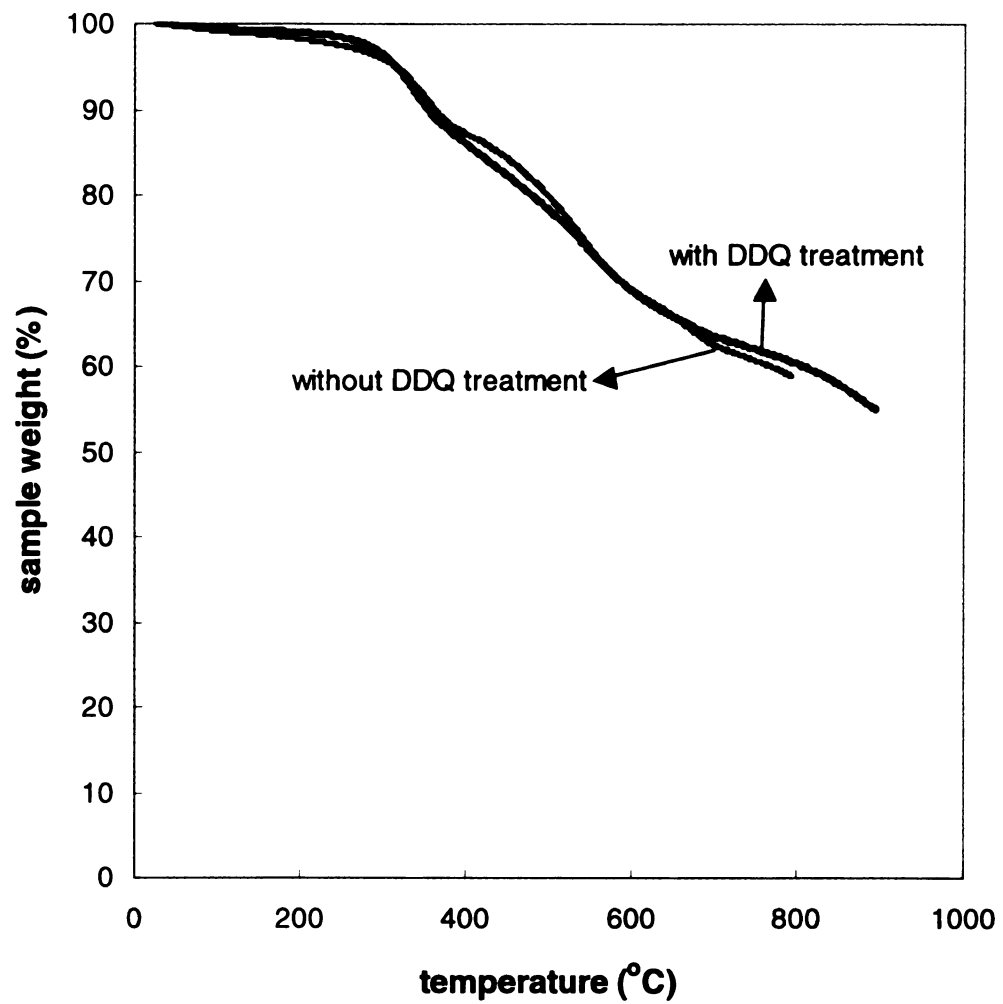


**Figure 18.** Thermogravimetric analysis results for poly(bis-1,4-(methoxymethyl)benzene) in nitrogen. Heating rate: 10 °C/min.

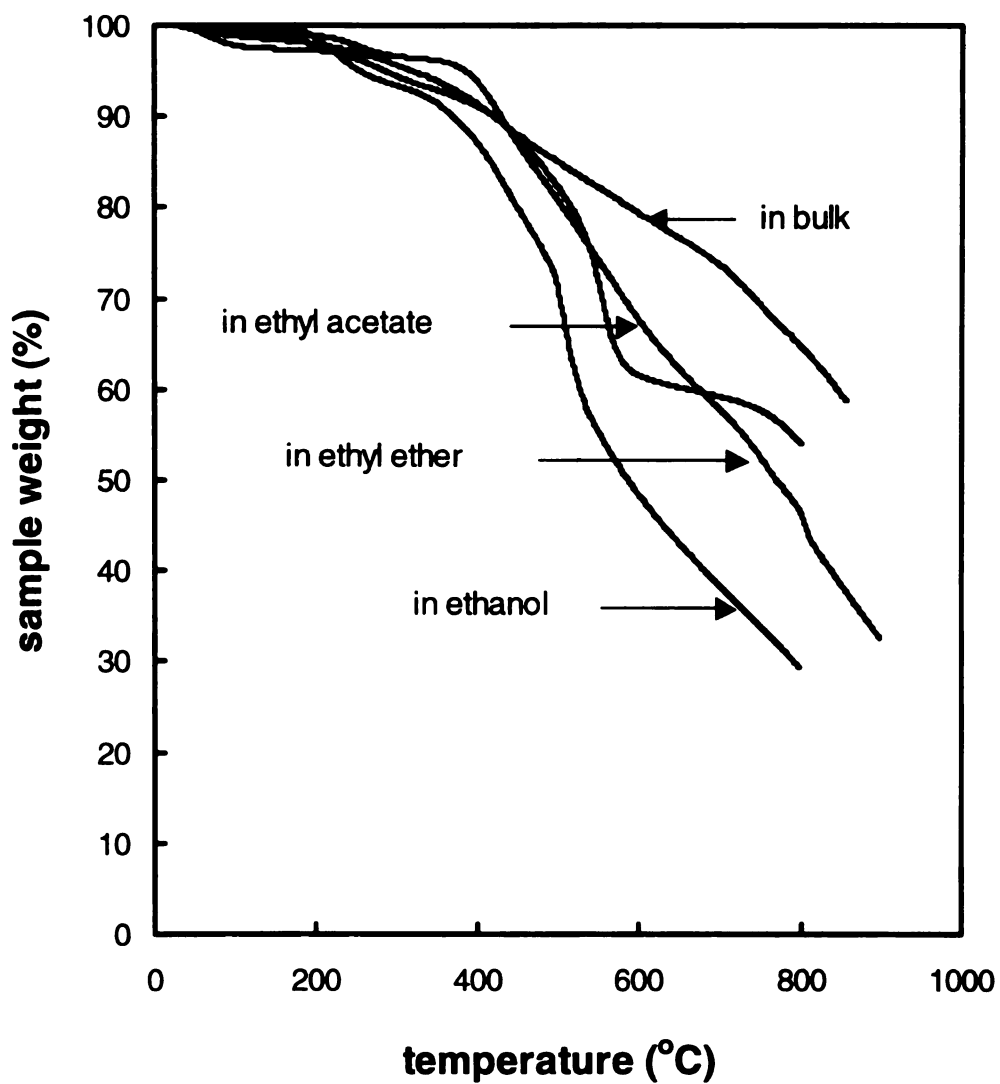


**Figure 19.** Thermogravimetric analysis results for poly(1,2-bis(methoxymethyl)benzene) prepared via solution and bulk reactions. Heating rate: 10 °C/min.

### 3.1.4. Characterization of acene-like materials

#### 3.1.4.1. Infrared

To better understand the structural changes that occur in the polymer derived from the *ortho* substituted monomer, we heated the products under nitrogen to various temperature in a TGA apparatus and the residues were analyze using infra red spectroscopy. The samples were made as KBr pellets, and for meaningful comparisons, the spectra were normalized for sample weight (mg sample/100 mg KBr) and the thickness of the pellet (related to the absolute concentration of sample in the pellet). An internal standard added to the sample (CBr<sub>4</sub>) and the residual water in the KBr also were used to normalize the IR spectra. As shown in **Figure 20**, the IR spectra clearly show progressive chemical structure evolution from that of the “as-obtained” polymer with a high proportion of C-H bonds to an intermediate structure with predominantly aromatic C-H bonds. Assuming the *ortho* precursor contains a large fraction of edge-fused rings, the sample treated at 500 °C should contain an appreciable fraction of polyacenes.

A signature of polyacenes would be the appearance of materials with a relatively low band gap, but with the retention of aromatic C-H bonds. From the IR spectra, we find that the 500 and 650° samples have a strong electronic absorption that tails into the infrared region, indicating extensive  $\pi$ -conjugation. In addition, the IR bands corresponding to C-H stretching are retained. The bands due to aliphatic C-H bands (2900-3000 cm<sup>-1</sup>) decrease in intensity while those due to aromatic C-H bonds increase, as expected for the formation of

acenes. Further treatment of the samples at 800 °C resulted in the near complete loss of C-H bonds and presumably the formation of a graphitic structure. The broad absorption at 3500 cm<sup>-1</sup> was due to residual moisture in the KBr.

#### 3.1.4.2. Raman

We also studied the structure of these acene-like materials using Raman spectroscopy. The polymer samples characterized were derived from the acid-catalyzed condensation of the *ortho*, *meta*, and *para* methoxymethylbenzenes that had been heat treated at 800 °C in an oxygen-free environment. The Raman spectra (**Figure 21**) are very similar to those of graphitic materials such as activated charcoal and carbon black.<sup>102</sup> Two characteristic peaks were observed for all samples, a peak at 1355 cm<sup>-1</sup> assigned to an A<sub>1g</sub> vibration mode of amorphous carbon, and a peak at 1600 cm<sup>-1</sup> from the E<sub>2g</sub> mode of graphite. Consistent with thermal gravimetric analyses of the precursors, the *ortho* derivative had the strongest 1600 cm<sup>-1</sup> band and thus the most ordered graphite structure. The same peak in the spectrum of the *meta* and *para* derivatives is weaker, consistent with their precursors being more polybenzyl-like compared to the *ortho* sample.

#### 3.1.4.3. Elemental Analysis

Elemental analyses of the condensation products of the methoxymethylbenzenes provide only limited structural information since the polybenzyls and polyacenes have identical chemical formulae. Elemental analysis can however provide some information about the purity of the

materials. The data obtained show that the samples are impure. Analysis for C, H, and S gave 76% C, 5.4% H and 2.2% S; the remainder is presumably oxygen. This gives a C/H ratio of 14 instead of the 16 that would be expected if the polymers were linear acene precursors ( $C_8H_6$  for each repeat unit). As expected, heat treatment increased the C/H ratio (to 71), and the elemental analysis results were 83% C, 1.2% H and 1.1% S. The presence of sulfur is a problem as it may substantially affect the properties of the polyacene product. How it is incorporated into the materials is unknown, but we suspect sulfonation of the polymer or occlusion of sulfates in the insoluble polymer. The lower than expected C/H ratio for the acene precursors is likely linked to incomplete condensation of the methoxymethyl groups, while the higher than expected C/H ratio after heat treatment is consistent with substantial graphitization.

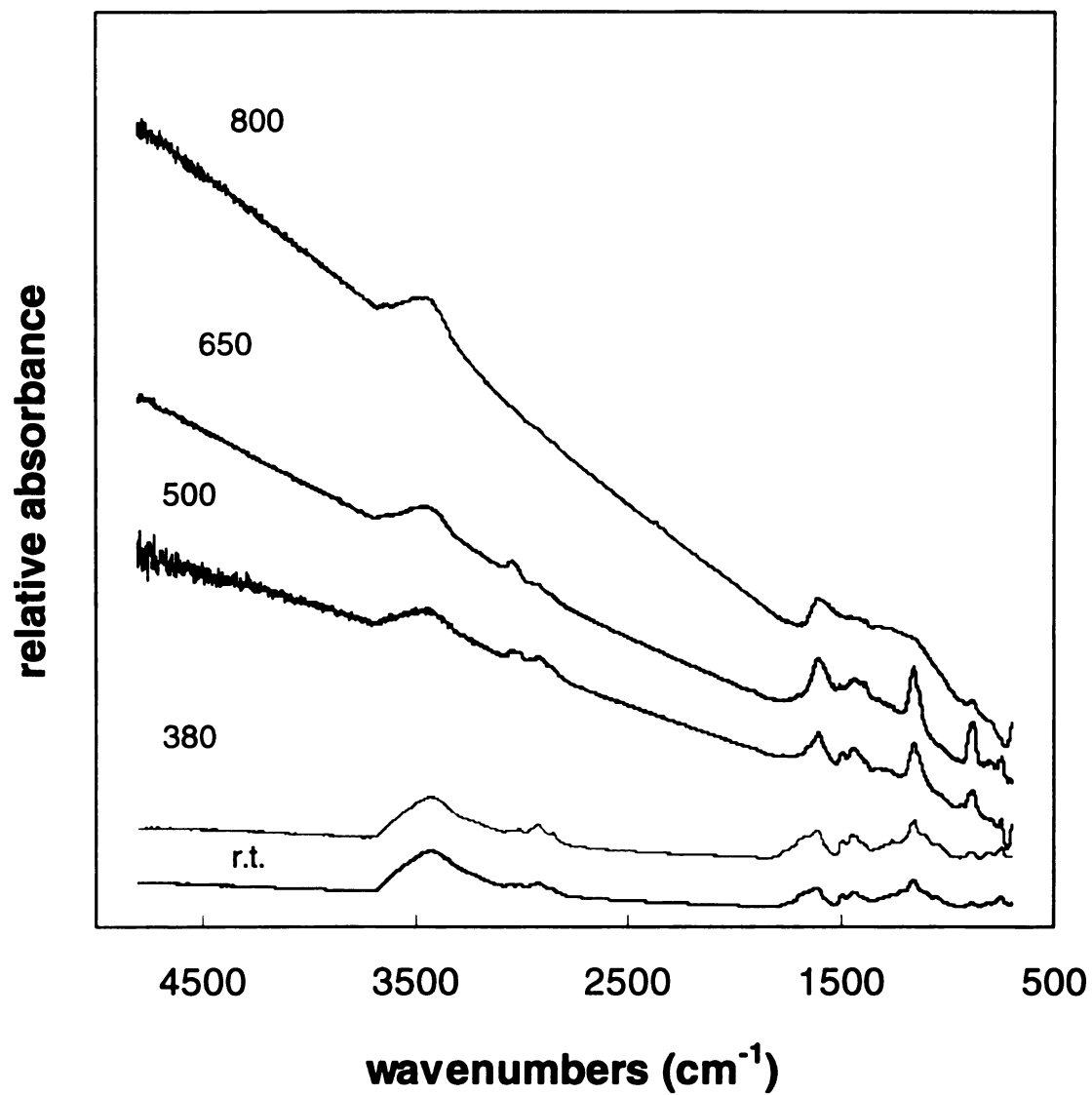


**Figure 20.** Infrared absorption spectra of the polybenzyl network formed from monomer 1 heated in nitrogen at 10 °C/min to 30 °C, 380 °C, 500 °C, 650 °C, and 800 °C.

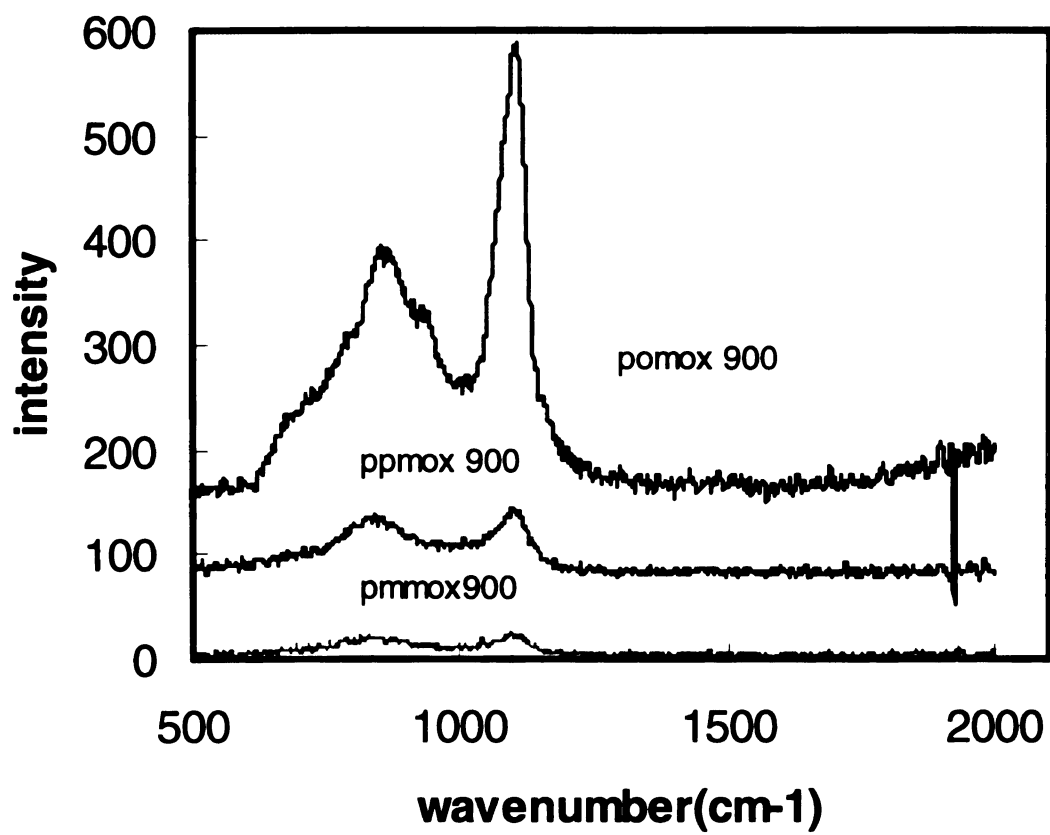


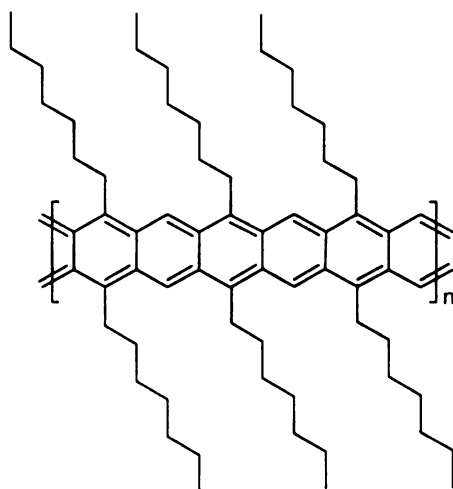
**Figure 21.** Raman spectra of ortho,para and meta-(methoxymethyl) benzene after heated to 800 °C.

### 3.2. Well-defined Soluble Polyacene

As seen in the previous sections, the poor solubility of polyacenes stymies characterization of the polymers. A new synthetic approach to soluble polyacenes is needed for there to be substantial progress toward their characterization. To improve the solubility of polyacene, we adopted a well-known strategy for solubilizing rigid-rod polymers like polyphenylenes (PPPs),<sup>103-106</sup> attaching flexible alkyl chains to the polymer backbone. Soluble PPP derivatives were obtained by adding *n*-hexyl chains to the polymer repeat units. As shown in **Scheme 11**, alkyl chains attached to the polyacene backbone will yield "hairy rods" that like PPPs, should be soluble.

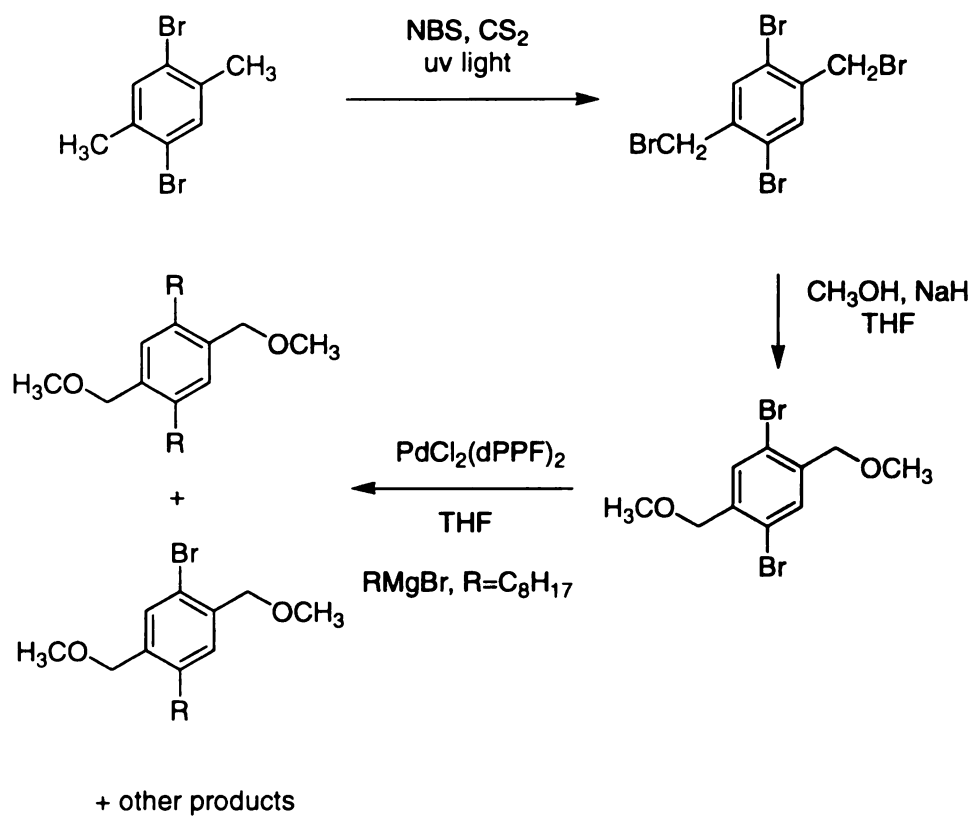
#### 3.2.1 Monomer design and synthesis

To obtain a substituted polyacene, a monomer must be designed that contains two methoxymethyl groups, unsubstituted sites capable of

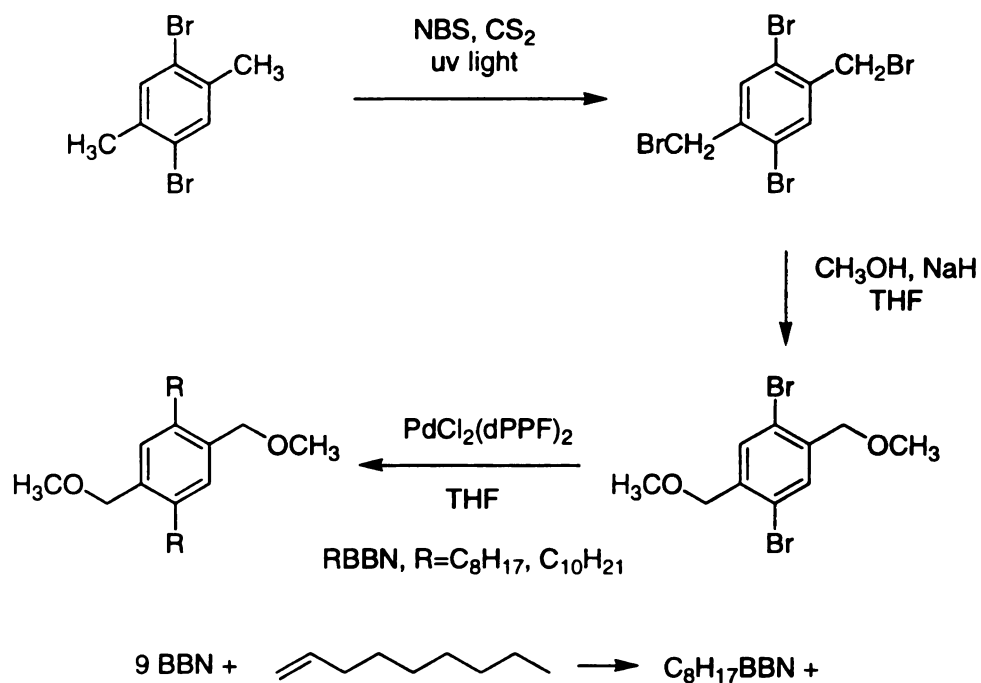


**Scheme 11.** Alkyl substituted polyacene.

electrophilic aromatic substitution, and alkyl groups to solubilize the polymer. **Scheme 12** shows the route chosen for the synthesis. The free-radical bromination of 2,5-dibromo-*p*-xylene using N-bromosuccinimide led to 1,4-bis(bromomethyl)-2,5-dibromobenzene (**4**) in 30% yield. The poor yield is due to the difficulty of separating **4** from impurities. Two equivalents of N-bromosuccinimide were used in the reaction, and the bromination yielded a statistical mixture of mono-, di-, and unbrominated products. Due to the symmetry of **4**, it could be recovered from the reaction mixture by repeated crystallization. Compound **4** was treated with 2 equivalents of sodium methoxide to give bis(methoxymethyl)-2,5-dibromobenzene **5**. When run in THF, this reaction forms a substantial amount of low molecular weight poly(phenylene vinylene). This side reaction was avoided by running the reaction in non-polar, non-coordinating solvents such as hexanes. Introduction of the alkyl group by a Pd-catalyzed coupling reaction via the Grignard reagent was not very successful. Clean disubstitution in high yield is needed, but TLC revealed at least 5 products with the disubstituted product present in low yield. While the coupling reaction works well on substrates like dibromobenzenes, the larger steric hindrance of our substrate presumably hinders the coupling reaction. In an alternative Pd-catalyzed coupling scheme (**Scheme 13**), we replaced the Grignard reagent with the 9BBN derivatives of 1-octene and 1-decene.<sup>107</sup> This reaction was successful, and we obtained a 56% of the coupled product.



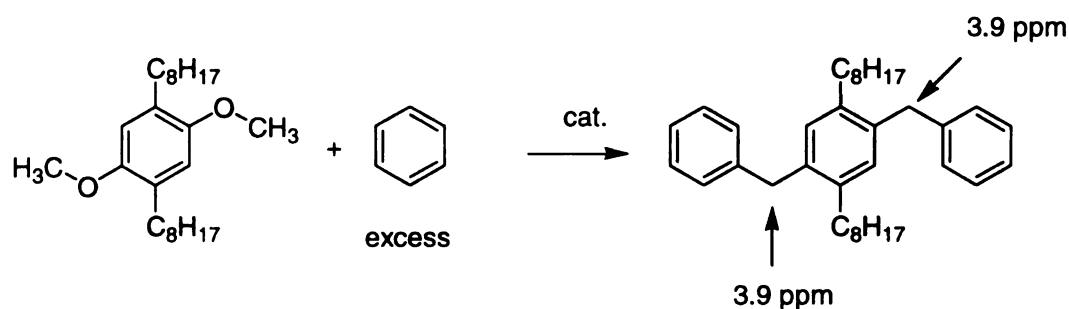
**Scheme 12.** First approach to the synthesis of 1,4-*bis*-(methoxymethyl)-2,5-dialkyl benzenes



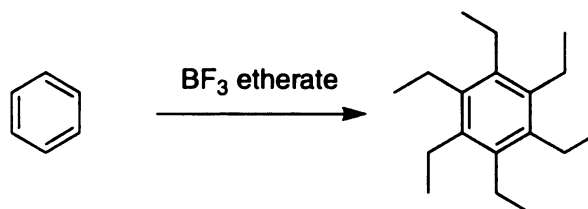
**Scheme 13.** Modified synthesis of 1,4-*bis*-(methoxymethyl)-2,5-dialkyl benzenes

### 3.2.2 Polymerization condition development

A model reaction was used to develop appropriate conditions for the condensation reactions of the monomer. Octylated bis(methoxymethyl)benzene was treated with different catalysts in an excess of benzene (Scheme 14). The reactions were assayed for the yield of 2,5-dibenzyl-1,4-dioctylbenzene and its purity. The reaction with concentrated  $\text{H}_2\text{SO}_4$  formed insoluble products.  $\text{BF}_3$ -etherate did not catalyze the desired reaction, but instead  $^1\text{H}$  NMR indicated formation of an ethylated aromatic product. This was confirmed when the reaction of  $\text{BF}_3$ -etherate and benzene alone yielded hexaethyl benzene (Scheme 15). However, a combination of  $\text{BF}_3$  and phosphoric acid resulted in clean formation of the dibenzylated product in 85% yield. When applied to bis(methoxymethyl)benzene,  $^1\text{H}$  NMR



**Scheme 14.** Control experiment used to develop polymerization conditions

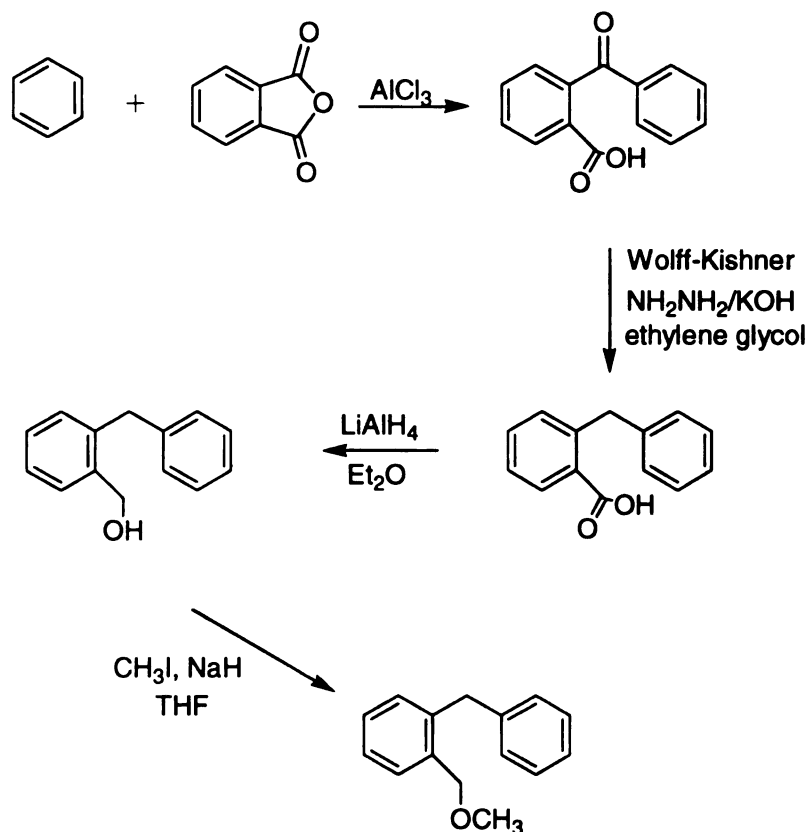


**Scheme 15.** Control experiment to prove  $\text{BF}_3$  caused side reactions.

showed the loss of the methoxymethyl group and the appearance of the benzyl linkages. The product was soluble, and based on GPC measurements, had a molecular weight of 3000 g/mol.

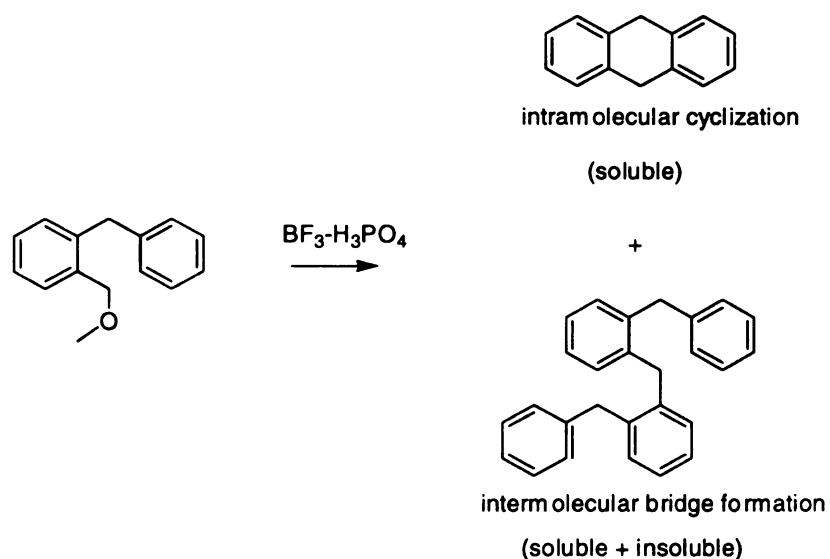
### 3.2.3. Model cyclization study

To optimize the cyclization conditions, we first synthesized the model compound shown in **Scheme 16**. The ring closing reaction of the benzyl substituted methoxymethyl benzene (**Scheme 17**) should provide a guide to the conditions that would best yield polyacenes. The model compound resembles the product of the first condensation step, which then can react



**Scheme 16.** Synthesis of a model compound for the cyclization study

intramolecularly to give the poyacene precursor, or intermolecularly to give hyperbranched polybenzyl products (**Scheme 19**). We tested a series of reaction conditions such as monomer concentration, monomer to catalyst ratio, temperature, reaction time, etc. to optimize the conditions that favor the intramolecular reaction. In each trial, we always observed some insoluble material, which must correspond to the branched polybenzyl product. After removing the insoluble fraction, we dried the soluble fraction, and determined the crude yield of 9,10-dihydroanthracene, the expected product. The crude product was analyzed by HPLC and the yield was corrected for purity. The results are tabulated in **Table 2-8**. From these series of experiments, we adopted standard conditions (monomer concentration = 2mM, catalyst/monomer ratio = 33, 12 hr reaction time in CH<sub>2</sub>Cl<sub>2</sub> at room temperature) for all polymerization reactions. When applied to the polymerization of dioctyl bis(methoxymethyl)benzene, we obtained an

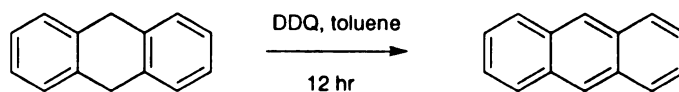


**Scheme 17.** Model cyclization condition study

85% yield of soluble product with a molecular weight of 7000. This corresponds to an average of 22 monomer units per chain.

With the presumed acene precursor in hand, we examined conditions for dehydrogenation by Pd/C<sup>108,109</sup> and DDQ<sup>110,111</sup> to form the acene structure. An advantage of Pd/C is that it can easily be removed from reaction mixtures via filtration, however we were concerned that the polyacene product might strongly bind to the catalyst. In addition, the mechanism of the hydrogenation reaction requires that the substrate come in contact with the catalyst, a step that might be hindered by the alkyl chains. DDQ, being soluble, should not have these problems. Nevertheless, one disadvantage of DDQ is that it may react with the acene and form a Diels-Alder adduct.

We carried out model dehydrogenations as shown in **Scheme 18** and found that the DDQ reaction worked well (no detected side reactions) as long as the temperature was held to no higher than the boiling point of toluene, and the reaction time was held to 12 hours. When this scheme was applied to the acene precursor polymer (**Scheme 20**), we did not see the characteristic absorption in the visible that one would expect from the  $\pi$ -conjugated system of a polyacene. This implies that the length of the acene segments must be small, and that the intermolecular condensation reaction dominated the desired intramolecular reaction needed to form rings.



**Scheme 18.** Model dehydrogenation test

**Table 2.** Concentration vs. yield in model cyclization study

Condition	Concentration (mol/L)	Acid ratio (mol) Model compound/acid	Crude Yield (%)	Purity from HPLC (%)	Overall Yield (%)
57.6 mg/30ml/1ml	$9.1 \times 10^{-3}$	1: 40.7	83.6	80.6	67.4
65.0 mg/140ml/1ml	$2.2 \times 10^{-3}$	1: 35.2	89.5	91.4	81.8
65.5 mg/700/1ml	$4.4 \times 10^{-4}$	1: 35.5	78.7	81.0	63.7
70.0 mg/1400ml/1ml	$2.3 \times 10^{-5}$	1: 33.3			

\*The best concentration is  $2.2 \times 10^{-3}$  M

**Table 3.** Reaction temperature vs. yield in model cyclization study

Condition	Concentration (mol/L)	Acid Ratio (mol) Model compound/acid	Crude Yield (%)	Purity from HPLC (%)	Overall Yield (%)
65.0 mg/140ml/1ml (25°C)	$2.2 \times 10^{-3}$	1: 35.2	89.5	91.4	81.8
65.0 mg/140ml/1ml (0°C)	$2.2 \times 10^{-3}$	1: 35.2	76.8	44.6	34.2

\* The better reaction temperature is at room temperature (25°C).

**Table 4. Reaction time vs. yield in model cyclization study**

Condition	Concentration (mol/L)	Acid ratio (mol) Model compound/acid	Crude Yield (%)	Purity from HPLC (%)	Overall Yield (%)
65mg/140ml/1ml 25°C/12hr/air	2.2* 10 <sup>-3</sup>	1: 35.2	89.5	91.4	81.8
65mg/140ml/1ml 25°C/24hr/air	2.2* 10 <sup>-3</sup>	1: 35.2	82.2	98.1	80.8

\* The better reaction time is 12 hr.

**Table 5. Argon purge vs. yield in model cyclization study**

Condition	Concentration (mol/L)	Acid ratio (mol) Model compound/acid	Crude Yield (%)	Purity from HPLC (%)	Overall Yield (%)
70 mg/140ml/1ml 25°C/12 hr/Ar	2.4* 10 <sup>-3</sup>	1: 33.3	97.0	92.1	89.2
65mg/140ml/1ml 25°C/12hr/air	2.2* 10 <sup>-3</sup>	1: 35.2	89.5	91.4	81.8

\* The better reaction condition is in argon.

**Table 6.** Acid ratio vs. yield in model cyclization study

Condition	Concentration (mol/L)	Acid ratio (mol) Model compound/acid	Crude Yield (%)	Purity from HPLC (%)	Overall Yield (%)
70 mg/140ml/lml 25°C/12 hr/Ar	$2.4 * 10^{-3}$	1: 33.3	97.0	92.1	89.2
70.6mg/140ml/0.25ml r.t./12 hr/Ar	$2.38 * 10^{-3}$	1:8.33	79.3	82.5	65.4
74.06mg/140ml/3ml/ r.t./12hr/Ar	$2.49 * 10^{-3}$	1:100	60.3	96.5	57.9

\* The best ratio of model compound to acid is: 1:33.3

**Table 7.** The rate of adding the acid vs. yield in model cyclization study

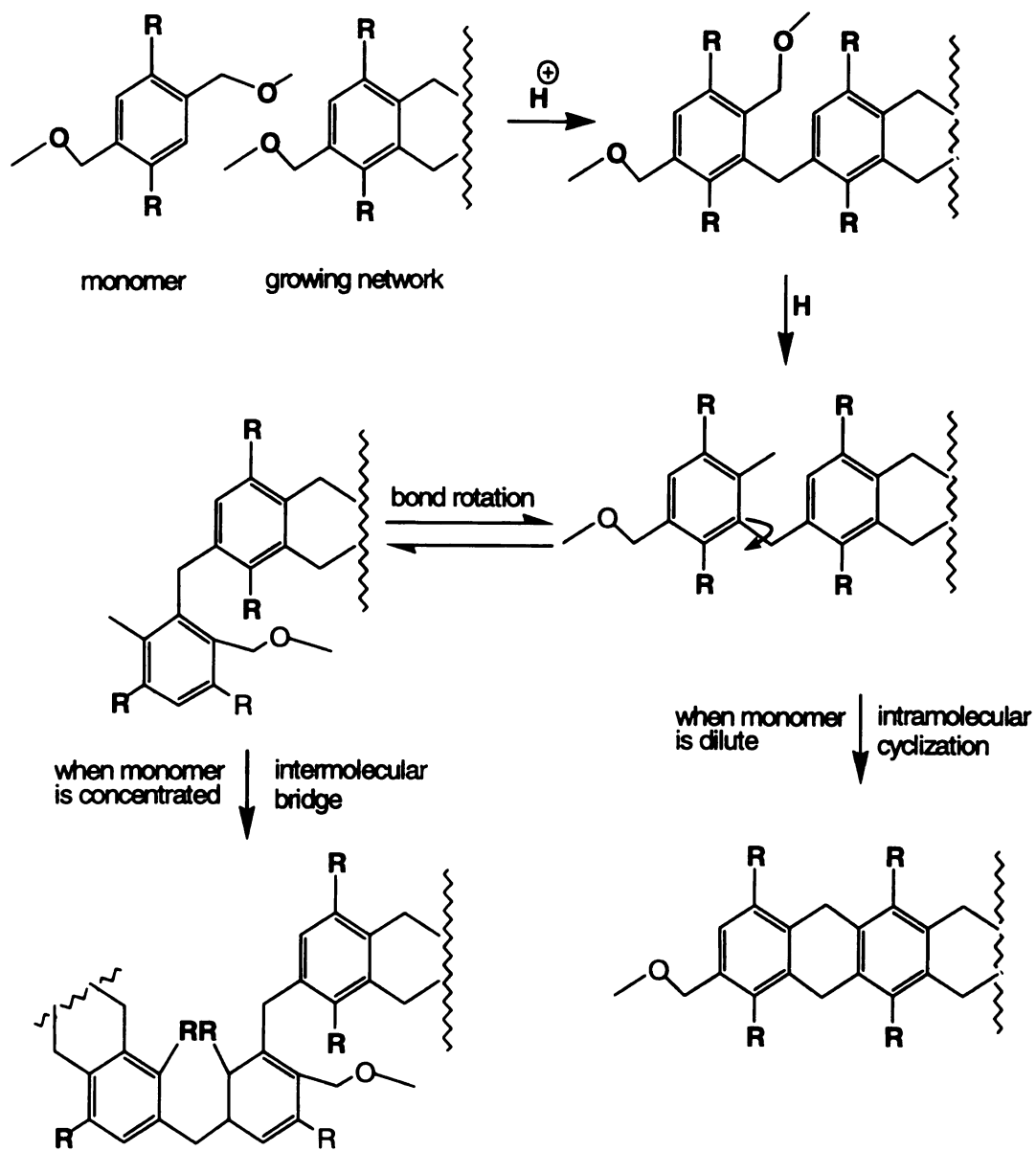
Condition	Concentration (mol/L)	Acid ratio (mol) Model compound/acid	Crude Yield (%)	Purity from HPLC (%)	Overall Yield (%)
70 mg/140ml/lml 25°C/12 hr/Ar adding acid in 10 minute	$2.36 * 10^{-3}$	1: 33.3	97.0	92.1	89.2
70 mg/140ml/lml 25°C/12 hr/Ar adding acid in 60 minute	$2.36 * 10^{-3}$	1: 33.3	60.0	84.5	50.7

\* The better condition is to add the acid in 10 minute

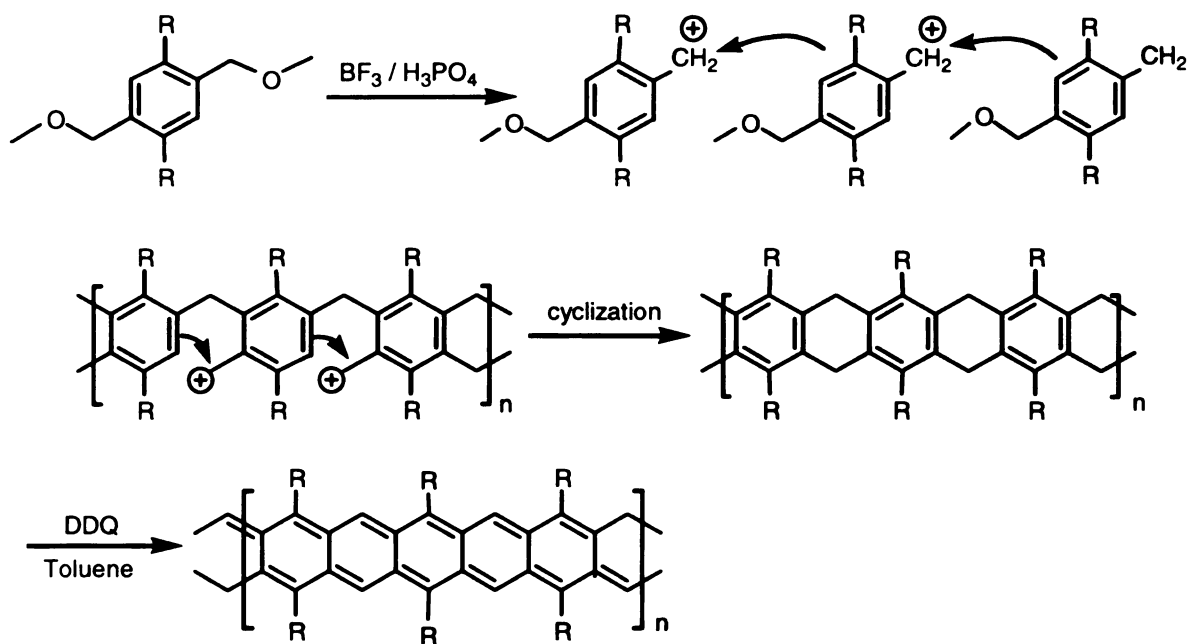
**Table 8.** Different solvent vs. yield in model cyclization study

Condition	Concentration (mol/L)	Acid ratio (mol) Model compound/acid	Crude Yield (%)	Purity from HPLC (%)	Overall Yield (%)
70 mg/140ml (CH <sub>2</sub> Cl <sub>2</sub> )/lml 25°C/12 hr/Ar adding acid in 10 minute	2.36 * 10 <sup>-3</sup>	1: 33.3	97.0	92.1	89.2
70 mg/140ml (CH <sub>3</sub> NO <sub>2</sub> )/lml 25°C/12 hr/Ar adding acid in 10 minute	2.36 * 10 <sup>-3</sup>	1: 33.3	NMR shows all the model compound Has reacted, but the result is messy Product is black oil.		

\* The better solvent is dichloromethane



**Scheme 19.** Intramolecular cyclization vs. intermolecular bridge formation



**Scheme 20.** Synthesis of alkylated polyacenes.

### 3.2.4. Characterization

Since the attachment of the alkyl chains improved the solubility of the acene precursor, we were able to better characterize the acene precursor polymer and the dehydrogenated product. UV and fluorescence spectroscopy (**Figure 22**) are the most direct techniques that can be used to assay the conjugation length of the polyacene product. When the soluble polymer was excited at 420 and 570 nm, the lowest energy emissions detected were near 480 and 610 nm, the longest wavelength absorption bands of tetracene and pentacene, respectively. Thus, the longest acene segments in the polymers contained 4 to and 5 fused rings. The bulk of the emission envelope appeared at shorter wavelengths, and we did not try to quantify the distribution of chain lengths.

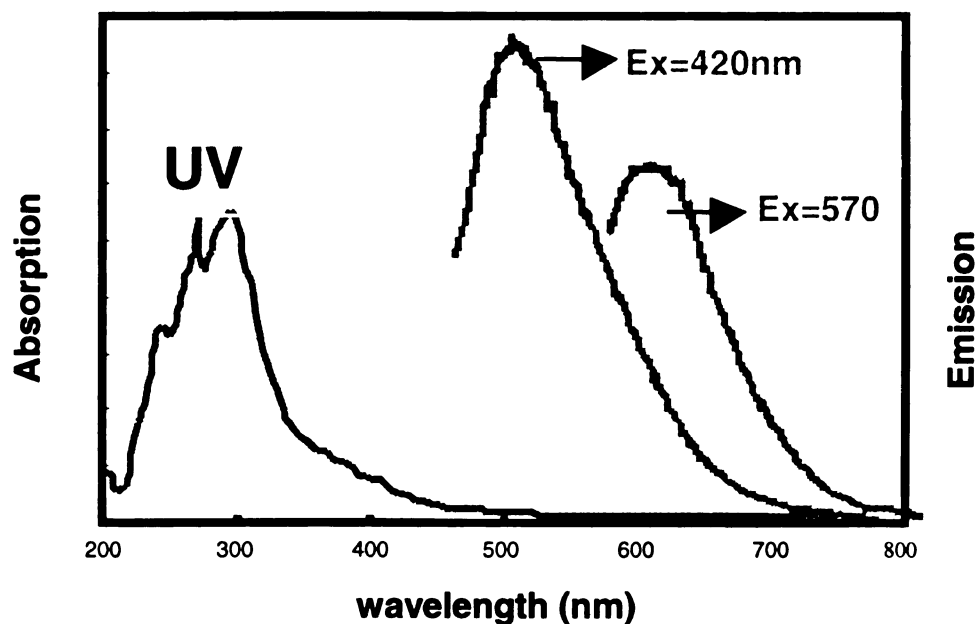


**Figure 22.** UV and fluorescence spectra of soluble polyacene products.

### 3.2.5. Discussion

Why were the lengths of the polyacene segments so short? We relied on the optimized reaction conditions of model compounds to favor cyclization over polybenzylation, but the data imply that the polymers had a higher degree of polybenzyl content than would be predicted from the model study. In the polymer system, the competition between intra and intermolecular cyclization apparently is biased toward the latter. It is possible that a different set of reaction conditions, such as a more dilute monomer concentration, would be more appropriate for the polymerization. There also may be undetected side reactions that are more prevalent in the polymerization. It is important to keep in mind that the polymerizations are probably best described as step growth systems, where monomers form dimers and dimers need to find each other to extend the chain. High concentrations favor more rapid growth, and possibly polybenzyl formation.

To solve this dilemma, the condensation and cyclization steps must be separated, i.e. a linear polymer must first be synthesized at high monomer concentrations, and after purification, the polymer can then be cyclized in dilute solution to give the acene precursor. Based on this idea, we propose the route shown in **Scheme 21**. By preparing a dialkylated monomer with the methoxymethyl and a second functional group, labeled X, the acid catalyzed reaction can be initiated to prepared a linear polybenzyl. After purification of the polymer, the second functional group can be accessed to close the ring.

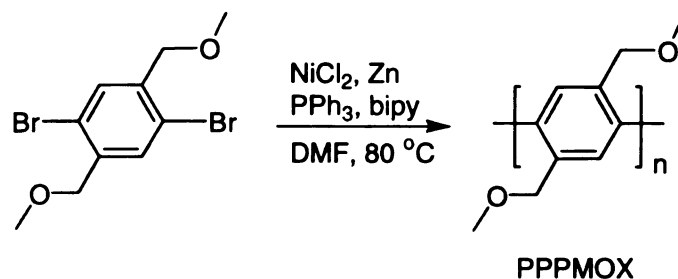
### 3.3. Acene/poly (*p*-phenylene) hybrids.

The lack of control over the electrophilic aromatic substitution reactions used to prepare polyacenic materials resulted in our inability to prepare perfectly linear polyacenes. An approach that should yield higher selectivity is to align the functional groups in a pre-ordered state. Designing monomers capable of organizing into an ordered phase may increase the probability of intramolecular cyclization. If a polyphenylene containing the reactive methoxymethyl functionalities is synthesized, then it should exhibit the same type of chemistry as bis(methoxymethyl)benzenes in the presence of strong acids and yield a network structure where the polymer backbones are cross-linked by benzyl bridges. Furthermore, if the polymer backbone has limited bond rotation, then the most probable cross-linking reaction is the formation of cyclized products. The overall structure of the product would resemble a sheet of graphite and should have high thermal stability.

To realize this idea, we synthesized 1,4-dibromo-2,5-bis(methoxymethyl)benzene from readily available starting materials as shown in **Scheme 12**. Methoxymethyl substituted poly(*p*-phenylene) was synthesized from the dibromobenzene monomer using a nickel catalyzed coupling reaction (**Scheme 22**). The resulting polymer was insoluble in DMF and precipitated from solution during the course of the polymerization. The polymer was collected by filtration and washed repeatedly with water and ethanol to remove any polymerization reagents. After drying, the polymer was obtained as a finely powdered, pale yellow solid. GPC analysis of the THF soluble fraction (5 wt.%)

indicated a degree of polymerization less than 10 (relative to polystyrene standards).

The polymer was reacted with sulfuric acid following the same procedure as the polymerization of bis(methoxymethyl)benzenes. Since the carbon atoms in PPP are  $sp^2$  hybridized, bond motion is limited to rotation about the central axis and the geometry of polyphenylenes is rigid rod; therefore the PPP chain can easily packed together. Once the PPP rods align with each other, intramolecular cyclization should be favored, leading to the formation of acene precursors (**Scheme 23**).



**Scheme 22.** Synthesis of a methoxymethyl-substituted polyphenylene

**Figure 23** shows the thermal stabilities of the polymer and that of the network resulting from the acid catalyzed cross-linking. The polymer is thermally stable to 350 °C at which point the side chains are evolved as volatile products leaving behind the polyphenylene backbone, which is stable to 700 °C. The weight loss observed in the TGA scans of the cross-linked network at lower temperatures is most likely due to the evolution of methanol resulting from the reaction of residual acid and methoxymethyl groups. Even though the product

from the cross-linking reaction was neutralized with base and rinsed repeatedly with water, some sulfuric acid did remain in the tacky solid. Despite the early weight loss, the network exhibits excellent thermal stability, producing a 70% char yield at 700 °C. There are two possible products from the heat dehydrogenation: one is the idealized 2D polyacene structure, the other is the more likely formed graphitized product. Both exhibit high thermal stability.

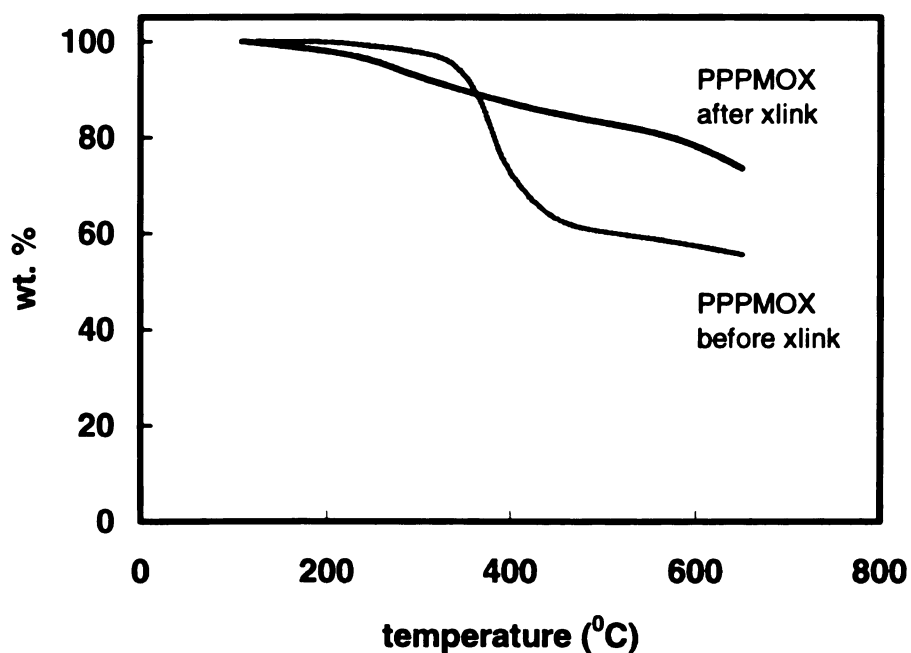
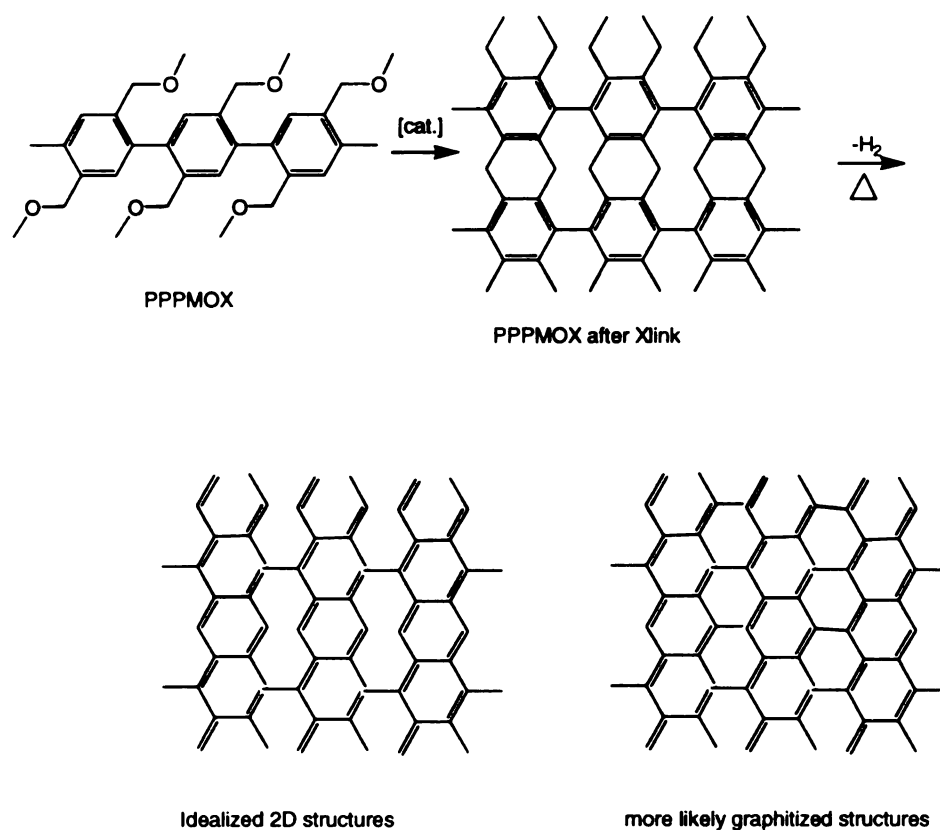


**Figure 23.** Thermogravimetric analysis of 2D polyacene



**Scheme 23.** Synthesis of sheet structures from methoxymethyl-substituted polyphenylenes.

These materials were also analyzed by IR spectroscopy, shown in **Figure 24**. The most noticeable evidence of the structural changes brought on by the acid catalyzed cross-linking of the polymer can be seen by the decreases in the C-H and C-O stretching intensities at 2900-3000 and 1100  $\text{cm}^{-1}$ , respectively, due to the loss of the methoxy groups. As seen in the pyrolysis of the networks formed from bis(methoxymethyl)benzenes, high temperature treatment of the polyphenylene-derived network at 700 °C also results in the near complete loss of C-H bonds and the tailing of the electronic absorption into the IR.

Raman spectrum also indicate a graphite-like material was formed after high temperature treatment (800 °C) of cross-linked PPPMOX (**Figure 25**). Among the two peaks observed, the one at 1355  $\text{cm}^{-1}$  belong to the  $A_{1g}$  vibration mode, attributed to the amorphous portion of graphite; the peak at 1600  $\text{cm}^{-1}$  is from the  $E_{2g}$  vibration mode, which is assigned to the lattice graphite. All the results from Raman, IR and thermal analysis indicate that thermal treatment of the cross-linked network structure also leads to materials with extensive  $\pi$ -conjugation and low H content.

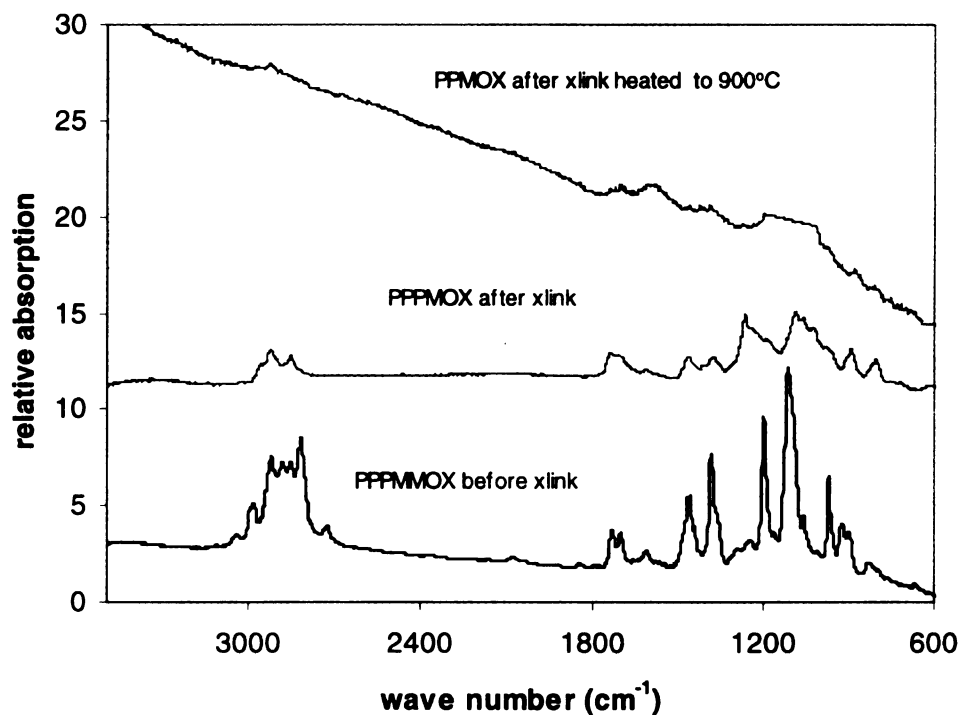


**Figure 24.** Infrared of cross-linked and heat treated samples of a methoxymethyl-substituted polyphenylene.

### 3.4. Conclusion

The high temperatures needed for the pyrolysis of phenolic and cellulose resins allows little control of the acene-like structural elements that are the precursors to graphite. If elements of the acene structure are designed into the starting material, it is possible to obtain partially graphitized structures at much lower temperatures that still retain some memory of the chemical structure before pyrolysis. Two types of polyacene syntheses based on a Lewis acid catalyzed electrophilic aromatic substitution reaction were investigated. The first targeted simple routes to acene-like materials that

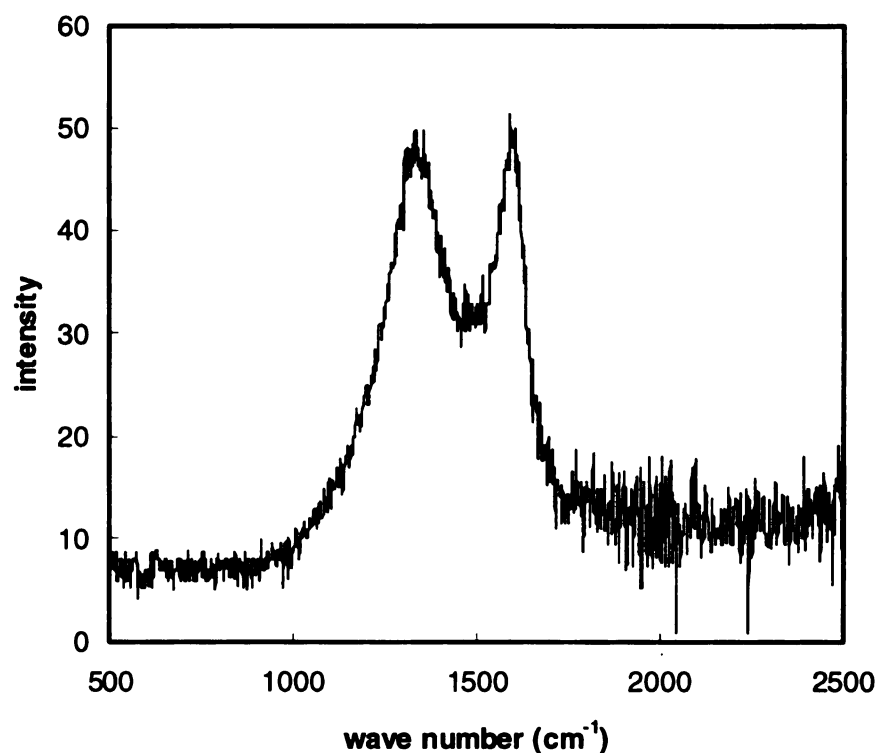


**Figure 25.** Raman spectrum of a cross-linked and heat treated sample of a methoxymethyl-substituted polyphenylene.

contain a substantial fraction of acene subunits. We found that bis(methoxymethyl)benzenes undergo acid-catalyzed polymerization to yield network structures. The idealized chemical structure for the polymerization of 1,2-bis(methoxymethyl)benzene is a linear polyacene precursor that after elimination of H<sub>2</sub>, yields polyacenic materials with an extended electron system. The second route targeted the synthesis of a methoxymethyl substituted poly(*p*-phenyl) that when chemically cross-linked, ideally formed a two-dimensional network closely resembling a graphite sheet. The IR and thermal analysis measurements indicate that much lower temperatures are required to pyrolyze these materials into partially graphitized structures. A synthetic route to a novel, soluble linear polyacene based on the same acid catalyzed electrophilic aromatic substitution reaction was also investigated. We obtained soluble polymer with molecular weights as high as 7000. However, fluorescence data show that the maximum length of the acene segments is ~5 units.

## BIBLIOGRAPHY

- 1 Kertesz, M. *Macromolecules* **1995**, *28*, 1475-1480.
- 2 Darosa, A. L. S.; Demelo, C. P. *Phys. Rev. B* **1988**, *38*, 5430-5437.
- 3 Mizes, H.; Conwell, E. *Phys. Rev. B* **1991**, *44*, 3963-3969.
- 4 Su, W. P.; Schrieffer, J. R.; Heeger, A. J. *Phys. Rev. Lett.* **1979**, *42*, 1698-1701.
- 5 Su, W. P.; Schrieffer, J. R.; Heeger, A. J. *Phys. Rev. B* **1980**, *22*, 2099-2111.
- 6 Wilbourn, K.; Murray, R. W. *J. Phys. Chem.* **1988**, *92*, 3642-3648.
- 7 Pietrass, P. *Proceedings of the 13th Annual International Symposium on Electronic Structure of Metals and Alloys*; Johnsbach: Dresden, 1983.
- 8 Boon, M. R. *Theoret. Chim. Acta* **1971**, *23*, 109-110.
- 9 Whangbo, M. H.; Hoffmann, R.; Woodward, R. B. *Proc. R. Soc. London Ser. A-Math. Phys. Eng. Sci.* **1979**, *366*, 23-46.
- 10 Cioslowski, J. *J. Chem. Phys.* **1993**, *98*, 473-477.
- 11 Tanaka, K.; Ohzeki, K.; Nankai, S.; Yamabe, T.; Shirakawa, H. *J. Phys. Chem. Solids* **1983**, *44*, 1069-1075.
- 12 Kertesz, M.; Lee, Y. S.; Stewart, J. J. P. *Int. J. Quantum Chem.* **1989**, *35*, 305-313.
- 13 Bredas, J. L. *Handbook of Conducting Polymers*; Dekker, New York:, 1986; Vol. 2.
- 14 Pomerantz, M.; Cardona, R.; Rooney, P. *Macromolecules* **1989**, *22*, 304-308.
- 15 Dewar, M. J. S.; Dougherty, R. C. *The PMO Theory of Organic Chemistry*, Plenum: New, York, 1975.
- 16 Carey, F. A.; Sundberg, R. J. *Advanced Organic Chemistry Part A*; 2nd ed.; Plenum: New York, 1984.
- 17 Wang, R. S.; Hou, W. L. *Synth. Met.* **1991**, *42*, 1637-1640.
- 18 Albery, W. J.; Doblhofer, K.; Lyons, M. E. G.; Mount, A. R.; Vorotyntsev, M. *Electroactive Polymer Electrochemistry*, Plenum: New York, 1994.

- 19 Feast, W. J. *Handbook of Conducting Polymer*, Marcel Dekker., 1986; Vol. 1.
- 20 Iyer, V. S.; Wehmeier, M.; Brand, J. D.; Keegstra, M. A.; Mullen, K. *Angew. Chem.-Int. Edit. Engl.* **1997**, *36*, 1604-1607.
- 21 Trick, K. A.; Saliba, T. E. *Carbon* **1995**, *33*, 1509-1515.
- 22 Dang, T. D.; Wang, C. S.; Click, W. E.; Chuah, H. H.; Tsai, T. T.; Husband, D. M.; Arnold, F. E. *Polymer* **1997**, *38*, 621-629.
- 23 Dhami, T. L.; Bahl, O. P.; Jain, P. K. *Carbon* **1995**, *33*, 1517-1524.
- 24 Tanaka, K.; Ohzeki, K.; Yamabe, T.; Yata, S. *Synth. Met.* **1984**, *9*, 41-52.
- 25 Yamabe, T.; Tanaka, K.; Ohzeki, K.; Yata, S. *J. Phys. (Paris) Colloq., Suppl.* **1983**, *44*, C3-645.
- 26 Yata, S.; Hato, Y.; Osaki, T.; Sakurai, K. In *US Patent No. 4 753 717* 1988.
- 27 Yata, S.; Hato, Y.; Sakurai, K.; Satake, H.; Mukai, K.; Tanaka, K.; Yamabe, T. *Synth. Met.* **1990**, *38*, 169-175.
- 28 Yata, S.; Osaki, T.; Hato, Y.; Takehara, N.; Kinoshita, H.; Tanaka, K.; Yamabe, T. *Synth. Met.* **1990**, *38*, 177-184.
- 29 Kojima, Y.; Matsuoka, T.; Sato, N.; Takahashi, H. *Macromolecules* **1995**, *28*, 2893-2896.
- 30 Giuliano, C. R.; Hess, L. R. *IEEE J. Quantum Electron* **1979**, *15*, D71.
- 31 Coulter, D. R.; Perry, J. W.; Wei, T. H. *Proc. SPIE* **1989**, *1105*, 42.
- 32 Perry, J. W.; Khundkar, L. R. *NATO ASI Ser. E* **1991**, *194*, 369.
- 33 Bunning, T. J.; Natarajan, L. V.; Schmitt, M. G.; Epling, B. L.; Crane, R. L. *Appl. Optics* **1991**, *30*, 4341-4349.
- 34 Tutt, L. W.; Kost, A. *Nature* **1992**, *356*, 225-226.
- 35 Wood, G. L.; Clark, W. W., III; Miller, M. J.; Salamo, G. J.; Sharp, E. *Proc. SPIE* **1989**, *1105*, 154.
- 36 Tutt, L. W.; McCahon, S. W. *Opt. Lett.* **1990**, *15*, 700-702.
- 37 Mansour, K.; Soileau, M. J.; Vanstryland, E. W. *J. Opt. Soc. Am. B-Opt. Phys.* **1992**, *9*, 1100-1109.

- 38 Branelik, D. M.; McLean, D. G.; Schmitt, M. G.; Epling, B. L.; Colclasure, C.; Tondiglia, V.; Pachter, R.; Obermeirer, K.; Crane, R. L. In *Electrical Optical and Magnetic Properties of Organic Solid State Materials*; Materials Research Society: Pittsburgh, 1992; Vol. 247, p 361.
- 39 Pochan, J. M.; Pochan, D. F.; Rommelmann, H.; Gibson, H. W. *Macromolecules* **1981**, *14*, 110-114.
- 40 Shacklette, L. W.; Chance, R. R.; Ivory, D. M.; Miller, G. G.; Baughman, R. H. *Synth. Met.* **1980**, *1*, 307-320.
- 41 Yata, S.; Hato, Y.; Sakurai, K.; Osaki, T.; Tanaka, K.; Yamabe, T. *Synth. Met.* **1987**, *18*, 645-648.
- 42 Jobst, K.; Sawtschenko, L.; Wuckel, L.; Doge, H. G.; Schwarzenberg, M. In *DD Patent 240 285* 1986.
- 43 Fauteux, D.; Koksang, R. *J. Appl. Electrochem.* **1993**, *23*, 1-10.
- 44 Yata, S.; Kinoshita, H.; Komori, M.; Ando, N.; Kashiwamura, T.; Harada, T.; Tanaka, K.; Yamabe, T. *Synth. Met.* **1994**, *62*, 153-158.
- 45 Zheng, T.; Xue, J. S.; Dahn, J. R. *Chem. Mat.* **1996**, *8*, 389-393.
- 46 Tatsumi, K.; Akai, T.; Imamura, T.; Zaghbi, K.; Iwashita, N.; Higuchi, S.; Sawada, Y. *J. Electrochem. Soc.* **1996**, *143*, 1923-1930.
- 47 Tanaka, K.; Koike, T.; Yamabe, T.; Yamauchi, J.; Deguchi, Y.; Yata, S. *Phys. Rev. B* **1987**, *35*, 8368-8373.
- 48 Tanaka, K.; Ueda, M.; Koike, T.; Yamabe, T.; Yata, S. *Synth. Met.* **1988**, *25*, 265-275.
- 49 Yazami, R.; Nakajima, T. *Synth. Met.* **1991**, *40*, 387-392.
- 50 Mohri, M.; Yanagisawa, N.; Tajima, Y.; Tanaka, H.; Mitate, T.; Nakajima, S.; Yoshida, M.; Yoshimoto, Y.; Suzuki, T.; Wada, H. *J. Power Sources* **1989**, *26*, 545-551.
- 51 Yata, S. In *US Patent No. 4 601 849788* 1986.
- 52 Tanaka, K.; Koike, T.; Yamabe, T.; Yata, S. *Synth. Met.* **1989**, *29*, E489-E494.
- 53 Sato, K.; Noguchi, M.; Demachi, A.; Oki, N.; Endo, M. *Science* **1994**, *264*, 556-558.
- 54 Ishikawa, M.; Sonobe, N. *Synth. Met.* **1991**, *40*, 231.

- 55 Zheng, T.; McKinnon, W. R.; Dahn, J. R. *J. Electrochem. Soc.* **1996**, *143*, 2137-2145.
- 56 Tokumitsu, K.; Mabuchi, A.; Fujimoto, H.; Kasuh, T. *J. Electrochem. Soc.* **1996**, *143*, 2235-2239.
- 57 Selwyn, L. S.; McKinnon, W. R.; Vonsacken, U.; Jones, C. A. *Solid State Ion.* **1987**, *22*, 337-344.
- 58 Nogami, T.; Mikawa, H.; Nawa, M. J. *J. Phys. Colloq. (France)* **1983**, *C3*, 573.
- 59 Yata, S.; Sakurai, K.; Osaki, T.; Inoue, Y.; Yamaguchi, K.; Tanaka, K.; Yamabe, T. *Synth. Met.* **1990**, *38*, 185-193.
- 60 Yata, S.; Okamoto, E.; Satake, H.; Kubota, H.; Fujii, M.; Taguchi, T.; Kinoshita, H. *J. Power Sources* **1996**, *60*, 207-212.
- 61 Sidman, J. W. *J. Chem. Phys.* **1956**, *25*, 122.
- 62 Kause, N. J.; Small, G. J. *J. Chem. Phys.* **1972**, *56*, 2985.
- 63 Clar, E. *Polycyclic Hydrocarbons*; Academic Press: London, 1964; Vol. 1,2.
- 64 Marschalk, C. *Bull. Soc. Chim. Fr.* **1938**, *5*, 306.
- 65 Marschalk, C. *Bull. Soc. Chim. Fr.* **1941**, *8*, 354.
- 66 Marschalk, C. *Bull. Soc. Chim. Fr.* **1950**, 311.
- 67 Notario, R.; Abboud, J. L. M. *J. Phys. Chem. A* **1998**, *102*, 5290-5297.
- 68 Horn, T.; Baumgarten, M.; Gerghel, L.; Enkelmann, V.; Mullen, K. *Tetrahedron Lett.* **1993**, *34*, 5889-5892.
- 69 Graham, R. J.; Paquette, L. A. *J. Org. Chem.* **1995**, *60*, 5770-5777.
- 70 Suh, M. C.; Shim, S. C. *Macromolecules* **1995**, *28*, 8707-8712.
- 71 Takahashi, T.; Kitamura, M.; Shen, B. J.; Nakajima, K. *J. Am. Chem. Soc.* **2000**, *122*, 12876-12877.
- 72 Molinski, T. F.; Fahy, E.; Faulkner, D. J.; Van Duyne, G. D.; Clardy, J. *J. Org. Chem.* **1988**, *53*, 1341-1343.
- 73 Mathias, J. P.; Stoddart, J. F. *Angew. Chem. Int. Ed. Engl.* **1987**, *26*, 805.

- 74 Alder, R. W.; Allen, P. R.; Edwards, L. S.; Fray, G. I.; Fuller, K. E.; Gore, P. M.; Hext, N. M.; Perry, M. H.; Thomas, A. R.; Turner, K. S. *J. Chem. Soc.-Perkin Trans. 1* **1994**, 3071-3077.
- 75 Herwig, P. T.; Mullen, K. *Adv. Mater.* **1999**, *11*, 480.
- 76 Girreser, U.; Giuffrida, D.; Kohnke, F. H.; Mathias, J. P.; Philp, D.; Stoddart, J. F. *Pure Appl. Chem.* **1993**, *65*, 119-125.
- 77 Ozaki, M.; Ikeda, Y.; Nagoya, I. *Synth. Met.* **1987**, *18*, 485-490.
- 78 Kim, D. S.; Suh, M. C.; Shim, S. C. *Synth. Met.* **1996**, *80*, 291-296.
- 79 Suh, M. C.; Shim, S. C. *Chem. Mat.* **1997**, *9*, 192-200.
- 80 Kertesz, M.; Ashertehrani, A. *Macromolecules* **1996**, *29*, 940-945.
- 81 Allison, G.; Bushby, R. J.; Jesudason, M. V.; Pailaud, J. L.; Taylor, N. J. *J. Chem. Soc. Perkin Trans.* **1997**, *2*, 147.
- 82 Vogel, T.; Blatter, K.; Schluter, A. D. *Makromol. Chem., Rapid Commun.* **1989**, *10*, 427-430.
- 83 Luo, J. H., H. J. *J. Org. Chem.* **1987**, *52*, 4833.
- 84 Netka, J.; Crump, S. L.; Rickborn, B. *J. Org. Chem.* **1986**, *51*, 1189-1199.
- 85 Goodings, E. P.; Mitchard, D. A.; Owen, G. J. *J. Chem. Soc. Perkin Trans.* **1972**, 1310.
- 86 Kobayashi, K.; Sugawara, S.; Toyoda, S.; Honda, H. *Carbon* **1968**, *6*, 359.
- 87 Jenkins, G. M.; Kawamura, K.; Ban, L. L. *Proc. Royal Soc. (London)* **1972**, A327, 501.
- 88 Kurosu, H.; Nakajima, Y.; Ando, I. *J. Mol. Struct.* **1995**, *355*, 27-32.
- 89 Tanaka, K.; Ago, H.; Matsuura, Y.; Kuga, T.; Yamabe, T.; Yata, S.; Hato, Y.; Ando, N. *Synth. Met.* **1997**, *89*, 133-139.
- 90 Tanaka, K.; Koike, T.; Nishino, H.; Yamabe, T.; Yamauchi, J.; Deguchi, Y.; Yata, S. *Synth. Met.* **1987**, *18*, 521-526.
- 91 Nijegorodov, N.; Ramachandran, V.; Winkoun, D. P. *Spectroc. Acta Pt. A-Molec. Biomolec. Spectr.* **1997**, *53*, 1813-1824.
- 92 Tuinstra, F.; Koenig, J. L. *J. Phys. Chem.* **1970**, *53*, 1126.

- 93 Ortiz, B.; Walls, F.; Yuste, F.; Barrios, H.; Sanchez-Obregon, R.; Pinelo, L. *Synth. Commun.* **1993**, *23*, 749-756.
- 94 Otsubo, T.; Kohda, T.; Misumi, S. *Bull. Chem. Soc. Jpn.* **1980**, *53*, 512-517.
- 95 Bedard, T. C.; Moore, J. S. *J. Amer. Chem. Soc.* **1995**, *117*, 10662-10671.
- 96 Zhang, S. S.; Liu, Q. G.; Yang, L. L. *J. Electrochem. Soc.* **1993**, *140*, L107-L108.
- 97 Yata, S.; Hato, Y.; Kinoshita, H.; Ando, N.; Anekawa, A.; Hashimoto, T.; Yamaguchi, M.; Tanaka, K.; Yamabe, T. *Synth. Met.* **1995**, *73*, 273-277.
- 98 Wang, T.; Kang, E. T.; Neoh, K. G.; Tan, K. L. *Synth. Met.* **1997**, *84*, 405-406.
- 99 Ago, H.; Nagata, K.; Yoshizawa, K.; Tanaka, K.; Yamabe, T. *Bull. Chem. Soc. Jpn.* **1997**, *70*, 1717-1726.
- 100 Tanaka, K.; Yata, S.; Yamabe, T. *Synth. Met.* **1995**, *71*, 2147-2149.
- 101 Salem, L.; Longuett-Higgins, H. C. *Proc. R. Soc. London, Ser. A* **1960**, *255*, 435.
- 102 Yazami, R.; Guerard, D. *J. Power Sources* **1993**, *43*, 39-46.
- 103 Voigtmartin, I. G.; Simon, P.; Bauer, S.; Ringsdorf, H. *Macromolecules* **1995**, *28*, 236-242.
- 104 Voigtmartin, I. G.; Simon, P.; Yan, D.; Yakimansky, A.; Bauer, S.; Ringsdorf, H. *Macromolecules* **1995**, *28*, 243-254.
- 105 Scherf, U.; Mullen, K. *Synthesis* **1992**, 23-38.
- 106 Rehahn, M.; Schluter, A. D.; Wegner, G.; Feast, W. J. *Polymer* **1989**, *30*, 1060-1062.
- 107 Miyaura, N.; Ishiyama, T.; Sasaki, H.; Ishikawa, M.; Satoh, M.; Suzuki, A. *J. Am. Chem. Soc.* **1989**, *111*, 314-321.
- 108 Buiel, E.; George, A. E.; Dahn, J. R. *J. Electrochem. Soc.* **1998**, *145*, 2252-2257.
- 109 Megahed, S.; Scrosati, B. *J. Power Sources* **1994**, *51*, 79-104.
- 110 Brandt, K. *Solid State Ion.* **1994**, *69*, 173-183.

111 Salomon, M.; Scrosati, B. *Gazz. Chim. Ital.* **1996**, *126*, 415-427.

MICHIGAN STATE UNIVERSITY LIBRARIES



3 1293 02364 4259